DEGREE PROJECT IN ENGINEERING PHYSICS
SECOND CYCLE, 30 CREDITS
STOCKHOLM, SWEDEN 2021

On the Possibility of Probing Early Matter Domination with Primordial Black Holes

Master's Thesis

Isak Stomberg

KTH ROYAL INSTITUTE OF TECHNOLOGY
SCHOOL OF ENGINEERING SCIENCES

Author

Isak Stomberg, isakst@kth.se
MSc Engineering Physics, track Subatomic and Astrophysics
KTH Royal Institute of Technology

Place for Project

Deutsches Elektronen-Synchrotron, DESY
Hamburg, Germany

Examiner

Prof. Sandhya Choubey KTH Royal Institutue of Technology

Supervisors

Dr. Kai Schmidt-Hoberg
Deutsches Elektronen-Synchrotron, DESY

Ass. Prof. Mattias Blennow
KTH Royal Institutue of Technology

TRITA-SCI-GRU 2021:058

Abstract

Primordial black holes (PBHs) are expected to form in the very early universe, and therefore, we could use them to probe pre-BBN times. Astrophysical observations permit the placement of bounds on the abundance of PBHs. Combining these bounds with predictions of PBH formation and the resulting PBH abundances, we explore the possibility to constrain an epoch of early matter domination (MD). For this analysis we incorporate the recently obtained and most stringent bounds on PBHs from 21 cm observations. We assume density perturbations described by a near-power-law form of the curvature power spectrum consistent with the Planck 2018 results and derive the corresponding PBH mass function using recent results from the literature. To place constraints on an early matter-dominated (MD) epoch, we compare this with up-to-date bounds on PBHs, adding those from 21 cm astronomy, using a formalism to apply monochromatic constraints to extended mass functions. We find that 21 cm bounds on PBHs may probe early MD if it lasts for a duration of at least ~ 12 e-folds and ends at a reheating temperature $T_{\text{min}} < T_{\text{reh}} \lesssim 10^{5.5}$ GeV, where T_{min} depends on the duration of the MD, the spectral index n_{s}, and α_{s}. For optimistic assumptions, our derived limits on the spectral index n_{s} extend into the Planck 2018 [3] 67% upper confidence region of $n_s = 0.9649 \pm 0.0042$, nearly reaching its median $n_{\text{s}} = 0.9649$, if we neglect the running α_{s}. Our bounds on the running α_{s} shows that early MD is incompatible with positive running $\alpha_{\text{s}} \gtrsim 0$.

Keywords

Primordial Black Holes, Early Matter Domination, Master's Thesis

Sammanfattning

Primordiala svarta hål förutsäges ha skapats i det mycket tidiga universum. Ur detta förstår vi att dessa svarta hål ger oss en länk till universums tillstånd under deras skapelse och att vi genom studiet av primordiala svarta hål kan skymta detta tillstånd. Restriktioner på mängden primordiala svarta hål i universum kan beräknas utifrån astrofysiska observationer. Jämförelse av dessa restriktioner med teoretiska förutsägelser av vilka mängder av primordiala svarta hål som skapats vid olika tillstånd medger att vissa tillstånd utesluts. I detta arbete undersöker vi just detta samband och avser etablera huruvida de starkaste restriktionerna på primordiala svarta hål, speciellt från 21 cm observationer av universum, kan utesluta ett kosmologiskt scenario med tidig materiadominans. För att göra detta antar vi att störningar i den annars homogena energidensiteten kan beskrivas med hjälp av ett nästan-storleksoberoende potenssamband vars form ges av resultat från Planck kollaborationen 2018. Givet denna potenslag beräknar vi en form för de primordiala svarta hålens massdistribution medelst resultat från den vetenskapliga litteraturen. Vi jämför sedan dessa förutsägelser med de senaste mängdrestriktionerna på primordiala svarta hål, inkluderat dem från 21 cm observationer, för att erhålla nya begränsningar på tidig materiadominans. Vi tar i beaktande att massdistributionen av primordiala svarta hål inte är monokromatisk, utan utbredd. Resultatet av denna analys är att tidig materiadominans är inom räckhåll för att uteslutas medelst studier av primordiala svarta hål om perioden av materiadominans är längre än ~ 12 e-folds och att den slutar vid återuppvärmningstemperaturen $T_{\text{min}} < T_{\text{reh}} \lesssim 10^{5.5}$ GeV, där T_{min} beror på hur länge den tidiga materiadominansen varar, på det spektrala indexet n_{s} och det spektrala indexets derivata α_{s}. För optimistiska antaganden äventyrar dessa restriktioner på materiadominans resultat från Planck kollaborationen 2018 i det att det övre konfidensintervallet på det spektrala indexet $n_s = 0.9649 \pm 0.0042$ är exkluderat, och att förändringen av detta index, α_{s}, inte kan vara positiv då vi låter

storleksordningen minska.

Nyckelord

Primordiala svarta hål, tidig materiadominans, mastersarbete

Acknowledgements

I extend my sincere gratitude to Dr. Camilo Garcia Cely and Dr. Thomas Konstandin, both of whom have judiciously guided me forward in this project through plentiful advice, support, and discussions. I am grateful to Oindrila Ghosh for helpful discussions, proofreading, and support during this difficult time of the COVID-19 pandemic. I am grateful to Prof. Mattias Blennow, my supervisor at KTH, for his support and help. This work was made possible and supported by the German Research Foundation (DFG, German Research Foundation) under Germany's Excellence 511 Strategy - EXC 2121 "Quantum Universe"- 390833306.

Finally, I would like to acknowledge my supervisor at DESY, Dr. Kai Schmidt-Hoberg, for an abundance of great ideas, incredible kindness, patience, and hospitality that always made me feel welcome and an integral part of the group, and express my immense appreciation for the great support he provided.

Definitions and Conventions

We use natural units $\hbar = c = 1.$, unless otherwise stated. The Planck mass is defined as $M_{\text{pl}} = 1/\sqrt{G} = 1.2211 \times 10^{19}$ GeV, where G is the gravitational constant. The reduced Planck mass is defined as $m_{\text{pl}} = M_{\text{pl}}/\sqrt{8\pi} = 2.4357 \times 10^{18}$ GeV. Converting between grams and solar masses, we use $M_{\text{sun}} = 1.986 \times 10^{33}$ g $= 1.116 \times 10^{57}$ GeV.

For the Hubble parameter, we use h=0.674, as derived by the Planck collaboration and presented in the 2018 results [4]. For the present entropy density of the universe, we use $s_0 = 2.23356 \times 10^{-26}$ GeV^3, and for the present (photon) temperature of the universe $T_0 = 2.725\,\text{K} = 2.349 \times 10^{-13}$ GeV. The temperature at matter-radiation equality $T_{\text{eq}} = 9840\,\text{K} = 8.482 \times 10^{-10}$ GeV. We also take the fraction of (cold) dark matter to the total energy density $\Omega_{\text{DM}} = 0.264$ [3].

We denote Four-vectors as x_μ with Greek indices, while three-vectors as x_i with Latin indices.

Throughout this work, we will assume that cosmological transitions from matter-domination to radiation-domination, and vice versa, occur abruptly.

We use the acronym MD to denote *matter domination* and *matter-dominated*, RD to denote *radiation domination* and *radiation-dominated*, and EQ to denote *matter-radiation equality*, the transition from radiation to matter domination at T_{eq}.

Prologue

I received the Quantum Universe Cluster of Excellence (QU) Masters Scholarship 2019-2020 to support my master's research. I thus joined the group DM1 at the German Electron Synchrotron (DESY) and the University of Hamburg as part of the QU, to pursue research under the supervision of Dr. Kai Schmidt-Hoberg and Dr. Camilo Garcia Cely. We explored a variety of topics: (i) We aimed to shed light onto a dark matter scenario that entailed a hidden sector with vector dark matter and a massless photon coupled to the standard model via a Higgs portal, generated via the breaking of SU(2) into U(1), in the context of early universe cosmology; (ii) we considered a classical approach to derive the momentum-transfer cross-section of dark matter interacting via a pseudoscalar mediator. The non-perturbative approach of solving the corresponding Schroedinger equation for a pseudo-scalar potential is plagued by divergence at its origin, which could be evaded through a classical treatment to derive the momentum transfer cross-section if indeed a classical regime could be established; for my master's thesis, we explored a third project, which constitutes my primary work: (iii) Stringent constraints on primordial black hole (PBH) abundances exist for most of the conceivable range of PBH masses, and 21 cm astronomy carry the potential to strengthen these significantly. We explore what these constraints can teach us about the thermal history of the universe, in particular periods of early matter domination.

While (i) was interesting and carried the potential to feed a long-term collaboration, lacking a clear objective, we decided against the continuation of this project as a foundation for my master's thesis, prioritizing instead a well-defined project with a clear objective. This led us to explore (ii). However, we rather quickly established that no such classical regime existed. Left with this result, we decided not to proceed further and begun exploring (iii), which I am now presenting to you in the form of this master's thesis.

To Herman Wilén, my dear friend and compatriot in the pursuit of knowledge, where we tirelessly fought side by side to realize our dreams.

Contents

1 Introduction **1**

1.1 Background 1

1.2 Science question 4

1.3 Outline 5

2 Cosmology **7**

2.1 Friedmann-Robertson-Walker-Lemaître Metric 7

2.2 The Friedmann equations 9

2.3 The Thermal Universe 13

2.3.1 Thermal equilibrium 13

2.3.2 Entropy 16

2.4 Early Matter Domination 17

2.5 Cosmological Perturbation Theory 18

2.5.1 Quantifying perturbations 19

2.5.2 Newtonian approximation 20

2.5.3 Results from relativistic perturbation theory 25

2.6 Inflation 28

2.6.1 Inflation as a solution to the horizon problem 28

2.6.2 The inflaton field 31

2.6.3 Primordial Perturbations from Inflation 33

3 Primordial Black Holes **35**

3.1 PBH evaporation 36

3.2 PBH Formation 37

3.2.1 Formation mass 37

3.2.2 Basic notions 37

3.2.3 Formation scenarios 38

3.2.4 Extended mass function 43
3.3 Constraints 51
3.3.1 Effects of cosmological histories 52
3.3.2 Various PBH constraints 54
3.3.3 Constraints from 21 cm observations 55
3.3.4 Combined constraints 60
3.3.5 Constraints for extended mass functions 61
3.4 Constraining early MD 62
3.5 Constraining $n_{\rm s}$ and $\alpha_{\rm s}$ 64

4 Discussion and Summary **68**
4.1 Results 68
4.2 Discussion 68
4.3 Conclusions 71

References **72**

Chapter 1

Introduction

1.1 Background

The idea that black holes may form from overdensities in the early universe has been around since 1967 when Zeldovich first proposed the idea [71]. Primordial in origin, they were referred to as Primordial Black Holes, to be abbreviated PBHs throughout this thesis. Hawking soon realized that PBHs, and indeed all black holes, are not entirely black, but evaporates via the radiation of particles, through a process that came to be known as Hawking radiation [44]. Bringing together the languages of general relativity, field theory, quantum mechanics, and thermodynamics, evaporating PBHs constitute a remarkable prediction that, more than 50 years later, is yet to be confirmed by observations. Despite an abundance of non-observations, interest in PBHs has spiked in recent years [1, 14, 24, 41]) due to a multitude of reasons, among which:

(i) convincing evidence suggests that a majority of matter in the universe reveals itself to us primarily through gravitational interactions (e.g. [13]). By this nature, the matter came to be known as Dark Matter (DM). While many new particle species have been proposed to account for this additional matter component, no conclusive evidence exists to date. One possibility is that PBHs constitute all, or at least part, of DM. While stringent constraints on the fraction f of DM as PBHs exist [22], it is permissible that PBHs in the mass windows $10^{16} - 10^{17}$ g, $10^{20} - 10^{24}$ g, and $10 - 10^3 M_\odot$ contribute significantly to the DM density [23]. Eager to uncover the nature of DM, PBHs have been explored as a DM candidate by many authors. However, because PBHs evaporate, those smaller than 10^{15}g no longer exist and cannot contribute to the present DM

density [22].

(ii) A new window to probe the universe was opened on September 14th, 2015, when the signal GW150914 [1] that reached the Advanced LIGO detector was found to be of gravitational origin, and indeed, the first gravitational wave (GW) signal was detected. This marked a milestone in astrophysics and made clear for the first time that the window of GW observations is viable, opening up the possibility to probe aspects of the universe up to the very dawn of time. This signal was the result of two Black Holes, with masses $29M_\odot$ resp $36M_\odot$, coalescing via a merger to form a larger black hole. Over the years of observation since, many more mergers have been detected. Given the relatively large masses of the merging black holes (compared to $1\ M_\odot$ black holes), which happen to coincide with the mass window above, the idea that LIGO had found both DM and PBHs arose [14]. PBHs are expected to give rise to different characteristic signatures than astrophysical black holes [14]. Future observatories, such as the Einstein telescope[62], Big Bang Observatory [60], and DECIGO [48], have greater sensitivities and probe complementary parts of the GW frequency spectrum, and may therefore help differentiate signals from astrophysical black holes from PBHs. Such differences include, e.g., high-frequency harmonics due to the initial high ellipticity not currently within the LIGO sensitivity and a stochastic background with more weight at the lower frequency part of the spectrum [14]. Thus, we can expect to somewhat conclusively answer the question of whether LIGO has indeed observed PBHs in the not-so-distant future. Given this recent surge in the interest in PBHs and the observational prospects of the near future, it is wise to develop a solid phenomenological foundation upon which observational interpretation is facilitated, improving our ability to draw inferences and test cosmological models.

One such scenario is a cosmology with an early epoch of matter domination (MD). It is typically assumed that the universe was radiation-dominated (RD) since after inflation until matter-radiation equality (EQ). In the literature on PBHs, therefore, it is generally considered [22, 24] that PBHs form during radiation domination (RD). During RD, radiation pressure prevents all but the most pronounced overdensities within the (Hubble) horizon from collapsing into PBHs, leading to exponentially suppressed abundances where PBHs form only from the tail of the density fluctuation distribution [26]. In this case the universe would fail to produce a significant fraction of DM in PBHs unless a UV-blue power spectrum with, e.g., a positive running of the spectral index or some other nontrivial UV-blue features, is assumed. If the universe

instead was matter-dominated (MD) during an early period, caused by, e.g., slow reheating after inflation [20] or the presence of some heavy long-lived particle species [6, 11], the lack of radiation pressure would lead to linear growth of overdensities in the early universe [8], analogous to structure formation during late times. These overdensities would eventually grow nonlinear and collapse into PBHs if nonspherical effects are small and the period of MD is long enough [23, 41]. For MD, then, the fraction of the universe that collapses to form PBHs depends on the probability that a perturbation, i.e. overdensity, is sufficiently spherical. This was recently studied in [41], whose results we will consider in greater detail later. Because of the increased PBH production during MD, it is attractive to study the consequences of introducing such a period and in particular whether the resulting PBH abundances are compatible with observations.

Constraints on PBH abundances are expressed as limits on the initial fraction β of PBHs to the total density, or the current DM fraction f, and stem from various phenomenological consequences. The strongest constraints arise due to non-observations of Hawking radiation or the effects this radiation would have on the surroundings. 21 cm cosmology probes the period between the time of last scattering, forming the cosmic microwave background (CMB) at $z \sim 1100$, and reheating, marked by the production of stars and other sources of light at $z \sim 10$. Importantly, on the first of March 2018 [15] reported in Nature that the *Experiment to Detect the Global Epoch of Reionization Signature*, EDGES, had observed an absorption feature in the radio spectrum around the redshift $z \sim 17$ that agrees in timing with predictions of reionization by early stars. However, the feature was more than twice as deep as expected. Arguing that PBHs would erase such an absorption feature, it was shown that PBHs of masses 6×10^{13} g $\lesssim M \lesssim 3 \times 10^{14}$ g are subject to the strong constraints [68], and that future 21 cm observations, such as the Square Kilometer Array (SKA) [17], may potentially provide the most stringent constraints at both smaller and larger masses [58]. We are not aware of any study that considers the 21 cm bounds in the context of early MD, and it is intriguing to consider the possibility that the increased production probability associated with MD leads to a PBH abundance in conflict with the 21 cm bounds.

In the literature, another common assumption is that all PBHs form at a given scale, and only at that scale, giving rise to a monochromatic mass function. The distribution of PBHs, in this case, forms a delta spike, or at least a narrow peak of width typically no

larger than the PBHs mass, centered on that mass [23]. While this may be a reasonable assumption for certain formation scenarios [23], a general treatment should not a priori make this assumption. It has been shown that when an extended, rather than monochromatic, mass function is considered, the constraints derived using a monochromatic mass function may be relaxed [29, 46]. It has also been shown that the numerous methods to account for an extended mass function sometimes lead to conflicting conclusions [25]. Particularly, in the light of a nearly scale-invariant power spectrum from inflation, as found by the Planck collaboration, one finds that the produced mass function of PBHs is extended, rendering a consistent method to adapt monochromatic constraints to an extended mass function necessary. Such a method is developed and presented in [25].

Big bang nuclosynthesis (BBN) denotes the period in the history of the universe when the light elements, D, ^{3}He, ^{4}He, and ^{7}Li, were produced from protons and neutrons. This period took place in the very early universe during the first couple of seconds after the universe's birth. See, e.g., [32] for a review. What is truly remarkable with BBN is that theoretical predictions of the abundances of the light elements agree well with astrophysical observations. Since these predictions include only physics that is well understood, such as the particle content of the standard model and their interactions, ΛCDM cosmology described by general relativity, etc., physicists can claim with great confidence that, reasonably well, we understand the universe all the way back to BBN, and that the standard hot Big Bang cosmology is consistent. Importantly, the BBN means that the universe was RD around the age $t \sim 1\,\mathrm{s}$ at a temperature $T \sim 1\,\mathrm{MeV}$.

While the history of the universe is well understood after BBN, the pre-BBN era is hard to probe observationally. Recent attempts include using gravitational wave production from cosmic strings that could be observed [31], but the state of the pre-BBN universe remains elusive.

1.2 Science question

PBHs are expected to form in the very early universe. In this regard, they stand in direct contact with the conditions of the very early universe, suggesting that we could use them to probe pre-BBN times and add new valuable information to our understanding of the early universe.

Given that strong limits on PBHs are available, particularly those from current and future 21 cm observations, we pose the question whether the increased PBH production probability associated with an early epoch of MD leads to an abundance of PBHs that exceeds the strictest limits. An epoch of MD leading to such a conflict would then be excluded. This, then, provides a means of accessing the conditions of the early universe. To explore this, we implement an analysis to investigate the possibility of probing early MD using predictions for PBHs, their abundance, and constraints from the scientific literature. We point to the possibility that this could rule out certain inflationary scenarios and add important new restrictions on the state of the early universe.

1.3 Outline

This thesis is organised as follows. In Chapter 2 we review relevant aspects of cosmology. This chapter contains section 2.1 which introduces the metric of a universe governed by the cosmological principle, 2.2 where the corresponding dynamical equations of the universe are derived, 2.3 covering basic aspects of thermal physics applied to cosmology, 2.4 where we describe consequences of an early epoch of MD. This is followed by section 2.5 covering fundamentals of cosmological perturbation theory and the description and evolution of density perturbations. The last section 2.6 introduces inflation, and concludes with the important result that the inflaton field sources scalar perturbations described by a near-scale-invariant power spectrum which may result in PBH formation.

In chapter 3 we review PBHs and implement the analysis as we proceed. Partial results and predictions are derived and presented throughout the chapter, while the most important results are presented at the end. This chapter contains section 3.1 that introduces Hawking radiation and basic properties of PBHs. Section 3.2 covers the essentials of PBH formation, such as formation mass, introduces quantities we need to describe the resulting PBH abundance, and various formation scenarios with emphasis on formation during MD. In 3.2.4, we obtain an analytical form for an extended mass function. Section 3.3 covers the constraints on PBHs. We discuss constraints from evaporated and non-evaporated PBHs, and review how 21 cm astronomy may place bounds on PBHs. We proceed to obtain the main results of this work: In section 3.4 we derive and present bounds on early MD, and in section 3.5 we obtain bounds on the

spectral index $n_{\rm s}$ and its running $\alpha_{\rm s}$.

The last chapter 4 contains section 4.1 where we summarize the results, section 4.2 where discuss the validity of our analysis and other sources uncertainty, and suggest future directions of research to complement our results, and section 4.3 where we conclude.

Chapter 2

Cosmology

In this chapter, we give a brief theoretical overview of cosmology, emphasizing aspects relevant to PBHs and their formation. For some results detailed derivations are provided, for others, we quote the results obtained in the literature, when a detailed derivation is beyond the scope of this thesis. Most results in this section have long been known. Hence, we will only give references to those results that are more recent or not so well-known, and declare that the majority of the results presented in this section is obtained from the following set of books and lecture notes [8, 9, 35, 53, 66]. In particular [8] has been useful, which is an excellent, comprehensive yet comprehensible, review of modern cosmology, covering most concepts that we will need.

This chapter is outlined as follows. First we walk the reader through the application of general relativity to cosmology, introducing the metric in section 2.1 in order to obtain the dynamical equations of the universe in section 2.2. In section 2.3 we briefly review thermal physics in the context of cosmology, and in section 2.4 we deviate from standard cosmology via the introduction of an early MD epoch. Section 2.5 touches upon the field of cosmological perturbation theory. In the last section 2.6 inflation as a source of scalar perturbations is introduced.

2.1 Friedmann-Robertson-Walker-Lemaître Metric

A universe governed by the cosmological principle is, at least on large scales, spatially isotropic and homogeneous. Such a universe is described by a metric whose only

nontrivial attributes include scaling of 3-space with time and a global curvature. These features were neatly encoded by Friedmann, Robertson, Walker, and Lemaître, in a metric that takes the form (using units where $c = 1$)

$$\mathrm{d}s^2 = \mathrm{d}t^2 - a^2(t)\gamma_{ij}\,\mathrm{d}x^i\,\mathrm{d}x^j \tag{2.1}$$

where $a(t)$ is a function of time only, and γ_{ij} is a metric on the comoving 3-space,

$$\gamma_{ij} \equiv \delta_{ij} + k\frac{x_i x_j}{1 - k\,(x_k x^k)}, \quad \text{for} \quad k \equiv \begin{cases} 0 & \text{Euclidean} \\ +1 & \text{spherical} \\ -1 & \text{hyperbolic} \end{cases} \tag{2.2}$$

Since in polar coordinates (r, θ, ϕ)

$$\begin{aligned} \mathrm{d}\boldsymbol{x}^2 &= \mathrm{d}r^2 + r^2\left(\,\mathrm{d}\theta^2 + \sin^2\theta\mathrm{d}\phi^2\right) \\ \boldsymbol{x}\cdot\mathrm{d}\boldsymbol{x} &= r\,\mathrm{d}r, \end{aligned} \tag{2.3}$$

we may write

$$\boxed{\mathrm{d}s^2 = \mathrm{d}t^2 - a^2(t)\left[\frac{\mathrm{d}r^2}{1-kr^2} + r^2\,\mathrm{d}\Omega^2\right]} \tag{2.4}$$

where $\mathrm{d}\Omega^2 \equiv \mathrm{d}\theta^2 + \sin^2\theta\mathrm{d}\phi^2$ denotes the angular part. Defining

$$\mathrm{d}\chi \equiv \frac{\mathrm{d}r}{\sqrt{1-kr^2}}, \tag{2.5}$$

the metric is recast to a form in which the comoving radial component has no explicit k dependence,

$$\mathrm{d}s^2 = \mathrm{d}t^2 - a^2(t)\left[\mathrm{d}\chi^2 + S_k^2(\chi)\mathrm{d}\Omega^2\right], \tag{2.6}$$

where

$$S_k(\chi) \equiv \begin{cases} \sinh\chi & k = -1 \\ \chi & k = 0 \\ \sin\chi & k = +1 \end{cases}. \tag{2.7}$$

It is furthermore fruitful to divide the time component by $a(t)^2$ to factorize the full metric by $a(t)^2$. Introducing the conformal time,

$$\mathrm{d}\tau = \frac{\mathrm{d}t}{a(t)}, \tag{2.8}$$

we obtain

$$\mathrm{d}s^2 = a^2(\tau)\left[\mathrm{d}\tau^2 - \mathrm{d}\chi^2 + S_k^2(\chi)\mathrm{d}\Omega^2\right] \tag{2.9}$$

We immediately notice why the recasting to this form is useful: for photons, $\mathrm{d}s^2 = 0$. Thus, choosing our coordinates such that $\mathrm{d}\Omega^2 = 0$ it follows that for photons (or massless particles),

$$\Delta\tau = \Delta\chi. \tag{2.10}$$

Thus, in conformal time and independent of the curvature parameter k, our choice of radial coordinate χ means that the change in conformal time is precisely the traveled distance as measured by χ. This will facilitate a conceptual understanding of certain concepts later on in this thesis.

2.2 The Friedmann equations

To obtain a description of the dynamical behavior of the universe, we start with the Einstein field equation

$$G_{\mu\nu} = 8\pi G T_{\mu\nu} \tag{2.11}$$

where

$$G_{\mu\nu} = R_{\mu\nu} - \frac{1}{2}Rg_{\mu\nu} \tag{2.12}$$

is the Einstein tensor, $T_{\mu\nu}$ is the stress-energy tensor,

$$R_{\mu\nu} \equiv \partial_\lambda \Gamma^\lambda_{\mu\nu} - \partial_\nu \Gamma^\lambda_{\mu\lambda} + \Gamma^\lambda_{\lambda\rho}\Gamma^\rho_{\mu\nu} - \Gamma^\rho_{\mu\lambda}\Gamma^\lambda_{\nu\rho} \tag{2.13}$$

is the Ricci tensor where

$$\Gamma^\mu_{\nu\rho} = \frac{1}{2}g^{\mu\sigma}\left(\partial_\rho g_{\sigma\nu} + \partial_\nu g_{\sigma\rho} - \partial_\sigma g_{\nu\rho}\right) \tag{2.14}$$

are the Christoffel symbols, and

$$R = R^\mu_\mu = g^{\mu\nu}R_{\mu\nu}. \tag{2.15}$$

In order to proceed, we need the form of $T_{\mu\nu}$, which for a perfect fluid under the

imposed symmetries of the metric takes the simple form

$$T^{\mu}_{\nu} = g^{\mu\lambda}T_{\lambda\nu} = \begin{pmatrix} \rho & 0 & 0 & 0 \\ 0 & -P & 0 & 0 \\ 0 & 0 & -P & 0 \\ 0 & 0 & 0 & -P \end{pmatrix}. \tag{2.16}$$

Conservation laws for the stress-energy tensor then give rise to the continuity equation

$$\boxed{\dot{\rho} + 3\frac{\dot{a}}{a}(\rho + P) = 0}. \tag{2.17}$$

To obtain the dynamics of the universe, we compute the non-vanishing elements of the Ricci tensor, which are found to be

$$\begin{aligned} R_{00} &= -3\tfrac{\ddot{a}}{a} \\ R_{ij} &= -\left[\tfrac{\ddot{a}}{a} + 2\left(\tfrac{\dot{a}}{a}\right)^2 + 2\tfrac{k}{a^2}\right] g_{ij} \end{aligned} \tag{2.18}$$

yielding

$$R = -6\left[\frac{\ddot{a}}{a} + \left(\frac{\dot{a}}{a}\right)^2 + \frac{k}{a^2}\right] \tag{2.19}$$

and consequently

$$\begin{aligned} G^0_0 &= 3\left[\left(\frac{\dot{a}}{a}\right)^2 + \frac{k}{a^2}\right] \\ G^i_j &= \left[2\frac{\ddot{a}}{a} + \left(\frac{\dot{a}}{a}\right)^2 + \frac{k}{a^2}\right]\delta^i_j \end{aligned} \tag{2.20}$$

Combining these results, we get the Friedmann equations:

$$\boxed{H^2 \equiv \left(\frac{\dot{a}}{a}\right)^2 = \frac{8\pi G}{3}\rho - \frac{k}{a^2}} \tag{2.21}$$

$$\boxed{\frac{\ddot{a}}{a} = -\frac{4\pi G}{3}(\rho + 3P)}. \tag{2.22}$$

We will take the curvature to be zero, due to the observed flatness of the universe [3]. Introducing the reduced Planck mass $m_{\rm pl} = M_{\rm pl}/\sqrt{8\pi} = 1/\sqrt{8\pi G}$, these equations take

the simple form

$$\boxed{H^2 = \frac{1}{3m_{\text{pl}}^2}\rho} \tag{2.23}$$

$$\boxed{\frac{\ddot{a}}{a} = -\frac{1}{6m_{\text{pl}}^2}(\rho + 3P)}. \tag{2.24}$$

The Hubble parameter H describes the expansion rate of the universe.

The equation of state relating pressure to the density is

$$P = w\rho. \tag{2.25}$$

Radiation is the energy component of the universe characterized by $w = 1/3$, and matter the component for which $w = 0$.

Generally, substituting $P = w\rho$ in equation 2.17 and prescribing $\rho \propto a^{\gamma}$ yields

$$\rho \propto a^{-3(1+\omega)} \tag{2.26}$$

The density corresponding to a curvature-free universe is often called *critical*. At the present time, which we will denote (and sometimes leave implicit) with subscript 0, the critical density reads

$$\begin{aligned} \rho_c \equiv \rho_{\text{c},0} \equiv 3m_{\text{pl}}^2 H_0^2 = 3m_{\text{pl}}^2 h^2 100^2 \left(\frac{\text{km}}{\text{s}}/\text{Mpc}\right)^2 &= 1.88 \times 10^{-26} h^2 \text{ kg m}^{-3} \\ &= 1.05 \times 10^{-5} h^2 \text{ GeV cm}^{-3} \\ &= 8.15051 \times 10^{-47} h^2 \text{ GeV}^4 \\ &= 3.706 \times 10^{-47} \text{ GeV}^4 \end{aligned} \tag{2.27}$$

using $h = 0.674$ as defined in . With the notion of the critical density introduced, we proceed to define the fraction

$$\Omega_{i,0} \equiv \frac{\rho_{i,0}}{\rho_{\text{c},0}} \tag{2.28}$$

where i denotes a sub-component of the energy density characterized by w_i, such as matter or radiation. The total density fraction is defined as

$$\Omega = \sum_i \Omega_{i,0} \equiv \sum_i \frac{\rho_{i,0}}{\rho_{c,0}}, \tag{2.29}$$

and equals 1 in case of a flat universe. For a universe composed of radiation (r), matter (m), curvature (k), and a cosmological constant (Λ), equation 2.26, means we can rewrite the Friedmann 2.21 as

$$H^2(a) = H_0^2 \left[\Omega_{r,0} \left(\frac{a_0}{a} \right)^4 + \Omega_{m,0} \left(\frac{a_0}{a} \right)^3 + \Omega_{k,0} \left(\frac{a_0}{a} \right)^2 + \Omega_{\Lambda,0} \right] \tag{2.30}$$

where $\Omega_{k,0} \equiv -k/\left(a_0 H_0\right)^2$, $|\Omega_{k,0}| \leq 0.01$, $\Omega_r = 9.4 \times 10^{-5}$, $\Omega_{m,0} = 0.32$, $\Omega_{\Lambda,0} = 0.68$. $\Omega_{m,0}$ has contributions both from baryons and (cold) DM, which contribute $\Omega_{\text{DM}} = 0.264$ [3]. Throughout this work, we will neglect curvature, i.e. we set $\Omega_k = 0$.

It is easy to estimate when the various components began to dominate over one another, or rather the time instances when they contributed equally. Equating $\Omega_\Lambda a^{-0} = \Omega_m a^{-3}$ leads to $a_{\Lambda m} \equiv \left(\frac{\Omega_m}{\Omega_\Lambda}\right)^{1/3} \approx 0.8$. Thus, Λ began dominating the universe only very recently at a scale factor of $a_{\Lambda m} = 0.8 \sim 1$. We will thus neglect Λ domination and assume MD until present time. Similarly, for matter and radiation, we compute $\Omega_r a^{-4} = \Omega_m a^{-3}$, leading to $a_{\text{eq}} \equiv \left(\frac{\Omega_r}{\Omega_m}\right) = 3 \times 10^{-4}$, corresponding to a redshift $z \approx 3400$.

For a flat universe dominated by a single component, equation 2.23 takes the form

$$\frac{\dot{a}}{a} = H_0 \sqrt{\Omega_{i,0}} a^{-\frac{3}{2}(1+\omega_i)}. \tag{2.31}$$

This equation is separable and has the solution

$$a(t) \propto \begin{cases} t^{\frac{2}{3(1+w_i)}} & w_i \neq -1 \\ e^{Ht} & w_i = -1 \end{cases} \tag{2.32}$$

Differentiating with respect to t for the case $\omega \neq -1$, the Hubble parameter obeys

$$H = \frac{\dot{a}}{a} = \frac{2}{3}\left(1 + \omega_i\right)\frac{1}{t} \propto a^{-\frac{3}{2}(1+\omega_i)} \tag{2.33}$$

These results are summarized in table 2.2.1, where the relations are presented for generic equation-of-state parameter w_i, and for matter and radiation explicitly. From this section, table 2.2.1 is most of what we need.

Throughout this work (and everywhere else), the scale factor is normalized to unity at present, $a_0 = 1$. We will often encounter expressions including only a factor $a(t)$. However, since the scale factor alone is not a physical quantity, rather merely a relative

Table 2.2.1: Important cosmological relations for single component universes. In section 2.3, we will see how the relations for RD are modified by the number of degrees of freedom.

	ωD	MD	RD	ΛD
ω	$= \omega$	$= 0$	$= 1/3$	$= -1$
ρ	$\propto a^{-3(1+\omega)}$	$\propto a^{-3}$	$\propto a^{-4}$	const.
a	$\propto t^{\frac{2}{3(1+w)}}$	$\propto t^{2/3}$	$\propto t^{1/2}$	$\propto e^{Ht}$
H	$\propto a^{-\frac{3}{2}(1+\omega)}$	$\propto a^{-\frac{3}{2}}$	$\propto a^{-2}$	const.

scaling, $a(t)$ in isolation must always be read as $a(t)/a_0$.

Of crucial importance in this work is the result that matter and radiation evolve as a^{-3} and a^{-4} respectively. PBHs evolve like matter. Thus, for an expanding universe, a fraction of PBHs that was initially small is enhanced relative to radiation during the era of RD, which is conventionally assumed to constitute the time after inflation until EQ. In this thesis, we will instead assume this era to constitute the time between the end of an early period of MD, until EQ. As a consequence, we have $(\rho_{\text{PBH}}/\rho_{\text{tot}})_{\text{now}} = (a_{\text{eq}}/a_{\text{reh}})\,(\rho_{\text{PBH}}/\rho_{\text{tot}})_{\text{reh}}$. Thus, the relative density of PBHs will increase during RD, but only from the end of early MD, in contrast to that for PBH formation during RD. This relative enhancement is crucial: an initially negligible PBH abundance may grow relative to radiation to be significant at late times.

Before proceeding, we take the opportunity to introduce the redshift z, defined as the relative difference in wavelengths between those at observation and emission,

$$z \equiv \frac{\lambda_{\text{obs}} - \lambda_{\text{em}}}{\lambda_{\text{em}}}. \tag{2.34}$$

Relating this to the scale factor, one finds

$$1 + z = \frac{1}{a\,(t_{\text{em}})} \tag{2.35}$$

2.3 The Thermal Universe

2.3.1 Thermal equilibrium

For a particle with g internal degrees of freedom, its density of states in phase space is $\frac{g}{(2\pi)^3}$ (in natural units where $\hbar = 1$). The likelihood of these states being occupied is described by a phase-space distribution function $f(\boldsymbol{x}, \boldsymbol{p}, t) = f(p)$, where we dropped

the space-dependence due to homogeneity of the universe, changed $\boldsymbol{p} \to p = |p|$ due to isotropy, and left the time-dependence implicit. We can now express the number density of particles as

$$n = \frac{g}{(2\pi)^3} \int \mathrm{d}^3 p f(p). \tag{2.36}$$

where we integrate over momentum space to obtain only the spatial density. For the dispersion relation $E = \sqrt{m^2 + p^2}$, the energy density is obtained by multiplying the integrand with $E(p)$ as

$$\rho = \frac{g}{(2\pi)^3} \int \mathrm{d}^3 p f(p) E(p). \tag{2.37}$$

Under the assumption that the particles exchange momentum and energy efficiently, kinetic equilibrium is reached and the distribution function takes the form

$$f(p) = \frac{1}{e^{(E(p)-\mu)/T \pm 1}} \tag{2.38}$$

where + gives the Fermi-Dirac distribution function for fermions and - the Bose-Einstein distribution function for bosons. We will neglect the chemical potential μ throughout this work.

Going to spherical coordinates and performing the angular part of the integrals 2.36,2.37, they become

$$n = \frac{g}{2\pi^2} \int_0^\infty \mathrm{d}p \frac{p^2}{\exp\left[\sqrt{p^2 + m^2}/T\right] \pm 1} \tag{2.39}$$

$$\rho = \frac{g}{2\pi^2} \int_0^\infty \mathrm{d}p \frac{p^2 \sqrt{p^2 + m^2}}{\exp\left[\sqrt{p^2 + m^2}/T\right] \pm 1} \tag{2.40}$$

For us, only relativistic and non-relativistic limits are of interest. We will only quote the results of performing the above integrals:

In the relativistic limit ($T >> m$), one obtains

$$\boxed{n = \frac{\zeta(3)}{\pi^2} g T^3 \begin{cases} 1 & \text{bosons} \\ \frac{3}{4} & \text{fermions} \end{cases}} \tag{2.41}$$

$$\boxed{\rho = \frac{\pi^2}{30} g T^4 \begin{cases} 1 & \text{bosons} \\ \frac{7}{8} & \text{fermions} \end{cases}} \tag{2.42}$$

where $\zeta(3) \approx 1.202$

In the non-relativistic limit ($T << m$), one obtains

$$\boxed{n = g\left(\frac{mT}{2\pi}\right)^{3/2} e^{-m/T}} \tag{2.43}$$

$$\boxed{\rho = mn + \frac{3}{2}nT \approx mn} \tag{2.44}$$

In the non-relativistic limit, we have two energy scales: the mass m, and the temperature T, both of which show up in 2.43. Number densities are suppressed by the exponential factor in this case. Furthermore, 2.44 makes it clear that the energy density is dominated by the particle masses.

With these results at hand, applicable to single particle species, we proceed to obtain equivalent expressions for the typical case involving multiple particles in which no single species dominates. We will take the temperature T to be that of photons.

Intuitively, the energy density of radiation is the sum of the contributing species

$$\boxed{\rho_{\mathrm{r}} = \sum_i \rho_i \equiv \frac{\pi^2}{30} g_\star(T) T^4}. \tag{2.45}$$

where we introduced $g_\star(T)$ to capture the *effective* number of degrees of freedom, which receives contributions from species in thermal equilibrium with the photons, $T_i = T$, and from decoupled species, $T_i \neq T$, such that $g_\star(T) = g_\star^{\mathrm{th}}(T) + g_\star^{\mathrm{dec}}(T)$ where

$$g_\star^{\mathrm{th}}(T) = \sum_{i \in \text{Bosons}} g_i + \frac{7}{8} \sum_{i \in \text{Fermions}} g_i \tag{2.46}$$

$$g_\star^{\mathrm{dec}}(T) = \sum_{i \in \text{Bosons}} g_i \left(\frac{T_i}{T}\right)^4 + \frac{7}{8} \sum_{i \in \text{Fermions}} g_i \left(\frac{T_i}{T}\right)^4 \tag{2.47}$$

Note that these sums should count only those particles that are relativistic, namely, those for which $T_i >> m_i$. We will use tabulated values for $g_\star(T)$ as presented in [8]. The values that we use are found, together with the related parameter $g_{\star s}(T)$, in figure 2.3.1.

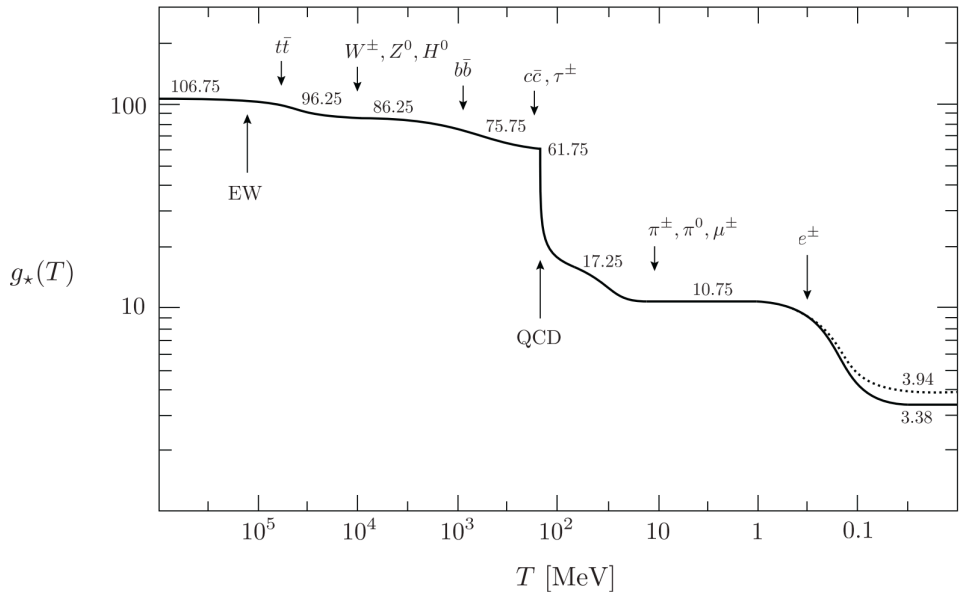

Figure 2.3.1: Relativistic effective (entropy) degrees of freedom (g_{*s}) g_* as function of temperature [8].

2.3.2 Entropy

Of tremendous importance is the second law of thermodynamics, which states that the incremental transport of heat, which always occurs from warmer to colder objects, is merely a manifestation of an incremental increase of entropy (weighted by temperature). In other words,

$$dS = \delta Q/T. \tag{2.48}$$

For an adiabatic system, this is clearly zero. If we could show that each and every volume of the universe behaves as such, entropy would be conserved. We will make this assumption. What this means physically is that to a good approximation the universe is assumed to be in equilibrium (or at least such that out-of-equilibrium processes are negligible), and this is the assumption that is typically made.

Rather than considering the entropy S, it makes more sense to consider the local quantity $s \equiv S/V$, namely the entropy density, which is computed as

$$s = \frac{\rho + P}{T}. \tag{2.49}$$

Using 2.42 and $P = \frac{1}{3}\rho$ for radiation, we find that

$$\boxed{s = \sum_i \frac{\rho_i + P_i}{T_i} \equiv \frac{2\pi^2}{45} g_{\star s}(T) T^3} \tag{2.50}$$

where

$$g_{\star s}(T) = g_{\star s}^{th}(T) + g_{\star s}^{\text{dec}}(T) \tag{2.51}$$

is the effective number of relativistic entropy degrees of freedom, in complete analogy to $g_\star$. Because of the T_i^3 rather than T_i^4 scaling, $g_\star = g_{\star s}$ only when all relativistic spices are in equilibrium. Note that the contribution to s from non-relativistic species is negligible. $g_{\star s}$ is plotted with $g_\star$ in figure 2.3.1. We see that for $T \lesssim 0.1$ MeV, to a good approximation $g_\star \approx g_{\star s}$. For lower temperatures, they differ by a factor of 1.17. This difference is negligible in the present context as other factors introduce greater uncertainties, and we will always use $g_{\star s} = g_\star$.

Multiplying s by a^3, one obtains the comoving entropy density, which is conserved. If the comoving number density $n_i a^3$ is constant, the ratio $Y \equiv n/s$ is conserved. This is an important quantity typically called the *yield*, which we will use later to discuss constraints on PBHs.

Conservation of entropy also allows us to relate the scale factor a to the temperature. This is because $sa^3 \propto g_{\star s} a^3 T^3 = const.$, which implies

$$\boxed{T \propto g_{\star s}^{-1/3} a^{-1}}, \tag{2.52}$$

but $\rho_{\text{r}} \propto g_\star T^4$. Thus, rather than $\rho_r \propto a^{-4}$, a more accurate statement is

$$\boxed{\rho_r \propto g_\star^{-1/3} a^{-4}}, \tag{2.53}$$

which is what we will use.

The temperature as a function of time may be obtained if one additionally assumes RD, equivalent to that $T \propto t^{-1/2}$. In this case, one finds after integration of the Friedmann equation that

$$\frac{T}{1\,\text{MeV}} \simeq 1.5 g_\star(T)^{-1/4} \left(\frac{1\,\text{s}}{t}\right)^{1/2}. \tag{2.54}$$

2.4 Early Matter Domination

A non-standard cosmology can be constructed by the introduction of some heavy particle ϕ that came to dominate the universe at some early time. Despite the possibility that ϕ formed in only small numbers, such that initially it was sub-dominant, scaling as

a^{-3} rather than a^{-4} (neglecting changes in g_*) for radiation, means that it will eventually dominate, provided it is sufficiently long-lived. As a result, the universe would deviate from the standard RD scenario due to the induced epoch of early MD. An early epoch of MD could also be the result of a rapidly oscillating field, such as the inflaton field during reheating. Independent of the cause of a period of early MD, it has immense consequences for the formation probability of PBHs, as we will see in chapter 3.

Suppose that ϕ decays with a decay rate given by Γ_ϕ. For as long as the decay rate $\Gamma_\phi \ll H$, ϕ may dominate. As soon as $\Gamma_\phi \approx H$, however, the decay rate is similar to the universal expansion rate leading to a transfer of the entropy to the decay products, which by assumption, belong to the standard model (SM). This leads to a transition to RD, which occurs at some temperature $T_{\rm reh}$, defined by $\Gamma_\phi = H\left(T = T_{\rm reh}\right)$, such that

$$\Gamma_\phi^2 = H\left(T_{\rm reh}\right)^2 = \frac{4\pi^3}{45} g_*^{\rm reh} \frac{T_{\rm reh}^4}{M_{\rm pl}^2}, \tag{2.55}$$

i.e.

$$\boxed{\Gamma_\phi = \sqrt{\frac{4\pi^3}{45} g_*^{\rm reh}} \frac{T_{\rm reh}^2}{M_{\rm pl}}, \text{ or inverted, } T_{\rm reh} = \left(\frac{45}{4\pi^3 g_*^{\rm reh}}\right)^{1/4} \sqrt{\Gamma_\phi M_{\rm pl}}} \tag{2.56}$$

where we assumed an abrupt transition to RD. Equation 2.56 is a useful relation between the reheating temperature and the decay rate of ϕ which we will apply later to our derivation of the PBH mass function.

Throughout this work, we will parameterize our MD epoch by the reheating temperature $T_{\rm reh}$ and its duration, which we express as the ratio of scale factors $\mathcal{A} \equiv a_{\rm reh}/a_{\rm md}$, $a_{\rm reh}$ being the scale factor at reheating and $a_{\rm md}$ at the onset of MD.

2.5 Cosmological Perturbation Theory

The purpose of this section is to examine the description, origin, and evolution of density perturbations in the universe, and to understand how these perturbations could contribute to the formation of PBHs. A rigorous treatment involves the application of general relativity, but since many important results and a qualitative understanding can be obtained assuming only Newtonian gravity, we will rely heavily on this description. In section 2.5.3 we will discuss the most important results from a full relativistic treatment.

2.5.1 Quantifying perturbations

Suppose with have a perturbation $Q(x)$. By construction, the expectation value $\langle Q(\boldsymbol{x})\rangle = 0$ so we need the two-point correlation function $\langle Q(\boldsymbol{x})Q(\boldsymbol{y})\rangle$ to extract statistical information. Fourier transforming the perturbations and using that Q is real, so that $\delta_{\boldsymbol{k}} = \delta^*_{-\boldsymbol{k}}$,

$$\langle Q(\boldsymbol{x})Q(\boldsymbol{y})\rangle = \int \frac{\mathrm{d}^3k}{(2\pi)^3}\frac{\mathrm{d}^3k'}{(2\pi)^3} e^{i\boldsymbol{k}\cdot\boldsymbol{x}} e^{-i\boldsymbol{k}'\cdot\boldsymbol{y}} \langle Q_{\boldsymbol{k}} Q^*_{\boldsymbol{k}'}\rangle \,. \tag{2.57}$$

Homogeneity demands that $\langle Q(\boldsymbol{x})Q(\boldsymbol{y})\rangle$ is a function of $|\boldsymbol{x}-\boldsymbol{y}|$, which is obtained if we impose

$$\langle Q_{\boldsymbol{k}} Q^*_{\boldsymbol{k}'}\rangle \equiv (2\pi)^3 F(\boldsymbol{k})\delta\left(\boldsymbol{k}-\boldsymbol{k}'\right). \tag{2.58}$$

Using this, and requiring that the universe is isotropic, namely, that $F(\boldsymbol{k}) = F(|\boldsymbol{k}|) = F(k)$, we obtain

$$\langle Q(\boldsymbol{x})Q(\boldsymbol{y})\rangle = \int \frac{\mathrm{d}^3k}{(2\pi)^3} e^{i\boldsymbol{k}\cdot(\boldsymbol{x}-\boldsymbol{y})} F(k). \tag{2.59}$$

Note that in this description $F(k)$ is nothing but the Fourier transform of the two-point correlation function $\langle Q(\boldsymbol{x})Q(\boldsymbol{y})\rangle$. Thus, if we set $\boldsymbol{x} = \boldsymbol{y}$, we obtain the variance

$$\sigma_Q^2 \equiv \langle Q(\boldsymbol{x})Q(\boldsymbol{x})\rangle = \int \frac{\mathrm{d}^3k}{(2\pi)^3} F(k) = \frac{1}{2\pi^2}\int_0^\infty k^3 F(k)\mathrm{d}\ln k. \tag{2.60}$$

But we can formally express

$$F(k) = \frac{\langle Q_{\boldsymbol{k}} Q^*_{\boldsymbol{k}}\rangle}{(2\pi)^3\delta\left(\boldsymbol{k}-\boldsymbol{k}\right)} = \frac{\langle Q_{\boldsymbol{k}} Q^*_{\boldsymbol{k}}\rangle}{(2\pi)^3\delta(0)} = \frac{\langle |Q_{\boldsymbol{k}}|^2\rangle}{V}, \tag{2.61}$$

where we obtain the volume of 3-space,

$$\delta(0) = \int \frac{\mathrm{d}^3x}{(2\pi)^3} e^{-ix\cdot(\boldsymbol{k}-\boldsymbol{k})} \equiv \frac{V}{(2\pi)^3} \tag{2.62}$$

to obtain

$$\sigma_Q^2 = \left\langle Q(\boldsymbol{x})^2\right\rangle = \frac{1}{2\pi^2}\int_0^\infty \mathrm{d}\ln k \frac{1}{V}\left\langle \left|Q_\parallel\right|^2\right\rangle k^3. \tag{2.63}$$

This leads us to define the dimensionless power spectrum for the perturbations $Q(x)$ as

$$\mathcal{P}_Q(k) \equiv \frac{k^3}{2\pi^2 V}\left\langle |Q_{\boldsymbol{k}}|^2\right\rangle, \tag{2.64}$$

and the variance

$$\sigma_Q^2 = \int_0^\infty \mathrm{d}\ln \mathrm{k} \mathcal{P}_\mathrm{Q}(\mathrm{k}), \tag{2.65}$$

which does not depend on scale. We note that this result agree with [10]. However, we will be interested in the size of the perturbations at a specific scale k, which will often be $k = aH$, i.e. horizon crossing. In this case, the variance of perturbations at k is

$$\sigma_Q^2(k) = \mathcal{P}_Q(k). \tag{2.66}$$

I refer the reader to [57] for a discussion on this result in case of density perturbations.

2.5.2 Newtonian approximation

A Newtonian treatment of of cosmological perturbation theory is valid for non-relativistic matter within the Hubble horizon. We will model the universe as a fluid of mass density ρ, pressure $P \ll \rho$ and velocity $\boldsymbol{u}$. Imposing mass conservation, we know that any change of mass contained within an infinitesimal volume must be accompanied by a non-zero flux through the enclosing surface area of this volume, or in other words,

$$\partial_t \rho = -\boldsymbol{\nabla}_{\boldsymbol{r}} \cdot (\rho \boldsymbol{u}), \tag{2.67}$$

which is the continuity equation (t denoting time and $\boldsymbol{\nabla}_{\boldsymbol{r}}$ being the spatial gradient operator for position coordinates $\boldsymbol{r}$). Newton's second law of motion formulated for a coflowing fluid volume-element leads to the Euler equation,

$$\left(\partial_t + \boldsymbol{u} \cdot \boldsymbol{\nabla}_{\boldsymbol{r}}\right) \boldsymbol{u} = -\frac{\boldsymbol{\nabla}_{\boldsymbol{r}} P}{\rho} - \boldsymbol{\nabla}_{\boldsymbol{r}} \Phi, \tag{2.68}$$

where we $(\partial_t + \boldsymbol{u} \cdot \boldsymbol{\nabla}_{\boldsymbol{r}})$ is the *convective* derivative, accounting for that the total change of a quantity is given by the change at a point $\boldsymbol{r}$ and the change in that quantity associated with the fluid motion. The gravitational potential Φ is sourced by the fluid itself and obeys the Poisson equation

$$\nabla_{\boldsymbol{r}}^2 \Phi = 4\pi G \rho = \frac{\rho}{2m_{\mathrm{pl}}^2}. \tag{2.69}$$

These equations are our starting point.

We will pursue a perturbative treatment, and thus express quantities as a background component, i.e. the global average, marked by an overline, plus a perturbation, preceded by δ, i.e.,

$$\begin{aligned}\rho(t,\boldsymbol{r}) &= \bar{\rho}(t) + \delta\rho(t,\boldsymbol{r}) \\ P(t,\boldsymbol{r}) &= \bar{P}(t) + \delta P(t,\boldsymbol{r}) \\ \boldsymbol{u}(t,\boldsymbol{r}) &= \boldsymbol{u}(t) + \delta\boldsymbol{u}(t,\boldsymbol{r}) \\ \Phi(t,\boldsymbol{r}) &= \bar{\Phi}(t) + \delta\Phi(t,\boldsymbol{r}).\end{aligned} \tag{2.70}$$

Note that the cosmological principle demands spatial homogeneity (and isotropy) for the background, rendering the background parts dependent only on time t. We will furthermore consider only terms linear in the perturbed quantities, neglecting terms of $\mathcal{O}(\delta^2)$ or larger order. In this representation, the continuity and Euler equations respectively take the form

$$\begin{aligned}\partial_t\bar{\rho} &= -\boldsymbol{\nabla}_{\boldsymbol{r}}\cdot(\bar{\rho}\bar{\boldsymbol{u}}) \\ \bar{\rho}\left(\partial_t + \bar{\boldsymbol{u}}\cdot\boldsymbol{\nabla}_{\boldsymbol{r}}\right)\bar{\boldsymbol{u}} &= -\boldsymbol{\nabla}_{\boldsymbol{r}}\bar{P} - \bar{\rho}\boldsymbol{\nabla}_{\boldsymbol{r}}\bar{\Phi}\end{aligned} \tag{2.71}$$

for the background contributions, and

$$\begin{aligned}&\partial_t\delta\rho = -\boldsymbol{\nabla}_{\boldsymbol{r}}\cdot(\delta\rho\bar{\boldsymbol{u}} + \bar{\rho}\delta\boldsymbol{u}) \\ &\bar{\rho}\left[\left(\partial_t + \bar{\boldsymbol{u}}\cdot\boldsymbol{\nabla}_{\boldsymbol{r}}\right)\delta\boldsymbol{u} + \left(\delta\boldsymbol{u}\cdot\boldsymbol{\nabla}_{\boldsymbol{r}}\right)\bar{\boldsymbol{u}}\right] + \delta\rho\left(\partial_t + \bar{\boldsymbol{u}}\cdot\nabla_r\right)\bar{\boldsymbol{u}} = -\boldsymbol{\nabla}_{\boldsymbol{r}}\delta P - \bar{\rho}\boldsymbol{\nabla}_{\boldsymbol{r}}\delta\Phi - \delta\rho\boldsymbol{\nabla}_{\boldsymbol{r}}\bar{\Phi}\end{aligned} \tag{2.72}$$

for the perturbations at linear order.

In an expanding universe, the physical coordinate $\boldsymbol{r}$ is related to the comoving coordinate $\boldsymbol{x}$ by

$$\boldsymbol{r}(t) = a(t)\boldsymbol{x} \tag{2.73}$$

which upon taking the time derivative yields

$$\boldsymbol{u} = \dot{\boldsymbol{r}} = H\boldsymbol{r} + \boldsymbol{v}. \tag{2.74}$$

Note how the velocity splits into two parts: $H\boldsymbol{r}$ due to the universal expansion, and $\boldsymbol{v} \equiv a(t)\dot{\boldsymbol{x}}$, a perturbation to the uniform expansion relative the comoving coordinate $\boldsymbol{x}$, often referred to as *proper motion*. We will phrase all our expressions in comoving coordinates $\boldsymbol{x}$. Our starting point is still 2.67, 2.68, and 2.69, but we will rewrite them in a form more enlightening for an expanding universe. The gradient operator in

physical coordinates relates to the gradient operator in comoving space as

$$\boldsymbol{\nabla}_{\boldsymbol{r}} = a(t)^{-1}\boldsymbol{\nabla}_{\boldsymbol{x}}. \tag{2.75}$$

The notion of a time derivative is also somewhat ambiguous since we must specify whether we hold $\boldsymbol{r}$ or $\boldsymbol{x}$ constant. Choosing to work in comoving coordinates, we find, analogous to the introduction of the convective derivative, that

$$\left(\frac{\partial}{\partial t}\right)_{\boldsymbol{x}} = \left(\frac{\partial}{\partial t}\right)_{\boldsymbol{r}} + H\boldsymbol{r}\cdot\boldsymbol{\nabla}_{\boldsymbol{r}} = \left(\frac{\partial}{\partial t}\right)_{\boldsymbol{r}} + H\boldsymbol{x}\cdot\boldsymbol{\nabla}_{\boldsymbol{x}}, \tag{2.76}$$

i.e. we can express the change at constant $\boldsymbol{r}$ in terms of comoving coordinates as

$$\left(\frac{\partial}{\partial t}\right)_{\boldsymbol{r}} = \left(\frac{\partial}{\partial t}\right)_{\boldsymbol{x}} - H\boldsymbol{x}\cdot\boldsymbol{\nabla}_{\boldsymbol{x}}. \tag{2.77}$$

Rather than describing density perturbations by $\delta\rho(t,\boldsymbol{r})$, we introduce the density contrast,

$$\delta \equiv \frac{\rho-\bar{\rho}}{\bar{\rho}} = \frac{\delta\rho}{\bar{\rho}} \tag{2.78}$$

which specifies the relative size of an overdensity.

We can now re-express the continuity, Euler, and Poisson equations in comoving coordinates and our choice of perturbations. The continuity equation takes the form

$$\left[\frac{\partial}{\partial t} - H\boldsymbol{x}\cdot\boldsymbol{\nabla}\right][\bar{\rho}(1+\delta)] + \frac{1}{a}\boldsymbol{\nabla}\cdot[\bar{\rho}(1+\delta)(Ha\boldsymbol{x}+\boldsymbol{v})] = 0. \tag{2.79}$$

Some algebraic manipulations quickly yield the equation,

$$\left(\frac{\partial\bar{\rho}}{\partial t}\right)_{\boldsymbol{x}} + 3H\bar{\rho} = 0 \tag{2.80}$$

for the spatially homogeneous background, and, using 2.80

$$\left(\frac{\partial\delta}{\partial t}\right)_{\boldsymbol{x}} = -\frac{1}{a}\boldsymbol{\nabla}_{\boldsymbol{x}}\cdot\boldsymbol{v} \tag{2.81}$$

for the perturbations at linear order.

The Euler equation takes the form

$$\bar{\rho}(1+\delta)\left[\left(\frac{\partial}{\partial t}\right)_{\boldsymbol{x}} + \frac{1}{a}\boldsymbol{v}\cdot\boldsymbol{\nabla}_{\boldsymbol{x}}\right](Ha\boldsymbol{x}+\boldsymbol{v}) = -\frac{1}{a}\left[\boldsymbol{\nabla}_{\boldsymbol{x}}P + \bar{\rho}(1+\delta)\boldsymbol{\nabla}_{\boldsymbol{x}}\Phi\right]. \tag{2.82}$$

Using, once again, the spatial homogeneity of the background, one finds

$$\bar{\rho}\left(\frac{\partial}{\partial t}Ha\boldsymbol{x}\right)_{\boldsymbol{x}}=0 \tag{2.83}$$

at zeroth order in the perturbations, which leads to

$$\left(\frac{\partial \boldsymbol{v}}{\partial t}\right)_{\boldsymbol{x}}+H\boldsymbol{v}=-\frac{1}{a}\left[\frac{\boldsymbol{\nabla}_{\boldsymbol{x}}\delta P}{\bar{\rho}}+\boldsymbol{\nabla}_{\boldsymbol{x}}\delta\Phi\right] \tag{2.84}$$

for the perturbations at linear order.

The Poisson equation, rather trivially, becomes

$$\boldsymbol{\nabla}^2_{\boldsymbol{x}}\delta\Phi=4\pi G a^2\bar{\rho}\delta. \tag{2.85}$$

To summarize, at linear order in the perturbations, the Continuity, Euler, and Poisson equations respectively read,

$$\begin{aligned}&\left(\tfrac{\partial\delta}{\partial t}\right)_{\boldsymbol{x}}=-\tfrac{1}{a}\boldsymbol{\nabla}_{\boldsymbol{x}}\cdot\boldsymbol{v}\\&\left(\tfrac{\partial\boldsymbol{v}}{\partial t}\right)_{\boldsymbol{x}}+H\boldsymbol{v}=-\tfrac{1}{a}\left[\tfrac{\boldsymbol{\nabla}_{\boldsymbol{x}}\delta P}{\bar{\rho}}+\boldsymbol{\nabla}_{\boldsymbol{x}}\delta\Phi\right]\\&\boldsymbol{\nabla}^2_{\boldsymbol{x}}\delta\Phi=4\pi G a^2\bar{\rho}\delta\end{aligned} \tag{2.86}$$

To simplify notation, we will use $\dot{X}\equiv\left(\frac{\partial X}{\partial t}\right)_{\boldsymbol{x}}$ to denote the time derivatives. Taking the time derivative of the first equation in 2.86 yields

$$\ddot{\delta}=-\frac{1}{a}\boldsymbol{\nabla}_{\boldsymbol{x}}\cdot\dot{\boldsymbol{v}}-H\delta. \tag{2.87}$$

Applying $\boldsymbol{\nabla}_{\boldsymbol{x}}$ to the second equation in 2.86 and using the third equation in 2.86 yield after some algebra (using $\delta P=w\delta\rho$)

$$\ddot{\delta}+2H\dot{\delta}-\frac{c_s^2}{a^2}\boldsymbol{\nabla}^2_{\boldsymbol{x}}\delta=4\pi G\bar{\rho}\delta, \tag{2.88}$$

where we introduced the speed of sound $c_s^2\equiv w$. This is our final equation describing the dynamics of the density contrast δ. Of particular importance is the effect of MD and RD on evolution of the density contrast. For MD we set $c_{\mathrm{s}}^2=w\equiv 0$, so that 2.88 takes the form

$$\ddot{\delta}_{\mathrm{md}}+2H\dot{\delta}_{\mathrm{md}}=4\pi G\bar{\rho}\delta_{\mathrm{md}}=\frac{3}{2}H^2\delta_{\mathrm{md}}. \tag{2.89}$$

For MD, table 2.2.1 gives $H = 2/3t$, which means that 2.89 becomes

$$\ddot{\delta}_{\text{md}} + \frac{4}{3t}\dot{\delta}_{\text{md}} = \frac{2}{3t^2}\delta_{\text{md}} \tag{2.90}$$

with the following two solutions:

$$\delta_{\text{md}} \propto \begin{cases} t^{-1} \propto a^{-3/2} \\ t^{2/3} \propto a \end{cases} \tag{2.91}$$

The implication is the following during MD, there are two behaviours; one for which matter density perturbations grow linearly with the scale factor; one where the matter density perturbations decay as $a^{-3/2}$, which we will disregard since they quickly disappear.

For radiation domination, we quote the following result from [8],

$$\delta_{\text{rd}} \propto \begin{cases} \text{const.} \\ \ln t \propto \ln a \end{cases}, \tag{2.92}$$

where δ_{rd} refers to the matter density perturbations in a RD universe. This means that during RD, matter overdensities grown only logarithmically with the scale factor. Perturbations in the radiation density oscillate within the Horizon due to radiation pressure, time-averaging out to zero. Because of this, only matter density perturbations contribute to the growth of structure.

In front of us we have the most important result of this section, and the reason for its inclusion in this thesis: During MD, matter overdensities grow linearly with the scale factor, whereas during RD, they hardly grow at all. As we will see, this conclusion has a tremendous impact on the formation of PBHs, as it takes that the universe is MD for the growth of overdensities to be significant.

It is useful to define the comoving wavenumber $\boldsymbol{k}$ such that we can Fourier decompose

$$\delta(t, \boldsymbol{x}) = \int \frac{\mathrm{d}^3 k}{(2\pi)^3} e^{i\boldsymbol{k}\cdot\boldsymbol{x}} \delta_{\boldsymbol{k}}(t), \tag{2.93}$$

and similarly for the other perturbations. Then, the Poisson equation in 2.86 can be written

$$-k^2 \delta\Phi_{\boldsymbol{k}}(t) = \frac{3a^2H^2}{2}\delta_{\boldsymbol{k}}(t) \tag{2.94}$$

where we used the Friedmann equation to write $\bar{\rho} = (3/8\pi G)\, H^2$. In section 2.6 about inflation, we will see how density perturbation will both exit and enter the comoving Hubble horizon $(aH)^{-1}$. Since a full general relativistic treatment of perturbation theory, for which we refer the reader to [8] and section 2.5.3, leads to the prediction that density perturbations remain constant outside of the Horizon and only starts growing $\propto a$ once they re-enter the horizon, we evaluate 2.94 at Horizon crossing $k = aH$, which results in

$$-\delta\Phi_{\boldsymbol{k}_*} = \frac{3}{2}\delta_{\boldsymbol{k}_*}, \tag{2.95}$$

where $*$ signifies that it should be evaluated at horizon crossing. In other words, at horizon crossing, the density and gravitational potential perturbations differ only by a constant factor independent of scale.

2.5.3 Results from relativistic perturbation theory

Beautiful as it is, a comprehensive and rigorous treatment of relativistic perturbation theory is lengthy and beyond the scope of this work. We will focus on certain aspects and highlight the most important results. For details on the presented results and the derivations, I refer the reader to [8].

In Newtonian gauge and neglecting anisotropic stress, the metric takes the form

$$\mathrm{d}s^2 = -(1+2\Phi)\mathrm{d}t^2 + a(t)^2(1-2\Phi)\mathrm{d}x^2. \tag{2.96}$$

The benefit of Newtonian gauge is that Φ is the gravitational potential in Newtonian gravity for non-relativistic matter on within the horizon. In this case, the potential obeys the Poison equation $\boldsymbol{\nabla}^2_{\boldsymbol{x}}\delta\Phi = 4\pi G a^2 \bar{\rho}\delta$. Defining the comoving Hubble parameter $\mathcal{H} = \frac{1}{a}\frac{da}{d\tau} = aH$, one finds that the Einstein equations take the form

$$\begin{aligned} \nabla^2\Phi - 3\mathcal{H}\left(\Phi' + \mathcal{H}\Phi\right) &= 4\pi G a^2 \delta\rho \\ \Phi' + \mathcal{H}\Phi &= -4\pi G a^2(\bar{\rho} + \bar{P})v \\ \Phi'' + 3\mathcal{H}\Phi' + \left(2\mathcal{H}' + \mathcal{H}^2\right)\Phi &= 4\pi G a^2 \delta P \end{aligned} \tag{2.97}$$

where $'$ denotes derivative with respect to conformal time τ. The *curvature*

perturbation is defined as

$$\mathcal{R} \equiv -\Phi - \frac{\mathcal{H}\left(\Phi' + \mathcal{H}\Phi\right)}{4\pi G a^2(\bar{\rho} + \bar{P})} \tag{2.98}$$

and is important because one can show that it remains constant on super-horizon scales $k << aH = \mathcal{H}$ for adiabatic fluctuations, and predictions from inflation may be succinctly expressed as a power spectrum of perturbations on $\mathcal{R}$.

Using $\frac{3}{2}\mathcal{H}^2 = 4\pi G a^2 \bar{\rho}$ and the equation of state $P = w\rho$, 2.98 becomes

$$\mathcal{R} = -\Phi - \frac{2}{3(1+w)}\left(\frac{\Phi'}{\mathcal{H}} + \Phi\right), \tag{2.99}$$

which, together with the Einstein equations 2.97, lead to the following equation describing the dynamics of the gravitational potential Φ:

$$\Phi'' + 3(1+w)\mathcal{H}\Phi' + wk^2\Phi = 0. \tag{2.100}$$

On super-horizon scales, $k << \mathcal{H}$, in which case we can neglect the third term in 2.100, to obtain the approximate equation

$$\Phi'' + 3(1+w)\mathcal{H}\Phi' = 0, \tag{2.101}$$

whose trivial solution is $\Phi = const.$, and another decaying solution which we neglect. Here, $\delta\rho$ is the total density perturbation with contributions from all particle species.

With this knowledge, $\Phi' \sim 0$ since only the decaying solution contributes, and we have that equation 2.99 becomes

$$\mathcal{R} = -\frac{5+3w}{3+3w}\Phi. \tag{2.102}$$

In MD, which is what we will need, this is simply

$$\mathcal{R} = -\frac{5}{3}\Phi \tag{2.103}$$

on super-horizon scales. However, for MD equation 2.100 becomes

$$\Phi'' + \frac{6}{\tau}\Phi' = 0 \tag{2.104}$$

with solution

$$\Phi \propto \begin{cases} \text{const.} \\ \tau^{-5} \propto a^{-5/2} \end{cases} \tag{2.105}$$

which means that the non-decaying solution to Φ is always constant. Therefore, we can start within the horizon, to write

$$\sigma_\delta^2(t,k) = \mathcal{P}_\delta(k,t) = \frac{k^3}{2\pi^2 V} \left\langle |\delta_{\boldsymbol{k}}(t)|^2 \right\rangle , \tag{2.106}$$

which using the Poisson equation

$$-k^2 \Phi_{\boldsymbol{k}}(t) = \frac{3a^2H^2}{2} \delta_{\boldsymbol{k}}(t). \tag{2.107}$$

yields

$$\sigma_\delta^2(k) = \frac{k^3}{2\pi^2 V} \frac{2^2 k^4}{3^2 (a^2H^2)^2} \left\langle |\Phi_{\boldsymbol{k}}(t)|^2 \right\rangle = \frac{k^3}{2\pi^2 V} \frac{2^2}{3^2} \left\langle |\Phi_{\boldsymbol{k}}|^2 \right\rangle , \tag{2.108}$$

evaluated at horizon crossing $k = aH$. Using the constancy of Φ on all scales during MD, we can go super-horizon, and use relation 2.103, to find,

$$\sigma_\delta^2(k) = \frac{k^3}{2\pi^2 V} \frac{2^2 3^2}{3^2 5^2} \left\langle |\mathcal{R}_{\boldsymbol{k}}(t)|^2 \right\rangle = \frac{2^2}{5^2} \mathcal{P}_\mathcal{R}(k) \tag{2.109}$$

i.e.

$$\boxed{\sigma_\delta(k) = \frac{2}{5} \sqrt{\mathcal{P}_\mathcal{R}(k)}} \tag{2.110}$$

This agrees with the definition used in [26]. It is possibly the most important equation of this section. This is because it connects predictions from inflation with the variance of density perturbations at much later times when they re-enter the horizon, and this variance is, as we will see, what determines the abundance of PBHs. Note that whenever we write just σ, we always refer to density perturbations unless explicitly stated otherwise.

2.6 Inflation

2.6.1 Inflation as a solution to the horizon problem

Expressed in terms of the reduced Planck mass, the Friedman equation reads

$$H^2 = \frac{\rho}{3M_{\text{pl}}^2} \tag{2.111}$$

for a flat space-time.

We showed that for photons (which travel on null geodesics) we have

$$\Delta\chi(\tau) = \pm\Delta\tau. \tag{2.112}$$

At a point P in the $\tau\chi$-plane, the worldlines of photons traveling in opposite directions emerge from below on the past conformal-time lightcone, starting their journey at some initial time τ_i, meet the point P at some later time τ_0, and continue past P, forming the future conformal lightcone. These conformal lightcones form the boundary of the regions that an observer may ever see or send signals to. In particular, we notice that, given an initial time τ_i, the comoving size of the observable universe, the particle horizon, is given by

$$\chi_{\text{ph}}(\tau) = \tau - \tau_i = \int_{t_i}^{t} \frac{\mathrm{d}t}{a(t)}. \tag{2.113}$$

Objects further away are always out of causal contact. Another horizon, the *event horizon*, emerges from considering that for signals emitted at P, an observer at some later time τ_f, may not observe such signals from any farther away than

$$\chi_{\text{eh}}(\tau) = \tau_f - \tau = \int_{t}^{t_f} \frac{\mathrm{d}t}{a(t)} \tag{2.114}$$

We can take τ_f to represent the *final* moment corresponding to $t_f = \infty$. However, since

$$\int_{\tau_i}^{\tau_f} d\tau = \int_{t_i}^{t_f} \frac{dt}{a(t)}, \tag{2.115}$$

the behaviour of $a(t)$ dictates the value of τ_f. It is therefore possible that, e.g., due to exponential expansion, τ_f is finite, while t_f is infinite, which would make the the Event Horizon finite.

Before we proceed, we would like to comment on the important distinction between the Hubble sphere and the particle horizon. The particle horizon is the greatest distance an observer has causal contact to. The Hubble sphere is the greatest distance over which two observers may communicate now. For us, the combination $(Ha)^{-1}$ is of great importance. It denotes the comoving distance a massless particle may travel during a Hubble time, and is thus called the comoving Hubble radius or, in short, just the Horizon. We will often write *horizon exit* in this thesis, with which we mean the exit from the Hubble sphere. *Horizon entry* similarly means the entry into the Hubble sphere.

For a single component universe, equation 2.26 yields $\rho = \rho_0 \left(\frac{a}{a_0}\right)^{-3(1+\omega)}$, which means that

$$H^2 = H_0^2 \Omega_{0,\omega} \left(\frac{a}{a_0}\right)^{-3(1+\omega)} . \tag{2.116}$$

Thus, the comoving Hubble radius may be expressed as

$$\begin{aligned} (Ha)^{-1} &= \left[H_0 \sqrt{\Omega_{0,\omega}} \left(\frac{a}{a_0}\right)^{-\frac{3}{2}(1+\omega)} a \right]^{-1} \\ &= H_0^{-1} \sqrt{\Omega_{0,\omega}}^{-1} \left(\frac{a}{a_0}\right)^{\frac{1}{2}(1+3\omega)} . \end{aligned} \tag{2.117}$$

We see that for $\omega > -1/3$, the comoving Hubble radius increases with the scale factor.

We may now relate the comoving Hubble radius to the particle horizon as follows:

$$\chi_{\text{ph}}(\tau) = \int_{t_i}^{t} \frac{\mathrm{d}t}{a} = \int_{a_i}^{a} \frac{\mathrm{d}a}{a\dot{a}} = \int_{\ln a_i}^{\ln a} (aH)^{-1} \, \mathrm{d} \ln a \tag{2.118}$$

which, using $(aH)^{-1} = H_0^{-1} a^{\frac{1}{2}(1+3w)}$ for a flat space, leads to the finite particle horizon

$$\chi_{\text{ph}}(t) = \frac{2H_0^{-1}}{(1+3w)} a(t)^{\frac{1}{2}(1+3w)} = \frac{2}{(1+3w)} (aH)^{-1} \tag{2.119}$$

after integration. Since this expression is finite, we should expect that patches of the sky separated by distances greater than the particle horizon be out of equilibrium, since they could never have communicated. This is contrary to observations of the cosmic microwave background (CMB), which is observed to have a uniform temperature to one part in 10^{15} and described by a black body [2]. To resolve the conundrum, referred to as the *horizon problem*, we need that two opposite points on the sky at the CMB

scale have had sufficient time to reach equilibrium in the past. In other words, if $\Delta\tau_{\text{CMB}} = \tau_0 - \tau_{\text{CMB}}$, the particle horizon at τ_{CMB} must obey $\chi_{\text{CMB}} > \Delta\tau_{\text{CMB}}$, as the past conformal light cones of the opposite points on the CMB would overlap. Thus, we resolve the horizon problem if we find a mechanism that makes $\chi_{\text{ph}}(\tau_{\text{CMB}})$ sufficiently large.

Notice then that

$$\chi_{\text{ph}}(a) = \frac{2H_0^{-1}}{(1+3w)}\left[a^{\frac{1}{2}(1+3w)} - a_i^{\frac{1}{2}(1+3w)}\right] \equiv \tau - \tau_i, \tag{2.120}$$

from which we see that $w < -1/3$ yields

$$\tau_i = \frac{2H_0^{-1}}{(1+3w)} a_i^{\frac{1}{2}(1+3w)} \longrightarrow -\infty \tag{2.121}$$

when $a_i \to 0$ and $w < -\frac{1}{3}$. Thus, while $t_i = 0$, τ_i could take negative values, rendering $\chi_{\text{ph}}(\tau_{\text{CMB}})$ sufficiently large to explain the isotropy of the CMB. Equation 2.117 also tells us that for $w < -\frac{1}{3}$ the comoving Hubble horizon would decrease, or equivalently that the universal expansion accelerates.

Thus, if we could establish a mechanism in the early universe that lasts long enough and is responsible for $\omega < -1/3$, the horizon problem is solved. Such a mechanism is part of most successful cosmological models and has generically been given the name inflation.

A simple yet conservative estimate of the required duration of inflation is obtained as follows: we require that the currently observable universe was contained within the comoving Hubble sphere before inflation such that equilibrium could be achieved, i.e.

$$(a_i H_i)^{-1} > (a_0 H_0)^{-1} = \left(\frac{a_0}{a_e}\frac{H_0}{H_e}\right)^{-1} (a_e H_e)^{-1} = \left(\frac{a_0}{a_e}\right)(a_e H_e)^{-1} \sim \frac{T_e}{T_0}(a_e H_e)^{-1}, \tag{2.122}$$

where subscript i (e) marks the beginning (end) of inflation and we assumed RD ($H \propto a^{-2}$) from the end of inflation until now. If we take $w \sim -1$, 2.116 tells us that $H \sim const.$ during inflation and 2.122 becomes

$$\frac{a_e}{a_i} > \frac{T_e}{T_0}. \tag{2.123}$$

If we take $T_0 \sim 10^{-3}$ eV and $T_e \in (10^{10}, 10^{15})$ GeV, $a_e/a_i > (10^{22} - 10^{27})$, corresponding to $\sim 50 - 65$ e-folds of inflation.

To characterize inflation, we define two useful quantities:

$$\varepsilon \equiv -\frac{\dot{H}}{H^2} = -\frac{d\ln H}{dN} < 1 \tag{2.124}$$

where $\mathrm{d}N \equiv \mathrm{d}\ln a = H\,\mathrm{d}t \equiv \frac{\mathrm{d}t}{t_H}$ is the logarithmic change of the scale factor, t_H the Hubble time, and

$$\eta \equiv \frac{d\ln\varepsilon}{dN} = \frac{\dot{\varepsilon}}{H\varepsilon} \tag{2.125}$$

The inequality follows since for inflation to take place, we showed that the comoving Hubble sphere must decrease, namely that

$$\frac{d}{dt}(aH)^{-1} = -\frac{\dot{a}H + a\dot{H}}{(aH)^2} = -\frac{1}{a}(1-\varepsilon) < 0, \tag{2.126}$$

from which the inequality follows. ϵ tells us how the expansion rate of the universe changes with the logarithmic change of the scale factor $\mathrm{d}N$. η measures how ϵ changes with N. We must require that η is small enough to make the condition 2.124 persist for a sufficient number of e-folds, typically $N \equiv \frac{a_E}{a_I} \sim 60$.

From this analysis, we understand that an important consequence of inflation is that regions of space, or perturbations, that were initially inside the Hubble horizon quickly exited. They thus remained outside the horizon until some time after the end of inflation, but eventually re-entered when the expansion of the universe decelerated. Inflation, therefore, sets up the scene for the later growth of these perturbations.

2.6.2 The inflaton field

As a driving source for inflation, we consider a scenario where the universe is initially dominated by a scalar field $\phi(t, \boldsymbol{x})$, which we refer to as the inflaton, governed by a potential $V(\phi)$. Since this field is assumed to dominate the universe, it will dictate the expansion of the universe during this period, and we make it our task to understand what features of this field give rise to inflation as described above. In general relativity, the energy-momentum tensor for a scalar field is given by

$$T_{\mu\nu} = \partial_\mu\phi\partial_\nu\phi - g_{\mu\nu}\left(\frac{1}{2}g^{\alpha\beta}\partial_\alpha\phi\partial_\beta\phi - V(\phi)\right) \tag{2.127}$$

The inflaton field expectation value must vary only in time to comply with the cosmological principle. Only quantum fluctuations on small scales lead to spatial dependence. Application of equation 2.127 yields for the time-time component

$$\rho_\phi \equiv T^0{}_0 \quad = (\partial_t \phi)^2 - g_{00}\left[\frac{1}{2}(\partial_t\phi)^2 - V(\phi)\right] = \frac{1}{2}\dot{\phi}^2 + V(\phi), \tag{2.128}$$

i.e. we see that the energy density of the inflaton carries contributions from its kinetic and potential energy, as expected. The space-space components obey

$$-P_\phi \delta^i_j \equiv T^i j = -\delta^i_j\left(\frac{1}{2}\dot{\phi}^2 - V(\phi)\right), \tag{2.129}$$

or simply

$$P_\phi = \frac{1}{2}\dot{\phi}^2 - V(\phi). \tag{2.130}$$

Inflation persists as long as the condition

$$P_\phi < -\frac{1}{3}\rho_\phi \Longleftrightarrow \frac{1}{2}\dot{\phi}^2 - V(\phi) < -\frac{1}{3}\left(\frac{1}{2}\dot{\phi}^2 + V(\phi)\right), \tag{2.131}$$

is met, or equivalently,

$$2\left(\frac{1}{2}\dot{\phi}^2\right) < V(\phi). \tag{2.132}$$

This condition tells us that the energy density of the inflaton is dominated by the potential energy for as long as inflation persists.

Given the inflaton density ρ_ϕ and the assumption that it dominates the energy, the evolution of the universe is now given by the Friedmann equation:

$$H^2 = \frac{1}{3M_{\text{pl}}^2}\left[\frac{1}{2}\dot{\phi}^2 + V(\phi)\right] \tag{2.133}$$

The evolution of the inflaton field obeys

$$\ddot{\phi} + 3H\dot{\phi} + V' = 0 \tag{2.134}$$

where we denote derivatives with respect to the inflaton field $' \equiv d/d\phi$. This is called the Klein-Gordon equation. Expanding the potential $V(\phi)$ around a local minimum $\phi_0 = 0$ to leading order,

$$\ddot{\phi} + 3H\dot{\phi} + V''(0)\phi = 0, \tag{2.135}$$

which makes explicit that the Klein-Gordon equation takes the form of a damped harmonic oscillator, where the gradient of the potential acts as a driving force, while the expansion rate of the universe introduces damping of the inflaton oscillations around the minimum.

2.6.3 Primordial Perturbations from Inflation

The most important reason to why a section on inflation is included is the following: scalar perturbations arise from quantum uncertainty in the inflation field value, leading to tiny variations in the amount of inflation a region of space undergoes. Thus, inflation induces adiabatic perturbations. These perturbations begun within the horizon $(aH)^{-1}$, but as the horizon shrunk due to accelerated expansion, they eventually left to become super-horizon. For this reason, it is useful to describe these as comoving curvature perturbations $\mathcal{R}$ once they exit the horizon, since $\mathcal{R}$ remain constant on super-horizon scales for adiabatic perturbations.

It can be shown [8] that the curvature power spectrum obeys

$$\mathcal{P}_{\mathcal{R}}(k) = \frac{1}{8\pi^2}\frac{1}{\varepsilon}\frac{H^2}{m_{\mathrm{pl}}^2}\bigg|_{k=aH}, \tag{2.136}$$

evaluated at Horizon exit $k = aH$, where $\varepsilon = \frac{\frac{1}{2}\dot{\phi}^2}{m_{\mathrm{pl}}^2 H^2}$. This is the main reason why inflation is introduced in this thesis: it sources perturbations that may eventually collapse into PBHs.

For perfect de-sitter expansion ($w = -1$), the Hubble rate $H = const.$, but in general, H and ε are time dependent. It is, however, expected that they vary only slowly with time, and we expect the power spectrum to vary with scale k since H and ε do. Assuming small deviations from scale invariance, we expand the spectrum around k_0 as

$$\ln \mathcal{P}_{\mathcal{R}}(k) = \ln \mathcal{P}_{\mathcal{R}}(k_0) + \frac{d\ln \mathcal{P}_{\mathcal{R}}}{d\ln k}\bigg|_{k_0}(\ln k - \ln k_0) + \frac{1}{2}\frac{d^2 \ln \mathcal{P}_{\mathcal{R}}}{d\ln k^2}\bigg|_{k_0}(\ln k - \ln k_0)^2 + \ldots \tag{2.137}$$

which, if we keep terms to second order, yields

$$\begin{aligned}\mathcal{P}_{\mathcal{R}}(k) &= \mathcal{P}_{\mathcal{R}}\left(k_0\right)\left(\frac{k}{k_0}\right)^{\left.\frac{d\ln\mathcal{P}_{\mathcal{R}}}{d\ln k}\right|_{k_0}+\frac{1}{2}\left.\frac{d^2\ln\mathcal{P}_{\mathcal{R}}}{d\ln k^2}\right|_{k_0}\ln\left(\frac{k}{k_0}\right)} \\ &\equiv A_{\mathrm{s}}\left(\frac{k}{k_0}\right)^{n_{\mathrm{s}}-1+\frac{1}{2}\alpha_{\mathrm{s}}\ln\left(\frac{k}{k_0}\right)}\end{aligned} \tag{2.138}$$

where $A_{\mathrm{s}} \equiv \mathcal{P}_{\mathcal{R}}\left(k_0\right)$, $n_{\mathrm{s}} \equiv 1 + \left.\frac{d\ln\mathcal{P}_{\mathcal{R}}}{d\ln k}\right|_{k_0}$ is the spectral index, and $\alpha_{\mathrm{s}} \equiv \left.\frac{d^2\ln\mathcal{P}_{\mathcal{R}}}{d\ln k^2}\right|_{k_0}$ is the running of the spectral index, all evaluated at the scale k_0

In our work, we aim for generality and therefore take 2.138 as a general form of the curvature power spectrum. We consult the Planck 2018 results ([5] [4]), for the values of A_{s}, n_{s} and n_{s}. At the Planck pivot scale $k_0 \equiv k_* = 0.05\mathrm{Mpc}^{-1}$, they obtain

$$\begin{aligned}\ln\left(10^{10}A_{\mathrm{s}}\right) &= 3.043 \pm 0.014 \quad (67\%\ \mathrm{CL}\ ) \\ n_{\mathrm{s}} &= 0.9649 \pm 0.0042 \quad (67\%\ \mathrm{CL}) \\ \alpha_{\mathrm{s}} &= -0.0045 \pm 0.0067 \quad (68\%\mathrm{CL})\end{aligned} \tag{2.139}$$

We will use these values throughout this work.

While the scalar power spectrum has been shown not to be perfectly scale-invariant [3] (i.e., $n_{\mathrm{s}} = 1$) at 8.4σ, the data is consistent with zero running, and we have $\alpha \equiv dn/d\ln k - 0.0045 \pm 0.0067 \quad (68\%\mathrm{CL})$. The near power-law form of the spectrum is established at comoving scales $0.005\mathrm{Mpc}^{-1} \lesssim k \lesssim 0.2\mathrm{Mpc}^{-1}$, but we adapt this form for all scales of interest. This, then, is a major assumption: we assume that we can extrapolate the form 2.138 of the power spectrum to all relevant scales.

In our analysis, we combine the parameters A_{s}, n_{s}, and α_{s} into sets of $(A_{\mathrm{s}}^{+}, n_{\mathrm{s}}^{+}, \alpha_{\mathrm{s}}^{+})$ (black), $(A_{\mathrm{s}}, n_{\mathrm{s}}, \alpha_{\mathrm{s}})$ (dark gray), $(A_{\mathrm{s}}^{-}, n_{\mathrm{s}}^{-}, \alpha_{\mathrm{s}}^{-})$ (light gray), corresponding to $+\sigma$, median, and $-\sigma$ values. Figure 2.6.1 shows the resulting scalar power spectra, in which we include various bounds for reference.

Figure 2.6.1: The scalar power spectrum $\mathcal{P}_{\mathcal{R}}(k)$, equation 2.138, for the combinations $(A_{\mathrm{s}}^{+}, n_{\mathrm{s}}^{+}, \alpha_{\mathrm{s}}^{+})$ (black), $(A_{\mathrm{s}}, n_{\mathrm{s}}, \alpha_{\mathrm{s}})$ (dark gray), $(A_{\mathrm{s}}^{-}, n_{\mathrm{s}}^{-}, \alpha_{\mathrm{s}}^{-})$ (light gray), corresponding to $+\sigma$, median, and $-\sigma$ values. Solid lines neglect the running of n_{s}, dashed lines include the running. The constraints are reproduced from [38] and references therein, to which we refer the reader for details. Dashed lines are potential future sensitivities.

Chapter 3

Primordial Black Holes

PBHs form a topic in physics and cosmology that beautifully unites general relativity, quantum mechanics, field theory, and thermodynamics. As such, one may consider their theoretical nature attractive enough to motivate their independent study. In cosmological contexts, it has been suggested that PBHs may constitute all or part of the DM [43]. PBHs form in the very early universe, much before EQ, which makes them nonbaryonic. They are furthermore stable on cosmological timescales if their initial mass $M \gtrsim 5 \times 10^{14}$ g [23]. DM constitutes approximately 85% of the matter content of the universe, which is stable on cosmological timescales, nonbaryonic, and typically described as cold [12]. Since PBHs satisfy this description of DM, the interest within the scientific community grew. It should, however, be noted that on large scales, PBHs behave as particle DM, but on scales similar to and smaller than galaxies, PBHs differs from particle DM in that their masses are nonuniformly distributed in space, leading to granularity, which can lead to observational signatures [38].

While a lot of work has been put down to study PBHs as DM, in this thesis we take the opposite approach and make explicit use of the fact that no conclusive evidence for PBHs as DM exists. Rather, for most PBHs masses there are strong constraints limiting their potential contribution to the total density of the universe.

There have been many reviews written on the topic of PBHs and, in particular, PBHs as a DM candidate (e.g., [23, 24, 38]), to which we refer the curious reader. Within the scope of this work, we aspire to provide a brief review of PBHs, emphasizing those aspects that are relevant for the progression of this thesis.

This chapter is outlined as follows. In section 3.1 we give a brief introduction to the

properties of PBHs and Hawking radiation. In section 3.2 we proceed to discuss formation scenarios, with emphasis on PBH production from overdensity growth during MD and introduce the necessary formalism to describe this quantitatively. This is followed by section 3.3 containing a review on PBH constraints, a review on 21 cm astronomy and how it has been used recently to place new stricter constraints, and a compilation of the strongest PBH bounds to date. Having presented the relevant theory and background, in section 3.4 we derive constraints on early MD, and in section 3.5 we place bounds on the spectral index $n_{\rm s}$ and its running $\alpha_{\rm s}$.

3.1 PBH evaporation

A tremendously important prediction was made by Hawking [44] that PBHs evaporate through a process that came to be known as Hawking radiation. Throughout this thesis, it is our working hypothesis that this prediction is true, as the tightest PBH bounds arise from the non-observation of Hawking radiation and its phenomenological consequences. Hawking radiation is thermal and is characterized by the temperature

$$T_{\rm BH} = \frac{\hbar c^3}{8\pi G M k_{\rm B}} \sim 10^{-7} \left(\frac{M}{M_\odot}\right)^{-1} \text{ K}, \tag{3.1}$$

which is inversely proportional to the PBH mass, i.e., the smaller the PBH, the larger the temperature, and PBHs warm up as they evaporate.

As PBHs evaporate, they lose mass which renders their lifetime finite. The lifetime τ of a PBH of (initial) mass M is given by [22]

$$\tau \approx 1.35 \times 10^9 \left(\frac{f(M)}{15.35}\right)^{1/3} \left(\frac{\tau}{1\,\text{s}}\right)^{1/3}, \tag{3.2}$$

where $f(M)$ counts the number of emitted particle species for a PBH of mass M (not averaged over the lifetime of the PBH, as a more precise calculation should entail), and is normalized to unity for PBHs that evaporate into only massless particles, i.e., those that have $M \gg 10^{17}$ g. It then follows that, for the age of the universe 13.8Gyr, PBHs that form with a mass

$$M = M_* \equiv 1.02 \times 10^{15} \left(\frac{f_*}{15.35}\right)^{1/3} \text{ g} \approx 5.1 \times 10^{14} \text{ g} \tag{3.3}$$

where $f_* = 1.9$, evaporate at the present time. This mass is called the critical mass and

thus divides the spectrum of PBH masses into two parts: those that have evaporated ($M < M_\star$) and those that have not ($M > M_\star$).

3.2 PBH Formation

3.2.1 Formation mass

PBHs are typically assumed to form with a mass similar to the horizon mass $M_{\rm H}$. A quick calculation relating the PBH mass M to the Hubble parameter H tells us that

$$M = \gamma M_{\rm H} = \gamma \frac{4\pi}{3} R_{\rm H}^3 \rho = \left\{ R_{\rm H} \equiv \frac{1}{H}, \quad \rho = \frac{3}{8\pi G} H^2 \right\} = \frac{\gamma}{2GH} = \gamma \frac{M_{\rm pl}^2}{2H}, \tag{3.4}$$

i.e.,

$$\boxed{M = \gamma \frac{M_{\rm pl}^2}{2H}}, \tag{3.5}$$

where ρ is the average total density of a flat universe and γ denotes the fraction of the horizon mass that collapses to a PBH. Throughout this thesis, we will take $\gamma = 1$. Equation 3.5 is model-independent in the sense that it only depends on H at any instant in time.

3.2.2 Basic notions

We begin this section by introducing some concepts and quantities needed to describe PBH formation and their resulting abundance. Unless explicitly mentioned, we will proceed as most often done in the literature, by assuming a *monochromatic* mass function for simplicity. By this, we mean that PBHs form with one and only one mass, and consequently at one and only one scale, or instant in time. We will see later in section 3.2.4 how to transition to an *extended* mass function. While we keep it simple for now and building upon the assumption of a monochromatic mass function, we will later analyze the more realistic case of an extended mass function.

One crucial ingredient in our treatment will be a quantity, typically denoted β, whose most straightforward definition is the *fraction of the energy density of the universe that collapses into PBHs of mass M at the time of formation*. As such, it may be defined

as

$$\beta(M) \equiv \frac{M n_{\mathrm{PBH}}\left(t_{\mathrm{i}}\right)}{\rho\left(t_{\mathrm{i}}\right)}, \tag{3.6}$$

where ρ is the total density of the universe at the time of formation and $n_{\mathrm{PBH}}\left(t_{\mathrm{i}}\right)$ is the PBH number density evaluated at the formation time t_{i}.

We furthermore define

$$\Omega_{\mathrm{PBH}} = \frac{M n_{\mathrm{PBH}}\left(t_0\right)}{\rho_{\mathrm{c}}} \tag{3.7}$$

and

$$f \equiv \frac{\Omega_{\mathrm{PBH}}}{\Omega_{\mathrm{CDM}}} \approx 3.8 \Omega_{\mathrm{PBH}}, \tag{3.8}$$

For non-evaporated PBHs, limits on their abundances are typically presented in terms of constraints on f. Note that f is only defined for non-evaporated PBHs and those that have not suffered significant mass loss, since $n_{\mathrm{PBH}}\left(t_0\right) = 0$ for PBHs smaller than M_*. However, one can still relate β to f even for evaporated PBHs, in which case f denotes the would-be fraction of DM had they not evaporated. In the coming sections, we will develop these concepts, and in particular provide explicit expressions for β and f in the cases of PBH formation during MD and RD.

3.2.3 Formation scenarios

PBH formation scenarios are abundant, and in all cases do PBHs form from some overdensity in the early universe [18]. These overdensities may arise from cosmic strings forming loops, whose configuration has a certain probability to be within its own Schwarzschild radius [42]. Another proposed mechanism for PBH formation is the collision of bubble walls arising from phase transitions in the early universe [30, 56]. See, e.g., [23] for a detailed review of these and other formation scenarios.

A different source of overdensities, as we have seen in section 2.6, are quantum fluctuations stemming from the presence of the inflaton field, which in the simplest case is just a scalar field. This leads to a spectrum of density perturbations that eventually enter the horizon, start growing, and collapse into PBHs.

Collapse of overdensities during radiation-domination

While not too important for the analysis in this thesis, it is historically important and conceptually enlightening to review the formation of PBHs during RD. In this case,

one naively assumes that RD was realized after inflation and that RD persisted until EQ. The main idea now is to identify a condition for PBH formation and calculate what fraction of the universe satisfied this condition. B. J. Carr suggested [19] that this condition can be placed on the density contrast $\delta > \delta_{\rm c}$, such that only those overdensities that are larger than $\delta_{\rm c}$ at Horizon entry collapse. He proposed $\delta_{\rm c} \sim w = 1/3$, where w is the equation of state parameter. Note that since the density contrast for those overdensities that form PBHs is large already at horizon entry, the collapse will take place quickly after entering the horizon. For $\delta < \delta_{\rm c}$, radiation pressure prevents the collapse from occurring. More recent analyses including numerical relativity simulations and aspherical overdensities have obtained values of $\delta_{\rm c}$ in the range $\delta_{\rm c} \simeq 0.42 - 0.66$ ([6, 22] and references therein).

Typically, one assumes that the density contrast δ is normally distributed. In this case, the fraction β of the energy density of the universe that collapses to form PBHs is [19]

$$\beta(M) = \frac{2}{\sqrt{2\pi}\sigma(M)} \int_{\delta_c}^{\infty} {\rm d}\delta \exp\left(-\frac{\delta^2}{\sigma(M)^2}\right) = {\rm Erfc}\left(\frac{\delta_c}{\sqrt{2}\sigma(M)}\right), \tag{3.9}$$

where Erfc is the complimentary error function. Thus, β is exponentially suppressed by $\delta_c/\sqrt{2}\sigma(M)$ since $\sigma\,(M) \ll \delta_{\rm c}$ [38]. This exponential dependence further complicates accurate predictions of β since it is very sensitive to the true value of σ and $\delta_{\rm c}$. In any case, this exponential suppression means that for any significant PBH abundance to form, the power spectrum amplitude would need to be large at small scales to enhance σ, i.e., a blue power spectrum of density perturbations [22]. This is not expected given a naive extrapolation of CMB observations [3], unless one includes a running of the spectral index or some other nontrivial UV-blue features.

If we want to relate the PBH mass M in equation 3.5 to a formation time, we must assume an expansion history. If we assume RD until EQ, then we can use the Friedmann equation $H = \frac{1}{\sqrt{3}m_{\rm pl}}\sqrt{\rho_{\rm r}}$ for a flat universe and proceed as

$$M = \gamma 4\pi\sqrt{3}\frac{m_{\rm pl}^3}{\sqrt{\rho_{\rm r}}} = \left\{\rho_{\rm r} = \frac{\pi^2}{30}g_*(T)T^4\right\} = \gamma\frac{12\sqrt{10}}{\sqrt{g_*(T)}}\frac{m_{\rm pl}^3}{T^2}, \tag{3.10}$$

i.e.,

$$\boxed{M = \gamma\frac{12\sqrt{10}}{\sqrt{g_*(T)}}\frac{m_{\rm pl}^3}{T^2}}, \tag{3.11}$$

which combined with equation 2.54 results in

$$M \sim 2.03 \times 10^5 \gamma \left(\frac{t}{1\,\mathrm{s}}\right) M_\odot \sim 4.03 \times 10^{15} \gamma \left(\frac{t}{10^{-23}\,\mathrm{s}}\right) \mathrm{g}. \tag{3.12}$$

where t is the time of formation. This normalization is chosen since PBHs with $M \sim 10^{15}$ g are evaporating at present. Note that because of the one-to-one correspondence between M and M_{H}, which determines the scale k, scale and mass can be used interchangeably.

A direct and very important consequence of 3.12 is that PBHs could in principle have formed over a vast mass range. If formed around the Planck time $t_{\mathrm{pl}} \sim 10^{-43}$s, then the mass would be $\sim 10^{-5}$ g, whereas those formed at $t \sim 1$s would have a mass of around $M \sim 10^5 M_\odot$. It is exciting to speculate whether the larger PBHs may have acted as seed black holes for supermassive black holes in the center of galaxies. Given such an enormous mass range, most PBHs could have formed with a mass dramatically different from astrophysical stellar core-collapse black holes. The detection of black holes of masses far from $M_\odot$, and in particular $M < M_\odot$, would then be the smoking gun that indeed their origin is primordial. Interestingly, [47] finds that a softening of the equation of state during the QCD phase transition may lead to a pronounced peak of the PBH mass spectrum around $1\mathrm{M}_\odot$, making these PBHs harder to distinguish from astrophysical black holes.

Collapse of overdensities during matter-domination

Standard cosmology assumes no epoch of early MD. There is, however, no evidence against such a period as long as it ends before big bang nucleosynthesis when the universe is shown to be RD. Indeed, early MD may arise as a result of the universe being dominated by some heavy non-relativistic particles [52] or by a period dominated by an oscillating scalar field, e.g. slow reheating after inflation [49]. In this work, in which we explicitly assume an early MD epoch, the cause of MD is unimportant as we aim for generality. What is important are the effects such a period has on the PBH abundance. Matter domination, or at least a softening of the equation of state due to, e.g., some phase transition, has been studied in, e.g., [16, 21, 26, 41, 47, 50, 52, 61]. Matter domination is key to the increased PBH production that, as we shall see, potentially allows us to constrain regions of the parameter space $(T_{\mathrm{reh}}, \mathcal{A})$ of MD, T_{reh} being the reheating temperature when the universe transitions to RD from early MD,

and $\mathcal{A} \equiv a_{\text{reh}}/a_{\text{md}}$ is the ratio of the scale factor at the beginning of MD to that at reheating.

It was shown [39] that an equation of state $p = w\rho$ leads to the analytical expression

$$\delta_{\text{c}} \simeq [3(1+w)/(5+3w)] \sin^2[\pi\sqrt{w}/(1+3w)]. \tag{3.13}$$

This seems to suggest that, if we naively proceed to compute the formation fraction β as we did for RD, any overdensity would collapse to a PBH since $\delta_{\text{c}} \sim 0$, leading to an overabundance of PBHs. In reality, there are two counteracting effects. On the one hand, the lack of pressure means that any overdensity that enters the horizon $k = aH$ during MD will grow as $\delta \propto a$, as found in section 2.5. As the pressure is negligible, it fails to thwart a collapse and PBHs could form provided the growth continues long enough and that pressure gradients remain negligible. On the other hand, because initially small overdensities may form PBHs, they must shrink considerably before finding themselves in such a configuration. Thus, aspherical effects and angular momentum may suppress the formation considerably. This is because instead of collapsing towards a point, a pancake- or cigar-like configuration is achieved [38, 40, 41]. The fraction of the universe collapsing into PBHs then depends upon what fraction of the overdensities that enter the horizon are spherical enough, and have low angular momentum.

Restricting themselves to the consequences of aspherical effects, this problem was studied in [41], upon which the present analysis relies heavily. In a later paper [40], the authors also include the effect of angular momentum. While they conclude that this is important and leads to an exponential suppression of the formation fraction β for sufficiently small overdensities, it is somewhat ambiguous whether this applies to the regions of the parameter space we are considering, as their analysis is subject to many assumptions and the corresponding results exponentially depend on uncertain quantities. Because of this uncertainty, we limit ourselves to account for only aspherical effects, as understood and studied in [41]. In this regard, our assumptions are optimistic.

In [41], they start by considering the Zel'dovich approximation [70] in which the physical coordinate for a particle is described as

$$\boldsymbol{r} = a(t)\boldsymbol{q} + b(t)\boldsymbol{p}(\boldsymbol{q}). \tag{3.14}$$

Here, $\boldsymbol{q}$ is not the comoving coordinate, but a time-independent coordinate, essentially a label of the particle, which would equal the comoving coordinate in the absence of perturbations. a is the scale factor as usual, and $b(t)\boldsymbol{p}(\boldsymbol{q})$ a perturbation which does depend on time. In this description, the evolution of the position of the particle is captured solely by the growing mode $b(t)$. They proceed to define the deformation tensor

$$D_{ik} := \frac{\partial r_i}{\partial q_k} = a(t)\delta_{ik} + b(t)\frac{\partial p_i}{\partial q_k}, \tag{3.15}$$

for which they make the choice of axes such that

$$\frac{\partial p_i}{\partial q_k} \equiv \text{diag}(-\alpha, -\beta, -\gamma), \tag{3.16}$$

being function of the comoving coordinate $\boldsymbol{q}$, yielding

$$D_{ik} = \text{diag}(a - \alpha b, a - \beta b, a - \gamma b). \tag{3.17}$$

Using the conservation of mass within an unperturbed comoving volume d^3q, they find the expression for the density

$$\rho = \frac{a^3}{(a - \alpha b)(a - \beta b)(a - \gamma b)}\bar{\rho}. \tag{3.18}$$

They proceed to argue that an aspherical overdensity would eventually collapse to a pancake-like shape after horizon crossing, and impose that the a PBH will form from this configuration only if the Hoop conjecture[65] is satisfied. The Hoop conjecture states that a black hole forms when a mass M contracts to the extent that the maximal circumference, i.e., the *hoop* $\mathcal{C}$, is approximately smaller than $4\pi MG$, the circumference of a spherical region the radius of which is given by the Schwarzschild radius $r_\text{s} = 2GM$. They define $h(\alpha, \beta, \gamma) := \mathcal{C}/\left(2\pi r_\text{s}\right)$,

$$h(\alpha, \beta, \gamma) = \frac{2}{\pi}\frac{\alpha - \gamma}{\alpha^2}E\left(\sqrt{1 - \left(\frac{\alpha - \beta}{\alpha - \gamma}\right)^2}\right), \tag{3.19}$$

resulting in the condition for PBH formation that $h(\alpha, \beta, \gamma) \lesssim 1$

The probability for $h < 1$ depends on α, β, and γ, whose probability distribution is

given by Doroshkevich's [36] as

$$\begin{aligned} & w(\alpha,\beta,\gamma)d\alpha d\beta d\gamma \\ = & -\frac{27}{8\sqrt{5}\pi\sigma_3^6}\exp\left[-\frac{1}{10\sigma_3^2}(\alpha+\beta+\gamma)^2-\frac{1}{4\sigma_3^2}\left\{(\alpha-\beta)^2+(\beta-\gamma)^2+(\gamma-\alpha)^2\right\}\right] \\ & \cdot(\alpha-\beta)(\beta-\gamma)(\gamma-\alpha)d\alpha d\beta d\gamma \end{aligned} \tag{3.20}$$

where σ_3 is a positive constant, relating to σ as

$$\sigma^2 = \overline{(\alpha+\beta+\gamma)^2}\left(\frac{b}{a}\right)^2(t_i) = 5\sigma_3^2 \tag{3.21}$$

The fraction of the universe collapsing into PBHs is then given by the integral

$$\beta = \int_0^\infty d\alpha \int_{-\infty}^{\alpha} d\beta \int_{-\infty}^{\beta} d\gamma\,\theta(1-h(\alpha,\beta,\gamma))w(\alpha,\beta,\gamma). \tag{3.22}$$

From this rather technical treatment, they arrive at the semianalytic formula

$$\beta(M) \simeq 0.056\sigma(M)^5, \tag{3.23}$$

which is their main result, applicable when $\sigma \ll 1$. We will use this. Figure 3.2.1 from [41] compares this result to the case of PBH formation during RD.

A couple of words of caution are required before we proceed. Equation 3.23 includes only the effect of asphericity. It could be argued that the increasing density associated with the collapse leads to a stiffening of the equation of state and consequently pressure gradients threatening the collapse. Escaping particles could also thwart the collapse [51], in which case one would instead have the dependence $\beta \sim \sigma^{13/2}$ [41]. However, they argue [41] that these assumptions are model-dependent and may be omitted for a general treatment. A discussion on the effect of spin follows in section4.2.

3.2.4 Extended mass function

For simplicity and model independence, monochromatic mass functions have generally been assumed to derive limits on PBH abundances, in which case the mass function is taken to be a delta spike at the PBH mass M or at least some distribution of width $\Delta M > M$ [24]. In this thesis, we will adapt the formalism as presented and used

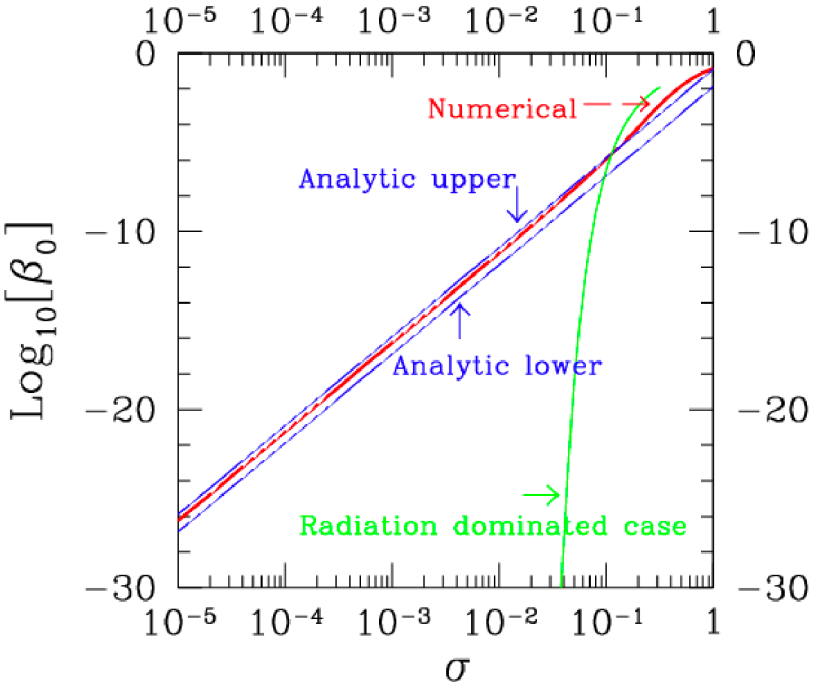

Figure 3.2.1: The initial fraction of PBHs produced during MD, as derived and presented in [41] to which we refer the reader for details.

in [25], in which a framework to treat an extended mass function is developed. Using this formalism, we can apply monochromatic constraints to place limits on extended mass functions and the resulting PBH abundances.

For an extended mass spectrum of PBHs, one proceeds to define the mass function as the differential contribution to the DM density in the mass range $(M, M+\mathrm{d}M)$, as

$$\psi(M)\mathrm{d}M \equiv \frac{1}{\rho_{\mathrm{DM}}}\frac{\mathrm{d}\rho_{\mathrm{PBH}}(M)}{\mathrm{d}M}\mathrm{d}M. \tag{3.24}$$

With $\psi(M)$ normalized to the DM density, one obtains the total contribution of PBHs to the DM fraction as

$$f_{\mathrm{PBH}} \equiv \frac{\Omega_{\mathrm{PBH}}}{\Omega_{\mathrm{DM}}} = \int \mathrm{d}M\psi(M) \tag{3.25}$$

In [26], the authors argue that, since $\rho_{\mathrm{PBH}} \propto a^{-3}$, while radiation, $\rho_{\mathrm{r}} \propto a^{-4}$, one can relate the initial mass fraction $\beta(M)$ to the mass function $\psi(M)$ at the present epoch as

$$\psi(M)\mathrm{d}M = \frac{a_{\mathrm{eq}}}{a}\frac{\beta(M)}{M}\,\mathrm{d}M, \tag{3.26}$$

where a is either the scale factor at formation if PBHs form during RD, or the scale factor at early reheating if PBHs form during MD, and a_{eq} is the scale factor at EQ.

We can, however, be more precise and express

$$\rho_{\rm r}^{\rm eq} = \frac{\pi^2}{30} g_*^{\rm eq} T_{\rm eq}^4 = \frac{g_*^{\rm eq}}{g_*^{\rm i}} \left(\frac{T_{\rm eq}}{T_{\rm i}}\right)^4 \rho_{\rm r}^{\rm i} \tag{3.27}$$

where we used equation 2.45, and

$$\rho_{\rm PBH}^{\rm eq} = n_{\rm PBH}^{\rm eq} M = s^{\rm eq} Y M = \left(\frac{s^{\rm eq}}{s^{\rm i}}\right) \rho_{\rm PBH}^{\rm i} = \left\{s \propto g_{*s} T^3\right\} = \left(\frac{g_{*s}^{\rm eq}}{g_{*s}^{\rm i}}\right) \left(\frac{T_{\rm eq}}{T_{\rm i}}\right)^3 \rho_{\rm PBH}^{\rm i}, \tag{3.28}$$

where we used the constancy of Y. Note that this is simply the well-known result that matter scales as $\propto a^{-3}$. What this calculation accounts for is that the simple relation $\rho_{\rm r} \propto a^{-4}$ is not strictly true, but should instead read $\rho_{\rm r} \propto g_*^{-1/3} a^{-4}$, if we use $g_* \approx g_{*s}$. Since g_* decreases, the radiation density will decrease less slowly than $\propto a^{-4}$.

Taking the ratio $\rho_{\rm PBH}^{\rm eq}$ to $\rho_{\rm r}^{\rm eq}$, and using that $g_{*s} \approx g_*$ before EQ, gives us that

$$\frac{\rho_{\rm PBH}^{\rm eq}}{\rho_{\rm r}^{\rm eq}} = \frac{T_{\rm i}}{T_{\rm eq}} \frac{\rho_{\rm PBH}^{\rm i}}{\rho_{\rm r}^{\rm i}}. \tag{3.29}$$

Thus, accounting for the changing effective (entropy) degrees of freedom, instead of 3.26 we should use

$$\psi(M) \mathrm{d}M = \frac{T}{T_{\rm eq}} \frac{\beta(M)}{M} \, \mathrm{d}M, \tag{3.30}$$

where T is evaluated at formation or reheating after early MD, whichever occurs later. In our case, we will exclusively take $T = T_{\rm reh}$, as we consider formation during MD and neglect PBH production beyond this period.

In an idealized scenario (excluding the effects of, e.g., critical collapse [59]), we expect abrupt cutoffs of the mass function at the masses associated with the earliest (and smallest) PBHs to form, $M_{\rm min}$, and the latest (and largest), $M_{\rm max}$. A naive guess would be to take

$$M_{\rm min} \equiv M_{\rm md} = \frac{M_{\rm pl}^2}{2H_{\rm md}}, \quad M_{\rm max} \equiv M_{\rm reh} = \frac{M_{\rm pl}^2}{2H_{\rm reh}}, \tag{3.31}$$

i.e, the horizon mass at the beginning of MD and at reheating. $M_{\rm max}$, however, is greatly overestimated, since it assumes that PBHs form until the very end of MD. This would imply instantaneous formation since the radiation pressure would otherwise thwart the formation of PBHs from the modes entering the horizon at reheating. Instead, we must consider that overdensities take time to grow. This is particularly important during MD when even initially small perturbations may grow sufficiently large to form

PBHs, provided MD lasts long enough. From this, we understand that it is only those overdensities that have, by the time of reheating, already grown large (nonlinear) would keep collapsing against the pressure and form PBHs.

For the smaller mass M_{min}, we find

$$M_{\text{min}} = \frac{M_{\text{pl}}^2}{2H_{\text{md}}} = \frac{M_{\text{pl}}^2}{2H_{\text{reh}}\frac{H_{\text{md}}}{H_{\text{reh}}}} = \frac{M_{\text{pl}}^2}{2H_{\text{reh}}}\left(\frac{a_{\text{md}}}{a_{\text{reh}}}\right)^{3/2} \tag{3.32}$$

where we used the result in table 2.2.1 that during MD $H \propto a^{-3/2}$. For the larger mass M_{max}, we simply replace a_{md} by a_{max}, which is the scale at which the last PBHs form. Since the density contrast within the horizon $\delta \propto a$ during matter domination and $\sigma^2 = \langle\delta^2\rangle$, we have that $a_{\text{max}}/a_{\text{reh}} \approx \sigma_{\text{max}}/\sigma_{\text{reh}}$. For the collapse to continue after reheating, we impose that the perturbations have grown nonlinear. For this we take as a proxy $\sigma_{\text{reh}} \sim 1$, as is also done in [26]. This choice of $\sigma_{\text{reh}} \sim 1$ seems rather arbitrary. It is, perhaps, natural to compare the formation criteria at the end of MD to those of pure RD, in which case we saw that one often imposes a density contrast $\delta_{\text{c}} \sim 0.42 - 0.50$. In this light, it seems reasonable that instead $\sigma_{\text{reh}} \sim \delta_{\text{c}} \sim 0.42 - 0.50$. To be conservative and to be able to compare with literature, we nevertheless choose $\sigma_{\text{reh}} \sim 1$. With this choice, we conclude that $a_{\text{max}}/a_{\text{reh}} \approx \sigma_{\text{max}}$, and thus that, if we assume that MD is achieved due to some heavy particle state of decay width Γ given by 2.56,

$$\boxed{M_{\text{min}} = \frac{M_{\text{pl}}^2}{2\Gamma}\mathcal{A}^{-3/2}, \quad M_{\text{max}} = \frac{M_{\text{pl}}^2}{2\Gamma}\sigma_{\text{max}}^{3/2}}. \tag{3.33}$$

where $\mathcal{A} \equiv a_{\text{reh}}/a_{\text{md}}$.

To find what σ_{max} is, we use equation 2.110, i.e.,

$$\sigma = \frac{2}{5}\sqrt{\mathcal{P}_{\mathcal{R}}(k)}, \tag{3.34}$$

which provides the important connection between observations of the power spectrum and the amplitude of density perturbations which are responsible for PBH formation during MD. For the expansion 2.138, i.e.,

$$\mathcal{P}_{\mathcal{R}}(k) = A_{\text{s}}\left(\frac{k}{k_*}\right)^{n_{\text{s}}-1+\frac{1}{2}\alpha_{\text{s}}\ln\left(\frac{k}{k_*}\right)} \tag{3.35}$$

we find

$$\boxed{\sigma^2_{\rm max} = \left(\frac{2}{5}\right)^2 \left(\frac{k_{\rm max}}{k_*}\right)^{n_{\rm s}-1+\frac{1}{2}\alpha_{\rm s}\ln\left(\frac{k_{\rm max}}{k_*}\right)}}. \tag{3.36}$$

$k_{\rm min}$ and $k_{\rm max}$ are the comoving scales for which smallest respectively largest PBHs form during the MD epoch. At horizon crossing, $k = aH$, which gives

$$k_{\rm min} \equiv k_{\rm md} = a_{\rm md}\, H_{\rm md} \; = a_{\rm md}\, \frac{H_{\rm md}}{H_{\rm reh}} H_{\rm reh} = a_{\rm md}\, \Gamma \left(\frac{a_{\rm reh}}{a_{\rm md}}\right)^{3/2} = \left(\frac{g^0_{*s}}{g^{\rm reh}_{*s}}\right)^{1/3} \frac{T_0}{T_{\rm reh}} \Gamma \sqrt{\mathcal{A}}, \tag{3.37}$$

and for

$$k_{\rm max} = a_{\rm max} \Gamma \left(\frac{a_{\rm reh}}{a_{\rm max}}\right)^{3/2} = \left(\frac{g^0_{*s}}{g^{\rm reh}_{*s}}\right)^{1/3} \frac{T_0}{T_{\rm reh}} \Gamma \frac{1}{\sqrt{\sigma_{\rm max}}} \tag{3.38}$$

where we used $g_{\star s}(T) T^3 a^3 = const.$.

We conclude,

$$\boxed{k_{\rm min} = \left(\frac{g^0_{*s}}{g^{\rm reh}_{*s}}\right)^{1/3} \frac{T_0}{T_{\rm reh}} \Gamma \sqrt{\mathcal{A}}, \quad k_{\rm max} = \left(\frac{g^0_{*s}}{g^{\rm reh}_{*s}}\right)^{1/3} \frac{T_0}{T_{\rm reh}} \Gamma \frac{1}{\sqrt{\sigma_{\rm max}}}}. \tag{3.39}$$

We can invert expression 3.39 for $k_{\rm max}$ and insert in 3.36, an equation which we numerically solve for $\sigma_{\rm max}$. The solution is shown in figure 3.2.2, which confirms that a naive guess for $M_{\rm max}$ where $\sigma_{\rm max} \sim 1$ is totally wrong. In fact, $\sigma_{\rm max}$ is so small that it typically takes many e-folds of MD for the overdensities to merely grow in a nonlinear manner.

Equipped with the solution $\sigma_{\rm max}(T_{\rm reh})$, we are ready to compute $M_{\rm min}$ and $M_{\rm max}$. In figure 3.2.3, $M_{\rm min}$ and $M_{\rm max}$ from equation 3.33 are plotted as a function of $T_{\rm reh}$. For a given reheating temperature $T_{\rm reh}$ and MD duration $\mathcal{A}$, the width of the produced PBH mass spectrum is given by the vertical range connecting the corresponding lower mass $M_{\rm min}$ (blue line, below) with the maximal mass $M_{\rm max}$ (black or gray). Note that when $\log_{10}\mathcal{A} \gtrsim 0$, i.e., when the duration of MD is very small, $M_{\rm min} = M_{\rm reh}$ (green line). As we increase $\log_{10}\mathcal{A}$, which is shown for integer values (light blue lines), $M_{\rm min}$ decreases (since MD commences earlier) and will eventually fall below the $M_{\rm max}$ line, which is shown for the combinations $(A_{\rm s}^+, n_{\rm s}^+, \alpha_{\rm s}^+)$ (black), $(A_{\rm s}, n_{\rm s}, \alpha_{\rm s})$ (dark gray), $(A_{\rm s}^-, n_{\rm s}^-, \alpha_{\rm s}^-)$ (light gray), corresponding to $+\sigma$, median, and $-\sigma$ values. In case of zero running of $n_{\rm s}$, this occurs for $\mathcal{A} \sim 10^5$. This is an important result: only if the duration of MD is greater than $\ln 10^5 = 11.5$ e-folds, may any PBH be expected to form. While a positive

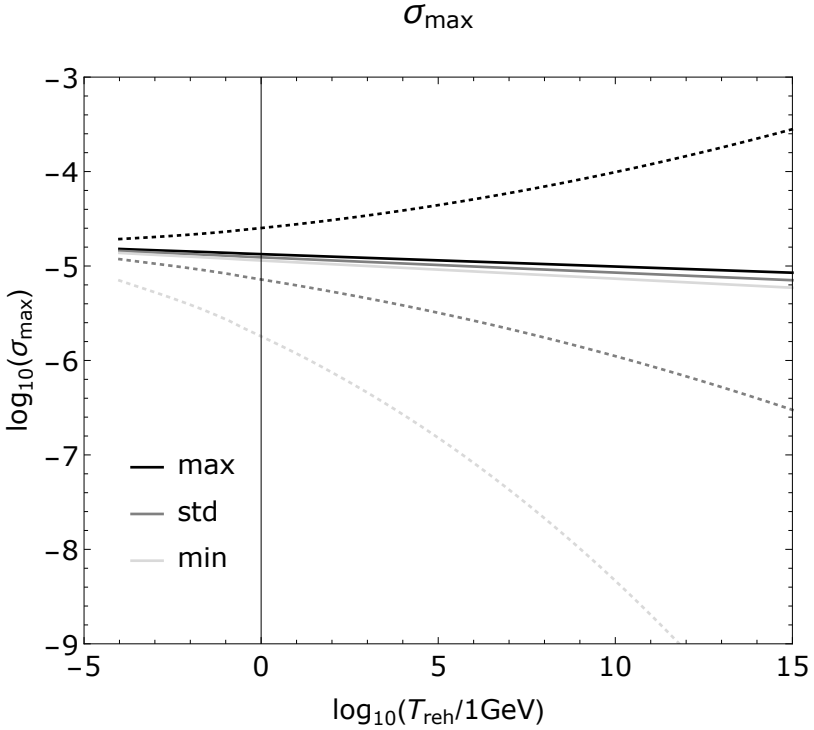

Figure 3.2.2: Plot of $\sigma_{\max}(T_{\rm reh})$, the numerical solution to 3.36, for the combinations $(A_{\rm s}^{+}, n_{\rm s}^{+}, \alpha_{\rm s}^{+})$ (black), $(A_{\rm s}, n_{\rm s}, \alpha_{\rm s})$ (dark gray), $(A_{\rm s}^{-}, n_{\rm s}^{-}, \alpha_{\rm s}^{-})$ (light gray), corresponding to $+\sigma$, median, and $-\sigma$ values. Solid lines neglect the running of $n_{\rm s}$, dashed lines include the running.

running may change this conclusion, as long as we stay within the 1σ-region of $\alpha_{\rm s}$, no PBHs are formed unless $\mathcal{A} > 10^4$. In case of negative running, the duration of MD must be even longer.

We can gain another very important piece of knowledge from figure 3.2.3: only for $T_{\rm reh} \lesssim 10^6$ GeV will PBHs form in the mass range of the strongest 21 cm PBH limits [68] (discussed in section 3.3.3). We will see how these bounds play the most important role, but for now, merely conclude that only for $T_{\rm reh} \lesssim 10^6$ GeV do we expect the 21 cm bounds to be important. If $T_{\rm reh} \ll 10^6$ GeV, the duration $\mathcal{A}$ must increase correspondingly to produce a PBH mass spectrum that extends into the 21 cm mass range mentioned above. This means, however, that the relative enhancement of the PBH fraction to radiation remains constant during a much longer period of MD, leading to a present PBH fraction that is lower since less time of relative enhancement could take place. This, therefore, means that it is only in the vicinity of $T_{\rm reh} \lesssim 10^6$ GeV that we expect the 21 cm limits to have the strongest constraining power. What this means will become clear in later sections.

We are almost ready to present the analytical form of the mass function $\psi(M)$. The

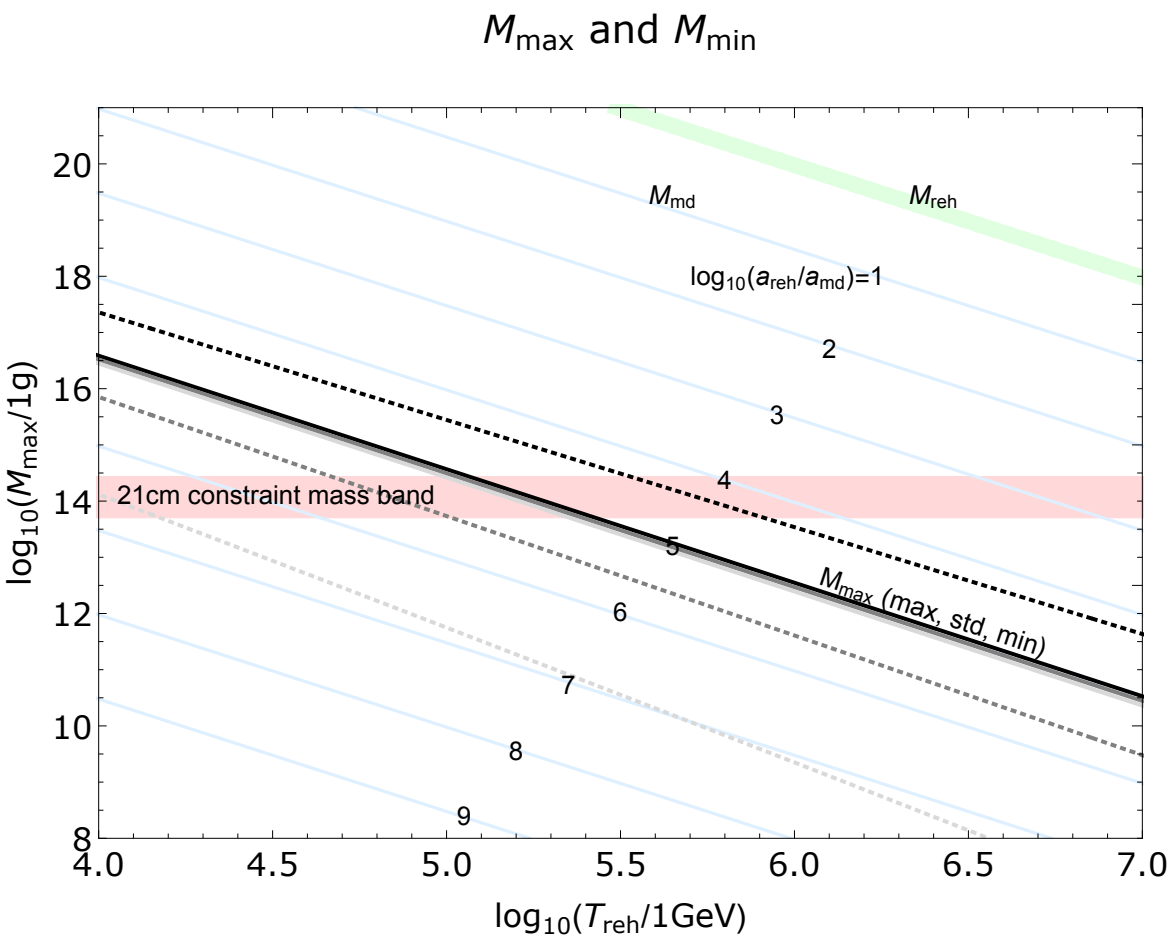

Figure 3.2.3: Plots of $M_{\rm max}$ and $M_{\rm min}$ as functions of the reheating temperature $T_{\rm reh}$, for various durations $\mathcal{A} \equiv a_{\rm reh}/a_{\rm md}$ of the MD epoch. $M_{\rm max}$ is shown for the combinations $(A_{\rm s}^+, n_{\rm s}^+, \alpha_{\rm s}^+)$ (black), $(A_{\rm s}, n_{\rm s}, \alpha_{\rm s})$ (dark gray), $(A_{\rm s}^-, n_{\rm s}^-, \alpha_{\rm s}^-)$ (light gray), corresponding to $+\sigma$, median, and $-\sigma$ values. The green line is the would-be smallest mass $M_{\rm min} = M_{\rm md}$ had MD lasted only very briefly, i.e., $\mathcal{A} \sim 1$. As we increase the duration $\log_1 0A$ in integer steps, $M_{\rm min}$ decreases. For successful PBH production, $\mathcal{A}$ must be large enough to make $M_{\rm min} < M_{\rm max}$.

only thing that is left is to relate the PBH mass M to the scale k at which an overdensity from which it formed entered the horizon, since given that relation, we could substitute k for M in 2.110, $\sigma = \frac{2}{5}\sqrt{\mathcal{P}_{\mathcal{R}}(k)}$, to express 3.23, $\beta(M) \simeq 0.056\sigma(M)^5$, as a function of the M. At horizon reentry, we then have

$$\begin{aligned} k = aH &= \frac{a}{a_{\rm reh}}\frac{a_{\rm reh}}{a_0}H = \left\{H \propto \frac{1}{a^{3/2}} \text{ during MD}\right\} \\ &= \left(\frac{H_{\rm reh}}{H}\right)^{2/3}\left(\frac{g_{*s}^0}{g_{*s}^{\rm reh}}\right)^{1/3}\frac{T_0}{T_{\rm reh}}H = \left(\frac{g_{*s}^0}{g_{*s}^{\rm reh}}\right)^{1/3}\frac{T_0}{T_{\rm reh}}\Gamma^{2/3}H^{1/3} \\ &= \left\{H = \frac{M_{\rm pl}^2}{2M}\right\} = \left(\frac{g_{*s}^0}{g_{*s}^{\rm reh}}\right)^{1/3}\frac{T_0}{T_{\rm reh}}\left(\frac{M_{\rm pl}^2\Gamma^2}{2M}\right)^{1/3}, \end{aligned} \tag{3.40}$$

i.e.,

$$\boxed{k \propto M^{-1/3}}. \tag{3.41}$$

where we used table 2.2.1, and equations 3.5 with $\gamma = 1$ and 2.52. This means that

$$\frac{k}{k_*} \equiv \left(\frac{M}{M_*}\right)^{-\frac{1}{3}} \tag{3.42}$$

where

$$M_* \equiv \left(\frac{k_{\rm reh}}{k_*}\right)^3 M_{\rm reh} = \left(\frac{k_{\rm reh}}{k_*}\right)^3 \frac{M_{\rm pl}^2}{2\Gamma\left(T_{\rm reh}\right)} \tag{3.43}$$

and

$$k_{\rm reh} = \left(\frac{g_{*s}^0}{g_{*s}^{\rm reh}}\right)^{1/3} \frac{T_0}{T_{\rm reh}} \Gamma\left(T_{\rm reh}\right). \tag{3.44}$$

Using 2.110, $\sigma = \frac{2}{5}\sqrt{\mathcal{P}_{\mathcal{R}}(k)}$, 3.23, $\beta(M) \simeq 0.056\sigma(M)^5$, and 2.138 for the power spectrum, we find

$$\begin{aligned}
\beta(M) &= 0.056 \cdot \left(\frac{2}{5}\right)^5 A_{\rm s}^{5/2} \left(\frac{k}{k_*}\right)^{\frac{5}{2}(n_{\rm s}-1)+\frac{5}{4}\alpha_{\rm s}\ln\left(\frac{k}{k_*}\right)} \\
&= 0.056 \left(\frac{2}{5}\right)^5 A_{\rm s}^{5/2} \left(\frac{M}{M_*}\right)^{-\frac{5}{6}(n_{\rm s}-1)-\frac{5}{12}\alpha_{\rm s}\ln\left(\frac{M}{M_*}\right)^{-\frac{1}{3}}} \\
&= 5.7 \cdot 10^{-4} A_{\rm s}^{5/2} \left(\frac{M}{M_*}\right)^{-\frac{5}{6}(n_{\rm s}-1)} e^{\frac{5}{36}\alpha_{\rm s}\ln^2\left(\frac{M}{M_*}\right)}
\end{aligned} \tag{3.45}$$

i.e.,

$$\boxed{\beta(M) = 5.7 \cdot 10^{-4} A_{\rm s}^{5/2} \left(\frac{M}{M_*}\right)^{-\frac{5}{6}(n_{\rm s}-1)} e^{\frac{5}{36}\alpha_{\rm s}\ln^2\left(\frac{M}{M_*}\right)}}, \tag{3.46}$$

where M_* is given by 3.43.

We are now equipped with the analytical results needed to express the mass function:

$$\boxed{\psi(M) = \begin{cases} \frac{T_{\rm reh}}{T_{\rm eq}} \frac{\beta(M)}{M} & (M_{\rm min} < M < M_{\rm max}) \\ 0 & (\text{ otherwise }) \end{cases}} \tag{3.47}$$

where $\beta(M)$ is given by 3.46, and $M_{\rm min}$ and $M_{\rm max}$ by 3.33.

This is one of the most important relations, as it provides a link between the curvature power spectrum and the mass spectrum of PBHs. We will use it extensively. The mass function is plotted for fixed MD duration $\mathcal{A} = \frac{a_{\rm reh}}{a_{\rm md}} = 10^7$ but different reheating

temperatures in figure 3.2.4.

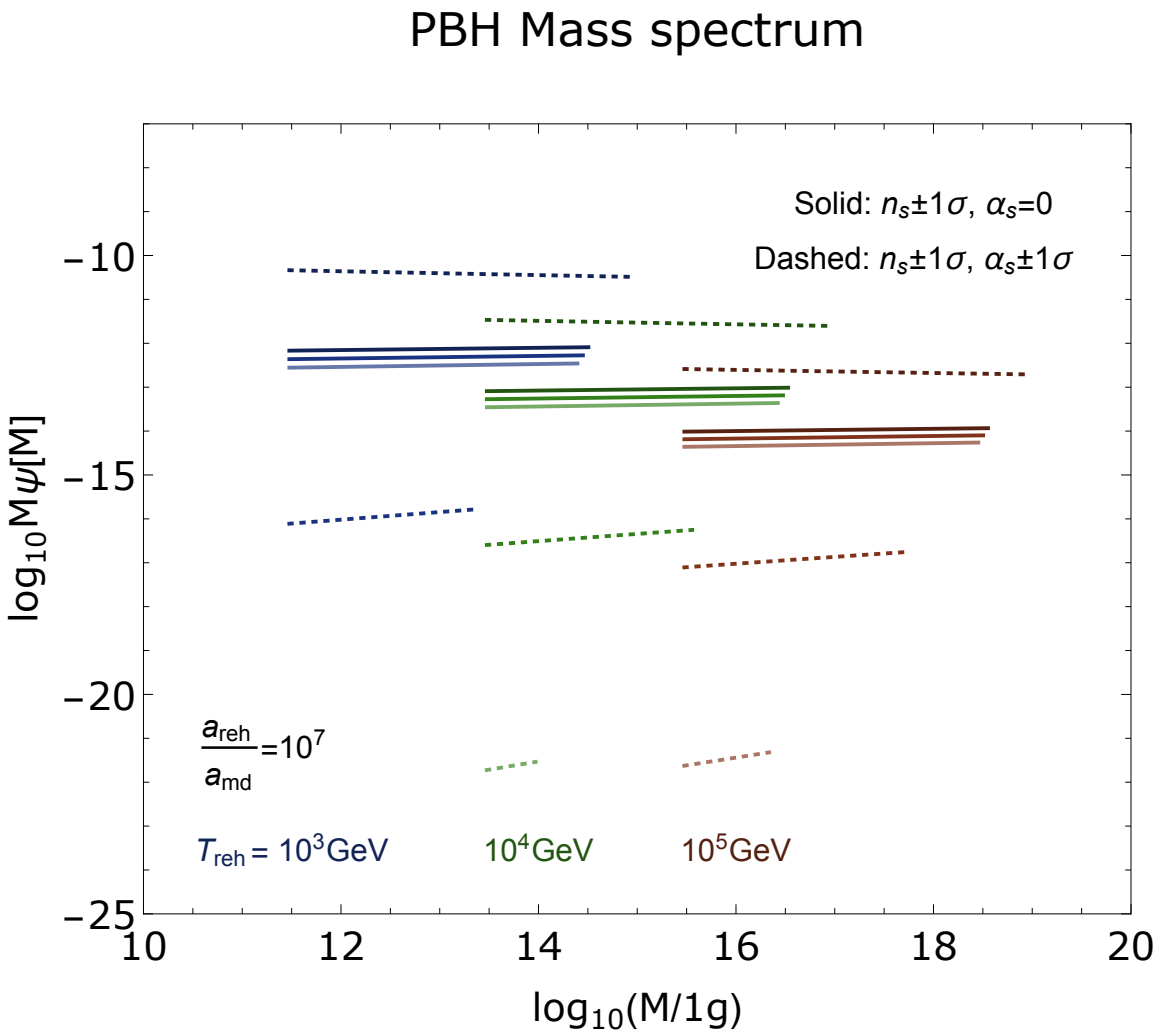

Figure 3.2.4: The mass function $\Psi(M)$. Plotted for fixed MD duration $\mathcal{A} = \frac{a_{\rm reh}}{a_{\rm md}} = 10^7$ but different reheating temperatures. Note that the $\alpha_{\rm s} - 1\sigma$ line has disappeared. This is because, in this case, the overdensities are so small that they must grow for a duration longer than that of MD in order to collapse against the pressure when RD sets in. Thus, no PBHs form.

3.3 Constraints

Constraints on PBH abundances are expressed as limits on the initial fraction β or the current (would-be) DM fraction$f$ and stem from various observational probes. For example, constraints may come from PBH evaporation, gravitational lensing, gravitational waves from PBH binary mergers, dynamical effects, and accretion [38]. For us, it turns out, only those due to evaporation are strong enough to be important in our attempt to place bounds on early MD, and the focus will henceforth mostly be on

these. Note that we implicitly assume that Hawking radiation is a correct prediction, as otherwise none of these constraints would be applicable. For completeness and comparability, the analysis will nevertheless include constraints over the whole mass range. Furthermore, any limits on PBHs are presented assuming a monochromatic mass function. In section 3.3.5, we will see how one can transition to an extended mass function while still using monochromatic constraints.

3.3.1 Effects of cosmological histories

Before we proceed, we would like to emphasize some often overlooked and implicitly assumed details regarding how PBH constraints are derived and presented. Most importantly, it is always assumed, unless explicitly stated otherwise, that PBHs form during RD. This is very important, since, as we will see, one must make assumptions on the expansion history of the universe to present constraints on the initial mass fraction $\beta(M)$, which is often the quantity that is constrained in the literature.

First, we consider the standard case of RD after inflation until EQ. We combine equation 2.53 and 2.50 to write $\rho_{\mathrm{r}} \approx 3sT/4$, which means

$$\beta_{\mathrm{RD}}(M) \equiv \frac{\rho_{\mathrm{PBH}}\left(t_{\mathrm{i}}\right)}{\rho\left(t_{\mathrm{i}}\right)} = \frac{4M}{3T_{\mathrm{i}}}\frac{n_{\mathrm{PBH}}(t)}{s(t)} = \frac{4M}{3T_{\mathrm{i}}}Y. \tag{3.48}$$

Equation 3.11, i.e.,

$$M = \gamma\frac{12\sqrt{10}}{\sqrt{g_*^i}}\frac{m_{\mathrm{pl}}^3}{T_{\mathrm{i}}^2},$$

relates the PBH mass to the formation temperature during RD.

Inverting this to express $T_{\mathrm{i}}(M)$ and inserting into equation 3.48 leads to

$$\beta_{\mathrm{RD}}(M) = \frac{4}{3}\left(\frac{\sqrt{g_*^{\mathrm{i}}}}{\gamma 12\sqrt{10}}\frac{M^3}{m_{\mathrm{pl}}^3}\right)^{1/2} Y, \tag{3.49}$$

which expresses the initial mass fraction as a function of the PBH mass M.

If they form intsead during MD,

$$\beta_{\mathrm{MD}} = \left(\frac{\rho_{\mathrm{PBH}}}{\rho_{\mathrm{tot}}}\right)_{\mathrm{i}} = \left(\frac{\rho_{\mathrm{PBH}}}{\rho_{\mathrm{reh}}}\right)_{\mathrm{reh}} = \frac{Mn_{\mathrm{PBH}}^{\mathrm{reh}}}{\frac{3}{4}s_{\mathrm{reh}}\,T_{\mathrm{reh}}} = \frac{4}{3}\frac{M}{T_{\mathrm{reh}}}Y \tag{3.50}$$

where we used that $\rho_{\rm PBH}$ evolves as matter until reheating, rendering the ratio $\rho_{\rm PBH}/\rho_{\rm tot}$ constant throughout MD, and evaluated $\rho_{\rm reh}$ assuming an abrupt transition to RD.

We note that 3.48 and 3.50 are similar only at the time of reheating and otherwise differ by a factor $T_{\rm i}/T_{\rm reh}$.

This difference is important to acknowledge because, in the literature, constraints are often presented as bounds on β, or β', which we will soon define (see the references [6, 34, 38] for a similar discussion). Given that the observations used to place limits on PBH abundances take place at late times, as long as one consistently uses the assumption of RD all the way from the end of inflation until EQ to both derive constraints on β and to convert back to late time abundances beyond EQ, artifacts of expansion history assumptions cancel. We will thus derive a relation between β and the current (would-be) DM fraction of PBHs f, assuming a standard cosmology with RD lasting from the end of inflation until EQ, since this is the assumption most often made when presenting constraints.

To do this, we express

$$f \equiv \left(\frac{\Omega_{\rm PBH}}{\Omega_{\rm DM}}\right)_{\rm now} = \frac{1}{\Omega_{\rm DM}}\frac{\rho_{\rm PBH}}{\rho_{\rm c}} = \frac{s_0}{\Omega_{\rm DM}}\frac{M}{\rho_{\rm c}}Y \tag{3.51}$$

which combined with 3.49 leads to

$$\begin{aligned} f_{\rm RD}(M) &= 106.75^{-1/4} \times \frac{3}{4}\sqrt{12\sqrt{10}} \times \frac{s_0 m_{\rm pl}^{3/2}}{\Omega_{\rm DM}\rho_{\rm c}} M^{-1/2} \left[\gamma^{1/2}\left(\frac{h}{0.674}\right)^{-2}\left(\frac{g_*^{\rm i}}{106.75}\right)^{-1/4}\beta_{\rm RD}(M)\right] \\ &\equiv 3.77 \times 10^8 \beta'_{\rm RD}(M)\left(\frac{M}{M_\odot}\right)^{-1/2} \\ &= 5.31 \times 10^{17}\beta'_{\rm RD}(M)\left(\frac{M}{10^{15}\,\mathrm{g}}\right)^{-1/2} \end{aligned} \tag{3.52}$$

where we defined

$$\boxed{\beta'_{\rm RD}(M) \equiv \gamma^{1/2}\left(\frac{g_*^{\rm i}}{106.75}\right)^{-1/4}\left(\frac{h}{0.674}\right)^{-2}\beta_{\rm RD}(M)}. \tag{3.53}$$

and used $s_0 = 2.234 \times 10^{-26}$ GeV^3 and 2.27 for ρ_c. We conclude,

$$\boxed{f_{\rm RD}(M) = 3.77 \times 10^8 \beta'_{\rm RD}(M) \left(\frac{M}{M_\odot}\right)^{-1/2} = 5.31 \times 10^{17} \beta'_{\rm RD}(M) \left(\frac{M}{10^{15}\,\text{g}}\right)^{-1/2}}. \quad (3.54)$$

Similar expressions have been derived in, e.g., [23]. Note that, in our case, we will set $\gamma = 1$, $h = 0.674$, and since we will consider mostly $T_{\rm reh} > 10^2$ GeV for which $g_*^{\rm i} \sim 106.75$, we have that $\beta'_{\rm RD}(M) \sim \beta_{\rm RD}(M)$. We will often drop the subscript RD.

For MD, we instead have

$$f_{\rm MD} = \frac{3}{4\Omega_{\rm DM}} \frac{s_0}{\rho_c} T_{\rm reh} \beta_{\rm MD} = 1.73 \times 10^9 \left(\frac{T_{\rm reh}}{1\,\text{GeV}}\right) \beta_{\rm MD}, \quad (3.55)$$

which should have been used, had the constrains been derived with the assumption of PBH formation during an MD epoch lasting until $T_{\rm reh}$. The dependence on $T_{\rm reh}$ makes this form very unappealing because the presented constraints would depend on what value of the reheating temperature one chooses. Perhaps more naturally, constraints should be presented as limits on the yield Y. Since this is not typically done in the literature on PBHs, we do not pursue this further but content ourselves with expression 3.54.

3.3.2 Various PBH constraints

Non-evaporated PBHs

Non-evaporated PBHs are those that have not fully evaporated, i.e., those for which the mass at formation $M > M_\star \approx 5 \times 10^{14}$ g. These will still contribute to the DM fraction, making equation 3.54 directly applicable if we neglect mass loss, which is a good approximation for $M > 2M_*$ [22], and assume RD until EQ. Limits on non-evaporated PBHs are derived from PBHs that are small enough ($M_\star < M \lesssim 10^{17}$ g) to emit significant amounts of radiation, gravitational lensing observations, various dynamical effects, accretion onto PBHs, and observations of gravitational waves [22].

Evaporated PBHs

We saw that PBHs whose mass $M < M_\star \approx 5 \times 10^{14}$ g have just evaporated. Below this mass, PBHs no longer contribute to the energy density of the universe but can be

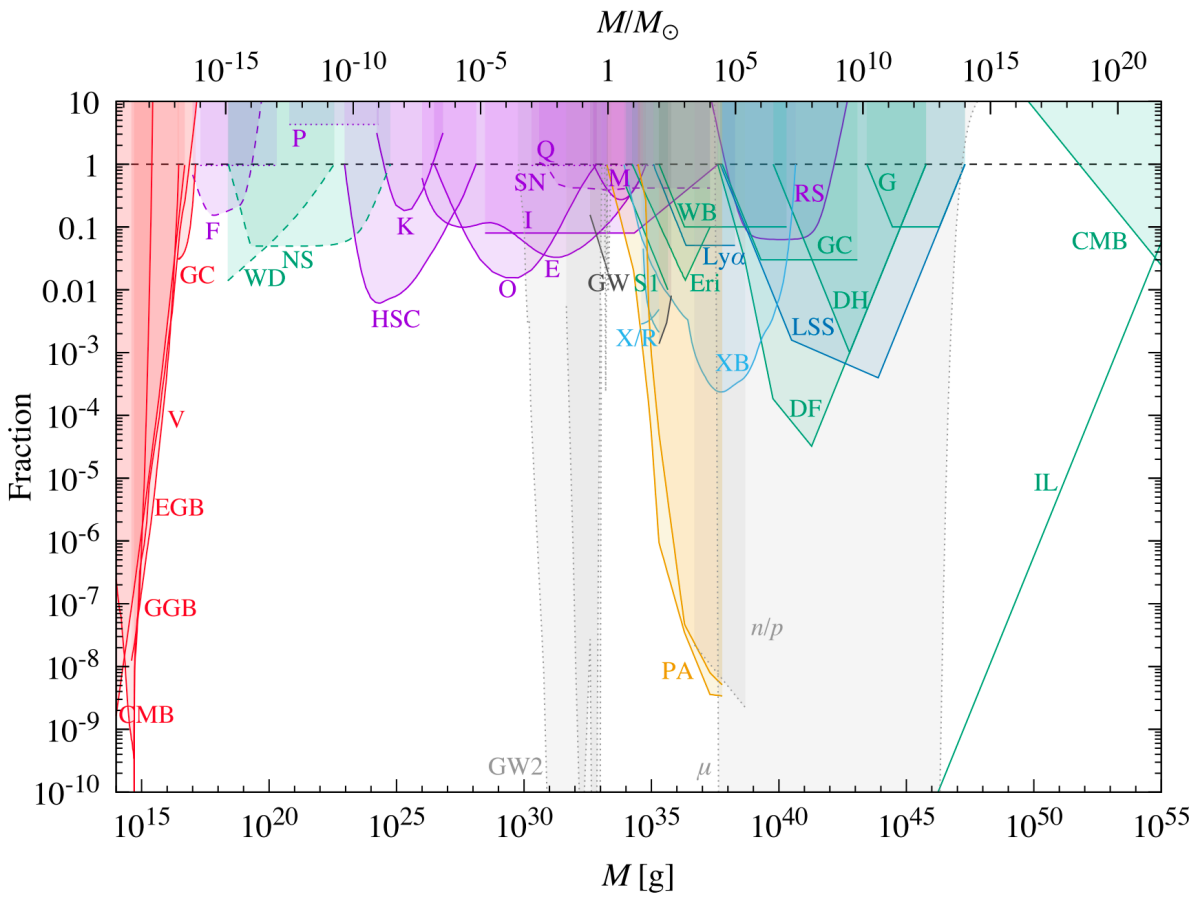

Figure 3.3.1: Compiled up-to-date (monochromatic) constraints on the mass fraction $f(M)$ for non-evaporated PBHs. Solid lines represent constraints that are considered secure, whereas dashed lines are uncertain and probably incorrect. We will use the solid lines for the present analysis. Adapted from [22], to which we refer the reader for details.

probed by the effect their emission products would have on the environment. Because these black holes do not contribute to the DM fraction, limits are often presented in terms of the initial mass fraction $\beta(M)$ (assuming RD from the end of inflation until EQ). We will, nevertheless, apply equation 3.54 to compute the would-be DM fraction $f(M)$ had they not evaporated.

Excluding the limits from 21 cm observations, which we discuss in the next section, an up-to-date summary of evaporation constraints is provided in [22], which we adapt for presentation in figure 3.3.2

3.3.3 Constraints from 21 cm observations

21 cm cosmology probe the cosmic dark ages, namely, the period between the time of last scattering, forming the cosmic microwave background (CMB) at $z \sim 1100$, and

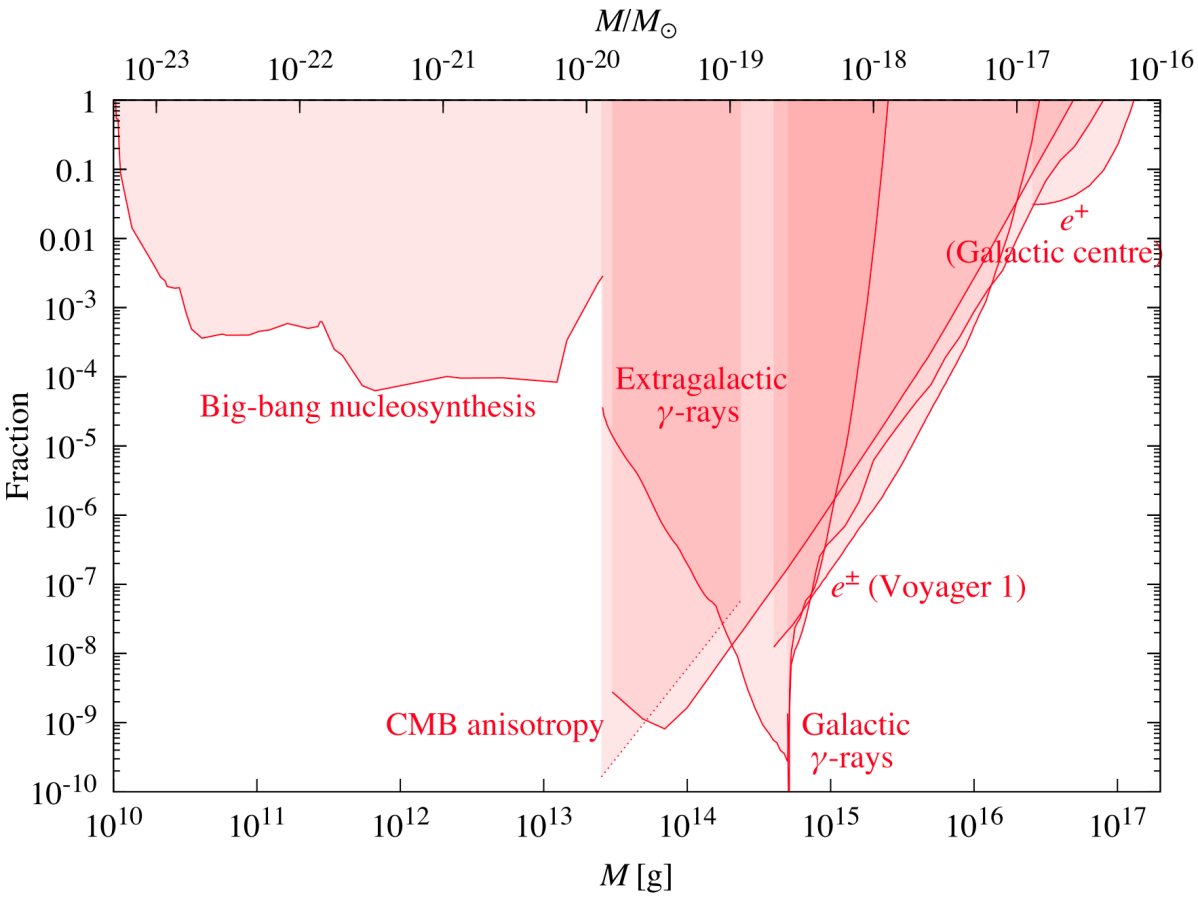

Figure 3.3.2: Compiled up-to-date (monochromatic) evaporation constraints on the would-be fraction $f(M)$. Adapted from [22], to which we refer the reader for details.

reionization, marked by the production of stars and other sources of light at $z \sim 10$. It is the hyperfine spin-flip transition of neutral hydrogen that gives rise to the emission or absorption of photons of 21 cm wavelength. The appearance as an emission or absorption feature, or lack thereof, in the photon spectrum is what 21 cm observations aim to detect. At present, this signal has redshifted to an observed wavelength of $21(1+z)$ cm. Given that the redshift z increases monotonically with radial distance, 21 cm observations could generate a three-dimensional map of the universe over a vast redshift range. This data could be sensitive to new physics and possibly the presence of a population of PBHs [58]. We will pursue this possibility in this work and review some of the work that has been done on the topic [28, 58, 68, 69].

21 cm cosmology

The sensitivity to new physics comes about because of the dependence of the 21 cm signal on the temperature evolution of the intergalactic medium (IGM). To describe

the evolution of the IGM, it is necessary to track the kinetic temperature of the gas T_{K}, the ionization fraction $x_{\mathrm{H_I}}$, and the spin temperature T_{S}. Neutral hydrogen absorbs CMB photons at the resonance energy of 1.42GHz, leading to a transition from the anti-aligned spin-0 singlet state of the electron-nucleus system to the excited aligned spin-1 triplet state. The ratio of the population numbers of exited spin-1 states to relaxed spin-0 states is determined by the spin temperature T_{S} as [28]

$$N_1/N_0 = 3\mathrm{e}^{-0.068\ \mathrm{K}/T_{\mathrm{S}}}. \tag{3.56}$$

where 0.068 K is the transition energy in units of Kelvin. The degree to which CMB photons are absorbed is determined by the 21 cm brightness temperature [69]

$$T_{21} \approx 0.023\ \mathrm{K} \cdot x_{\mathrm{H_I}}(z) \left(\frac{0.15}{\Omega_{\mathrm{m}}} \cdot \frac{1+z}{10}\right)^{\frac{1}{2}} \frac{\Omega_{\mathrm{b}} h}{0.02} \left(1 - \frac{T_{\mathrm{CMB}}}{T_{\mathrm{s}}}\right) \tag{3.57}$$

where $x_{\mathrm{H_I}}$ is the fraction of neutral hydrogen to the total amount of hydrogen in the IGM, T_{CMB} is the photon temperature of the CMB, and Ω_{m} and Ω_{b} the total matter and baryon fractions of the critical energy density. Before reionization at $z \sim 20$, $x_{\mathrm{H_I}} \approx 1$ in standard cosmology. Absorption ($T_{21} < 0$) or emission ($T_{21} > 0$) occurs when the spin temperature T_{s} deviates from T_{CMB} and $x_{\mathrm{H_I}} > 0$. Thus, for the case of absorption, $T_{\mathrm{S}} < T_{\mathrm{CMB}}$, which could be caused by IGM heating from decaying DM or evaporating PBHs.

Naively, as soon as hydrogen decouples from the CMB at around $z \sim 200$, it will evolve like $T_{\mathrm{K}} \propto a^{-2} \propto (1+z)^2$, while $T_{\mathrm{CMB}} = 2.7\ \mathrm{K} \cdot (1+z)$. Thus, the IGM temperature decreases faster than the CMB in the absence of other energy transferring processes, and we expect to see the 21 cm feature in absorption. However, gradually the CMB photons will excite neutral hydrogen to the spin-1 state, increasing T_{S}, while its kinetic gas temperature T_{K} maintains its $a^{-2} \propto (1+z)^2$ scaling. As stars begin to form, they begin reionizing the universe. The transition from the 2nd to 1st electron orbital leads to emission of the Lyman-α photons which re-couple T_{K} to T_{S} via the Wouthuysen-Field effect [67]. As a consequence, T_{S} approaches T_{K} and regains the $a^{-2} \propto (1+z)^2$ scaling. The evolution of T_{K}, T_{CMB}, and T_{S} for standard cosmology without energy injection from new physics has been solved for and presented in [28], a result we adapt for presentation in figure 3.3.3. An absorption feature is now expected to emerge, because T_{S} gets coupled to T_{K} and drops suddenly. According to 3.57, T_{21} then also

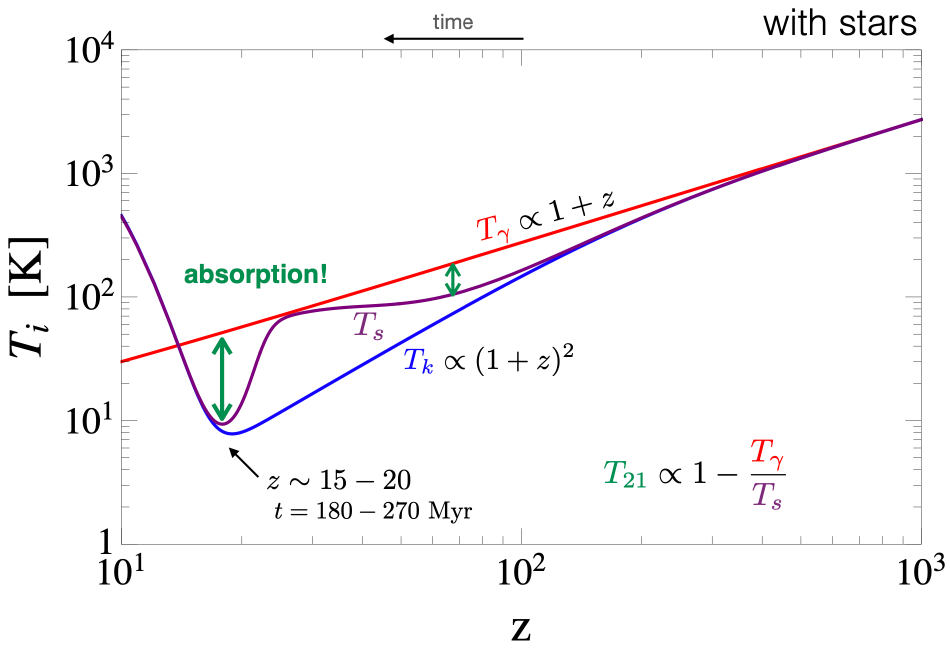

Figure 3.3.3: Evolution of $T_{\rm K}$, $T_{\rm CMB}$ (here denoted as T_γ) and $T_{\rm S}$ for a standard cosmology without energy injection from new physics. Adapted from [63].

drops because of the increased ratio $T_{\rm CMB}/T_{\rm S}$, which implies absorption.

EDGES

On the first of March 2018 [15] reported in Nature that the *Experiment to Detect the Global Epoch of Reionization Signature*, EDGES, had observed a "flattened absorption profile in the sky-averaged radio spectrum, which is centered at a frequency of 78 megahertz and has a best-fitting full-width at half-maximum of 19 megahertz and an amplitude of 0.5 kelvin." They report that this observation coincides with predictions of an absorption feature due to reionization by early starts, but that, very importantly, the amplitude is more than twice as large as expected from even the largest predictions. They interpret this as if either the IGM gas "was much colder than expected, or the background radiation temperature was hotter than expected," both of which would reduce the 21 cm brightness temperature T_{21} according to 3.57.

This discovery prompted studies to constrain DM scenarios [28, 33, 55, 68], with the argument that any model of DM that heats the IGM, e.g., via the decay of DM particles or PBH evaporation, would suppress the 21 cm absorption feature. It has been shown that PBHs of masses 6×10^{13} g $\lesssim M \lesssim 3 \times 10^{14}$ g are subject to the strongest constraints from 21 cm observations [68], and future 21 cm observations may lead to strong constraints at both larger and smaller masses [58]. In [68], one of their main

results is a constraint plot, including their own results and potential 21 cm constraints from [58], which we adapt for presentation in figure 3.3.4.

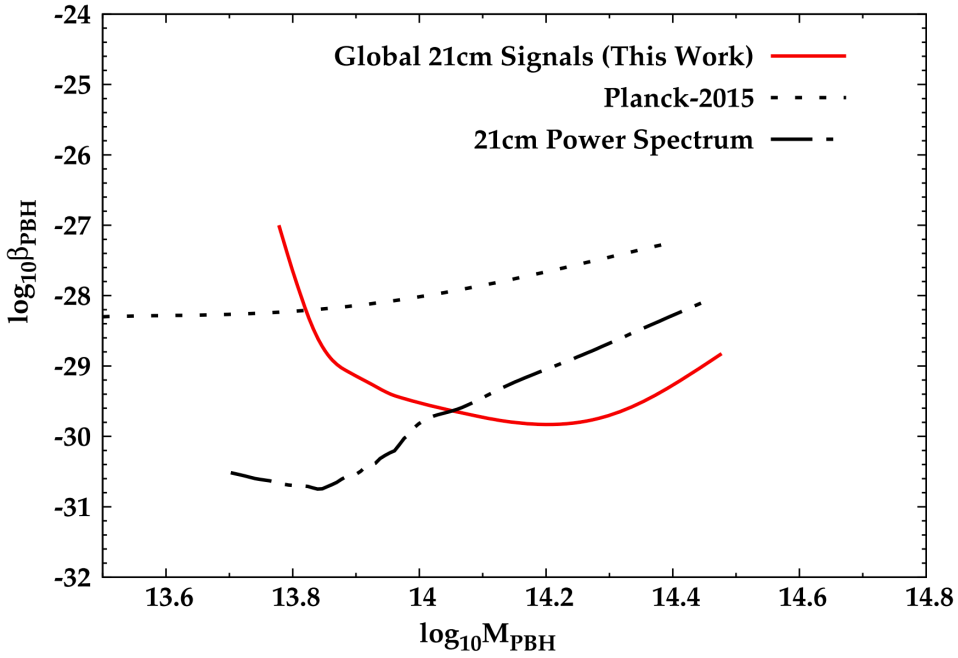

Figure 3.3.4: Constraints on PBHs derived from 21 cm observations by EDGES [68] and potential 21 cm constraints [58]. Adapted from [68], to which we refer the reader for details.

These constraints are the strongest to date and will prove to be the most important. While these limits are strong, they are not directly derived from EDGES data but assume that the global differential brightness temperature of the 21 cm signal be $T_{21} \lesssim -100$ mK for a 21 cm absorption feature in the same redshift range as that of the EDGES signal. Note that this is much shallower than $T_{21} \sim -500$ mK, according to the the result presented in [15]. One should furthermore comment on that EDGES requires new physics to explain the signal. PBHs would not be part of this new physics, since they would merely weaken the signal. Thus, PBHs and new physics would compete, partially canceling the effects of each other. However, to make use of the results in [68], we assume that the excess absorption is due to modeling errors and other issues [45, 64]. We discuss this further in section 4.2. In this case, $T_{21} \lesssim -100$ mK might be a conservative assumption, and the actual PBH constraints could in principle be much stronger.

3.3.4 Combined constraints

In this work, we combine the 21 cm constraints (figure 3.3.4) with those from evaporating PBHs (figure 3.3.2) and from non-evaporated PBHs (figure 3.3.1), to form a new set of PBHs limits covering a broad mass range. Note that we exclude the dashed lines in figure 3.3.1 since they are very uncertain and probably incorrect [22]. To convert the 21 cm constraints in figure 3.3.4, which are presented as bounds on $\beta'(M)$, to bounds on the (would-be) DM fraction f we use equation 3.54. The resulting limits are shown in figure 3.3.5 These are the constraints we adapt for the present

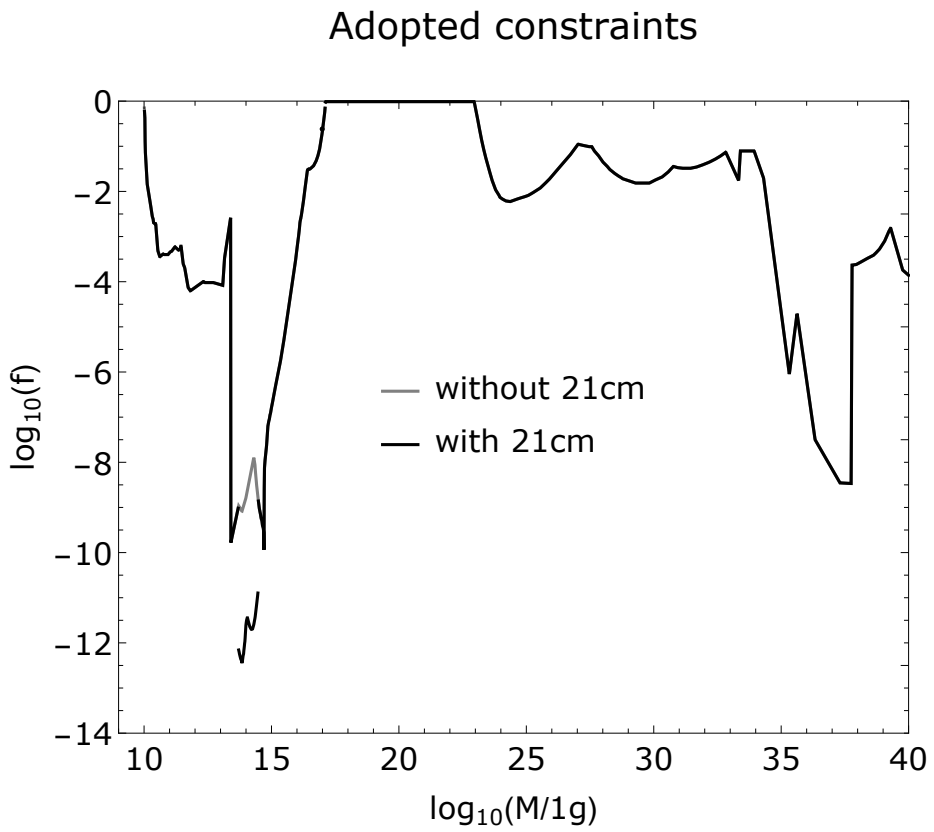

Figure 3.3.5: Combined constraints on PBHs from 21 cm observations (figure 3.3.4), evaporating PBHs (figure 3.3.2), and non-evaporated PBHs (figure 3.3.1). We exclude the dashed lines in figure 3.3.1 due to uncertainties [22]. To convert the 21 cm constraints in figure 3.3.4, which are presented as bounds on $\beta'(M)$, to bounds on the (would-be) DM fraction f we use equation 3.54.

analysis. It should be emphasized that these are constraints on monochromatic mass functions, thus assuming that all PBHs are formed with the same mass M. We will see next in section 3.3.5 how monochromatic constraints may be used to place bounds on extended mass functions.

3.3.5 Constraints for extended mass functions

To account for extended mass functions, provided only monochromatic constraints, is a nontrivial matter. In [25], they introduce a method to generalize monochromatic constraints to any PBH mass function $\psi(M)$ normalized to $f = \int \psi(M)\mathrm{d}M$, and do this by arguing as follows.

An astrophysical observable $A[\psi(M)]$ (such as the number of lensing events), can be expanded as

$$\begin{aligned} A[\psi(M)] &= A_0 + \int \mathrm{d}M \psi(M) K_1(M) \\ &+ \int \mathrm{d}M_1 \, \mathrm{d}M_2 \psi\left(M_1\right) \psi\left(M_2\right) K_2\left(M_1, M_2\right) + \ldots \end{aligned} \tag{3.58}$$

for some background A_0 and functions K_i depending on the specific physical processes behind the measurement. Furthermore, if PBHs of different masses contribute to the observable A independently of each other, 3.58 may be truncated after the first two terms, which result in the requirement

$$\boxed{\int \frac{\psi(M)}{f_{\max}(M)} \mathrm{d}M \leq 1}, \tag{3.59}$$

where, for an observed limit limit $A[\psi(M)] \leq A_{\text{exp}}$,

$$f_{\max}\left(M_{\mathrm{c}}\right) \equiv \frac{A_{\text{exp}} - A_0}{K_1\left(M_{\mathrm{c}}\right)} \tag{3.60}$$

is the maximally allowed fraction of PBH as DM for a monochromatic mass function at M_{c}. A caveat with this method is that, physically, it only make sense in case of non-evaporated PBHs, since otherwise $f \equiv 0$. However, we may still formally define f neglecting PBH absorption, as we have done before, interpreting f as the would-be DM fraction in PBHs, had PBHs not evaporated. Then, we can formally use 3.59 below $M < M_\star \approx 5 \times 10^{14}$ g. In [25], they note that the mass function may evolve nontrivially if PBHs merge or new black holes form of similar masses. We proceed without further considering such effects.

Equation 3.59 is strictly valid only if applied to each observable A independently. Applied to a set of observables, one must add the contributions in quadrature as

$$\sum_{j=1}^{N} \left(\int \mathrm{d}M \frac{\psi(M)}{f_{\max,j}(M)} \right)^2 \leq 1. \tag{3.61}$$

At any given mass, however, for most parts one observable dominates over the others, rendering the effect of all others insignificant. Furthermore, we are overwhelmingly dominated by the 21 cm bounds which will dominate the sum in 3.61. We, therefore, proceed with the insight that 3.61 should be approximated by 3.59, and declare the use of 3.59 with $f_{\max}$ given by figure 3.3.5 throughout this work.

3.4 Constraining early MD

We are now equipped with the necessary framework and tools to translate the limits on PBHs to the limits on early matter domination. The necessary ingredients are the following:

The assumption of formation during MD leads us to the expression 3.47,

$$\psi(M) = \begin{cases} \frac{T_{\text{reh}}}{T_{\text{eq}}} \frac{\beta(M)}{M} & (M_{\min} < M < M_{\max}) \\ 0 & (\text{ otherwise }) \end{cases} , \tag{3.62}$$

which, combined with the initial mass fraction 3.46,

$$\beta(M) = 5.7 \cdot 10^{-4} A_s^{5/2} \left(\frac{M}{M_*}\right)^{-\frac{5}{6}(n_s-1)} e^{\frac{5}{36}\alpha_s \ln^2\left(\frac{M}{M_*}\right)}, \tag{3.63}$$

and the range of masses 3.33,

$$M_{\min} = \frac{M_{\text{pl}}^2}{2\Gamma} \mathcal{A}^{-3/2}, \quad M_{\max} = \frac{M_{\text{pl}}^2}{2\Gamma} \sigma_{\max}^{3/2}, \tag{3.64}$$

predicts the shape of the mass function $\psi(M)$. To evaluate this numerically, we assume the power spectrum amplitude A_{s}, spectral index n_{s}, and running α_{s}, to take values given by 2.139 [3],

$$\begin{aligned} \ln\left(10^{10} A_{\text{s}}\right) &= 3.043 \pm 0.014 \quad (67\%\ \text{CL}\ ) \\ n_{\text{s}} &= 0.9649 \pm 0.0042 \quad (67\%\ \text{CL}) \\ \alpha_{\text{s}} &= -0.0045 \pm 0.0067 \quad (68\%\text{CL}) \end{aligned} , \tag{3.65}$$

which enter the power spectrum expansion 2.138 as,

$$\mathcal{P}_{\mathcal{R}}(k) = A_s \left(\frac{k}{k_0}\right)^{n_{\text{s}}-1+\frac{1}{2}\alpha_{\text{s}} \ln\left(\frac{k}{k_0}\right)} . \tag{3.66}$$

Equipped with this prediction of $\psi(M)$, we find what region of the parameter space $(T_{\rm reh},\ \mathcal{A})$ leads to a violation of 3.59,

$$\int \frac{\psi(M)}{f_{\rm max}(M)} \mathrm{d}M \leq 1. \tag{3.67}$$

If a violation is found, we conclude that the theory predicts a PBH abundance larger than that permitted by the PBH bounds, and we must therefore declare the corresponding MD epoch during which the PBHs formed incompatible with current limits.

To present the result of this computation, the function

$$I_f \equiv \int \frac{\psi(M)}{f_{\rm max}(M)} \mathrm{d}M \tag{3.68}$$

is defined. Contours of I_f are then plotted in the $(T_{\rm reh}, \mathcal{A})$-plane. The result is presented with and without the inclusion of the 21 cm constraints in figures 3.4.1 and 3.4.2. The first row of plots in each figure represents the case of zero running $\alpha_{\rm s} = 0$, whereas the second row includes the running. Figure 3.4.1 includes 21 cm constraints whereas 3.4.2 does not.

Regions where $I_f < 1$ are marked by green, while regions where $I_f > 1$ are marked red. Overlaid in the same plot are also contours of the DM fraction f. We immediately note some features that we already expected and mentioned in the comments to figure 3.2.3 (i): Only when $\mathcal{A} = a_{\rm reh}/a_{\rm md}$ exceed $\sim 10^5$ does f become non-zero. In other words, PBHs form only when the duration of the MD epoch is long enough, and this limit is marked by the transition from white to green color. Because of the scale dependence of the power spectrum, this line is neither exactly horizontal nor flat, as is clear from the second row of plots with non-zero running α. (ii): The regions where MD is constrained coincides with the 21 cm mass band in figure 3.2.3. As the reheating temperature, $T_{\rm reh}$, creeps lower, the largest PBH of mass $M_{\rm max}$ (and thus the last to form) begin to fall within the range of masses covered by the 21 cm constraints. This is precisely when bounds on MD start to emerge since the 21 cm constraints are the strongest. As $T_{\rm reh}$ decreases further, more and more of the mass function ψ falls within this mass band, strengthening and broadening the MD bounds. Eventually $M_{\rm max}$ exits the 21 cm mass band, in which case $\mathcal{A}$ must increase further and further to produce PBHs of smaller mass that would still fall within the mass band. In this case, there is less time for the

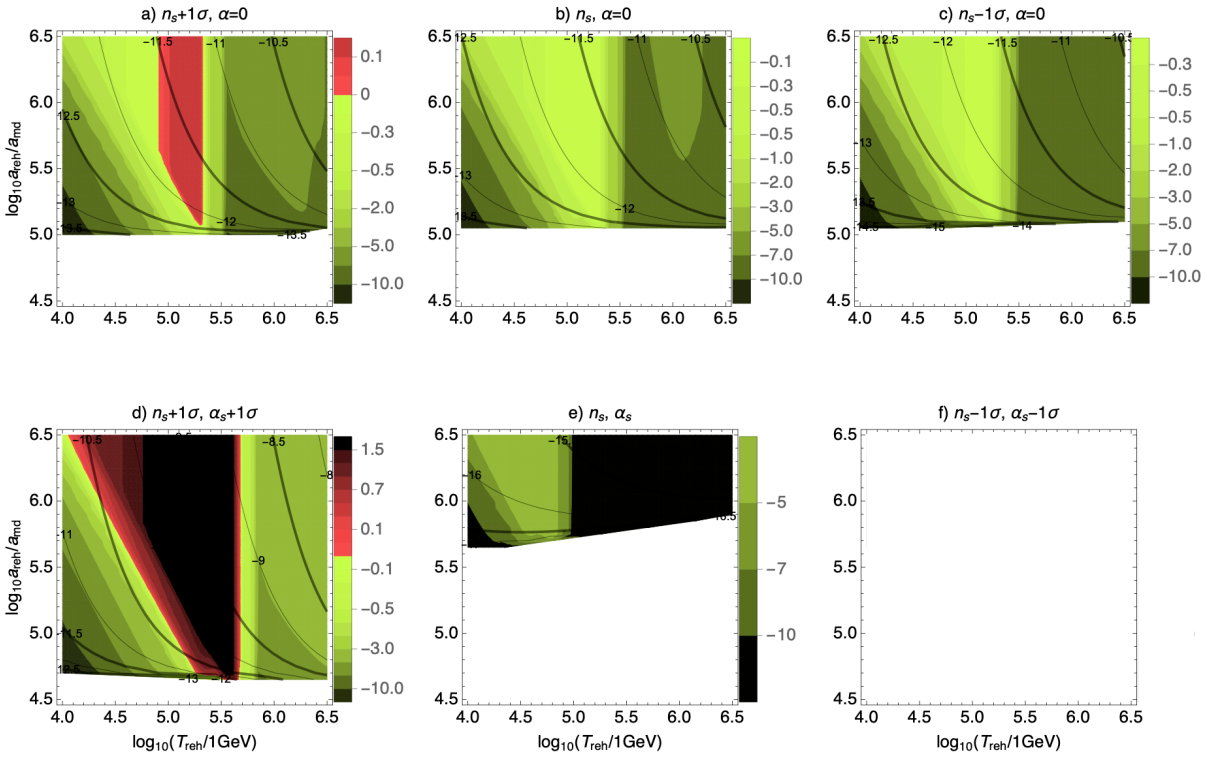

Figure 3.4.1: Contours of I_f plotted in the ($T_{\rm reh}$, $\mathcal{A}$)-plane computed using constraints including the 21 cm limits. Regions where $I_f < 1$ (allowed) are marked by green, while regions where $I_f > 1$ (excluded) are marked red. The black lines are contours of the DM fraction f. White regions mean no PBHs are formed. The upper row neglects the running, i.e., $\alpha_{\rm s} = 0$. The lower row includes the running.

PBH density to increase relative to radiation, leading to a lower PBH fraction f. Thus, at a certain point, simply extending the duration of MD is not sufficient to push I_f above 1, and we can no longer constrain MD. This explains the wedge shape of the bounds. Regarding figure 3.4.2, which we include for comparison, there is not much to say, as it is now apparent that without the 21 cm constraints, we may place no bounds on MD. This is why the 21 cm observations are so important.

3.5 Constraining $n_{\rm s}$ and $\alpha_{\rm s}$

Constraints on $n_{\rm s}$ and $\alpha_{\rm s}$ are obtained by finding for what values of $n_{\rm s}$ and $\alpha_{\rm s}$ equation 3.59 evaluates to 1. Any value $n_{\rm s}$ and $\alpha_{\rm s}$ larger than this is then constrained. We present the constraints as a function of reheating temperature for various durations $\mathcal{A} = a_{\rm reh}/a_{\rm md}$ of the MD epoch. In constraining the spectral index $n_{\rm s}$, we take the running $\alpha_{\rm s} = 0$, and $A_{\rm s}^+$ (black), $A_{\rm s}$ (dark gray), and $A_{\rm s}^-$ (light gray), corresponding

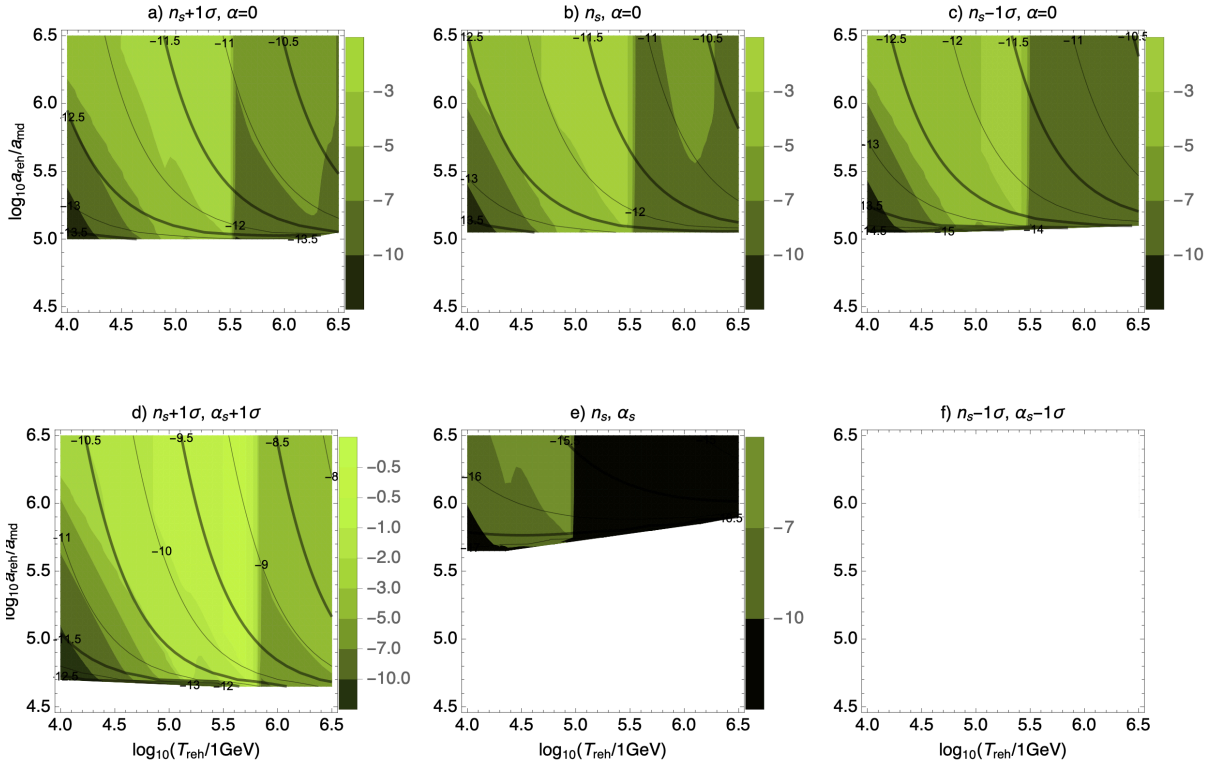

Figure 3.4.2: Contours of I_f plotted in the ($T_{\rm reh}$, $\mathcal{A}$)-plane computed using constraints excluding the 21 cm limits. Regions where $I_f < 1$ (allowed) are marked by green. The black lines are contours of the DM fraction f. White regions mean no PBHs are formed. The upper row neglects the running, i.e., $\alpha_{\rm s} = 0$. The lower row includes the running. Since $I_f < 1$ everywhere, there are no bounds on early MD.

to $+\sigma$, median, and $-\sigma$ values. For the running, we obtain constraints on $\alpha_{\rm s}$ for the combinations $(A_{\rm s}^+, n_{\rm s}^+)$ (black), $(A_{\rm s}, n_{\rm s})$ (dark gray), $(A_{\rm s}^-, n_{\rm s}^-)$ (light gray).

The results are presented in figures 3.5.1 and 3.5.2.

Qualitatively, both figures reflect the same result: the larger $n_{\rm s}$ and $\alpha_{\rm s}$, the larger the power spectrum $\mathcal{P}_\nabla(k)$, the more PBHs are produced, which leads to stronger constraints. Once again, we see that the constraints are the strongest around $T_{\rm reh} \sim 10^5$ GeV and that for large reheating temperatures $T_{\rm reh} \gtrsim 10^6$ GeV, the constraints weaken due to the largest PBH mass $M_{\rm max}$ falling below the strong evaporation and 21 cm constraint mass window. Once $M_{\rm max}$ falls within or exceeds the 21 cm constraints mass window, we can always extend the MD duration to produce PBHs in the the 21 cm mass window. However, this comes at the cost of reducing the relative enhancement of PBHs during the period of RD, leading to progressively less stringent constraints as we decrease $T_{\rm reh}$.

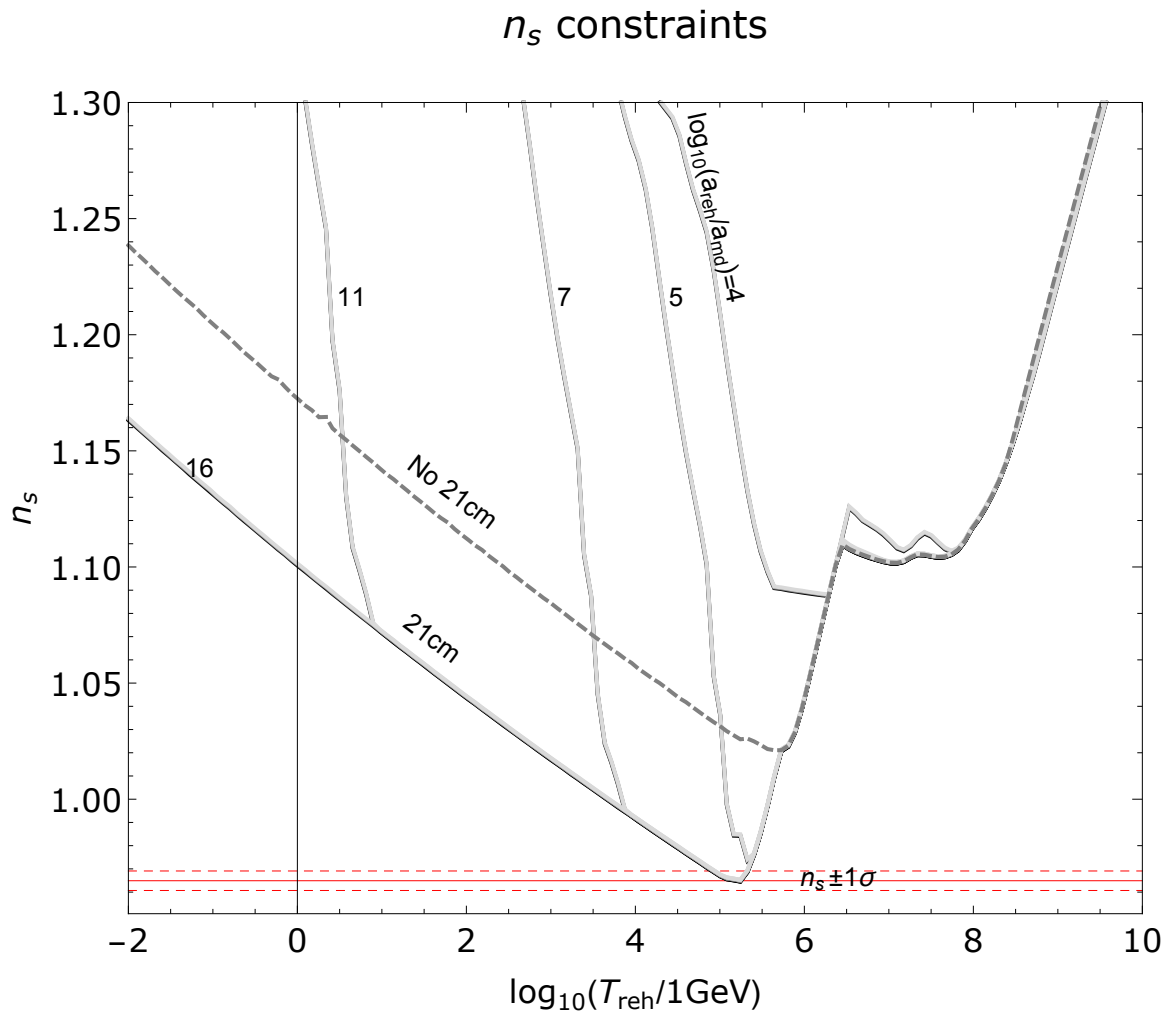

Figure 3.5.1: Constraints on the spectral index n_s, assuming PBH formation during an early MD epoch of duration $\mathcal{A} = a_{\rm reh}/a_{\rm md}$ and reheating temperature $T_{\rm reh}$. We take the running $\alpha_s = 0$, and obtain the constrains for A_s^+ (black), A_s (dark gray), and A_s^- (light gray), corresponding to $+\sigma$, median, and $-\sigma$ values. Note that the difference is so small that the lines almost coincide. The dashed gray line is included for reference and shows the constraints neglecting 21 cm PBH bounds for an MD epoch duration longer than $\mathcal{A} > 10^{16}$.

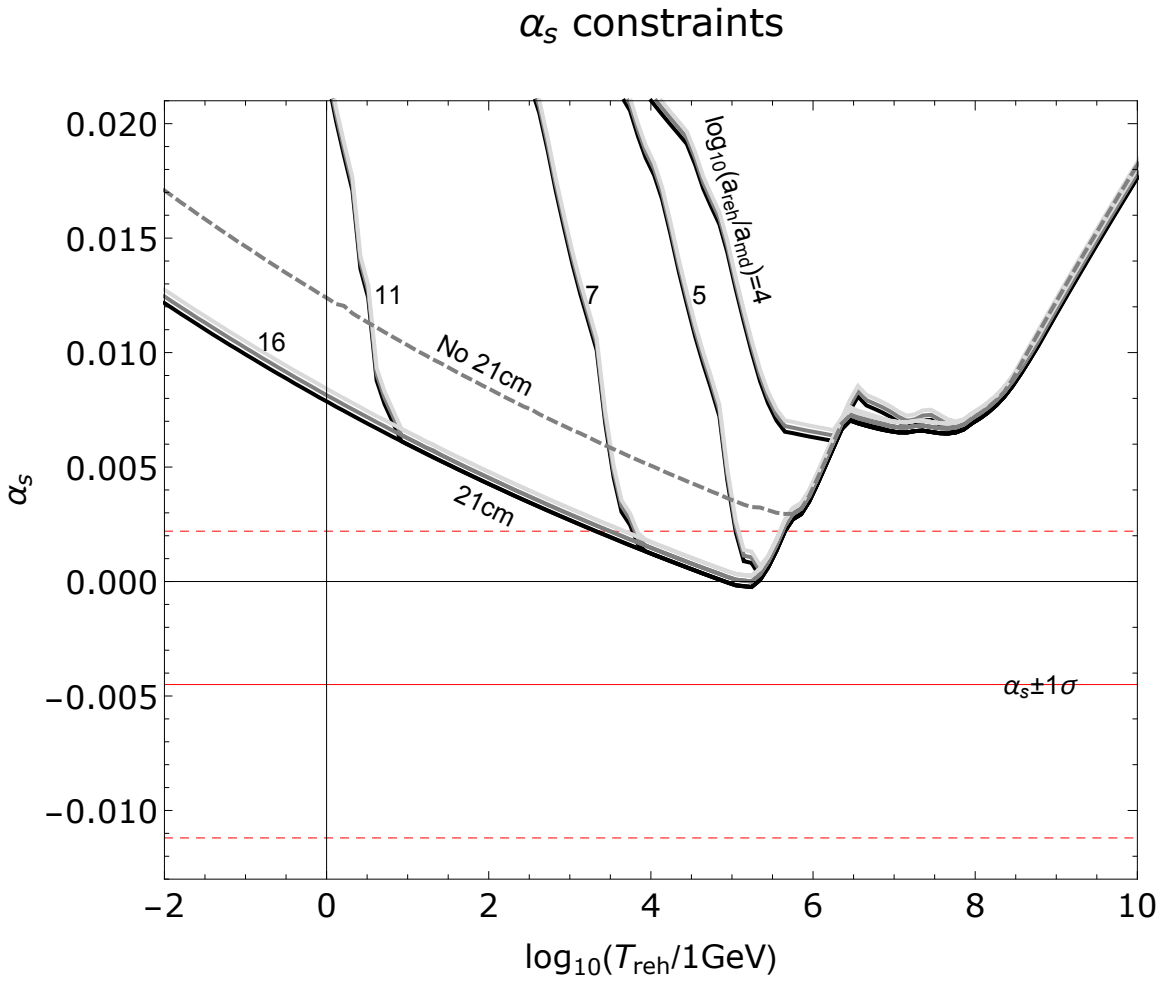

Figure 3.5.2: Constraints on the running of the spectral index α_s, assuming PBH formation during an early MD epoch of duration $\mathcal{A} = a_{\rm reh}/a_{\rm md}$ and reheating temperature $T_{\rm reh}$. We obtain the constrains for the combinations $(A_{\rm s}^+, n_{\rm s}^+)$ (black), $(A_{\rm s}, n_{\rm s})$ (dark gray), $(A_{\rm s}^-, n_{\rm s}^-)$ (light gray). The dashed gray line is included for reference and shows the constraints neglecting 21 cm PBH bounds for an MD epoch duration longer than $\mathcal{A} > 10^{16}$.

Chapter 4

Discussion and Summary

4.1 Results

We have derived bounds on a possible early MD epoch assuming an extended PBH mass function, and placed limits on the spectral index $n_{\rm s}$ and the running of the spectral index $\alpha_{\rm s}$ by comparing the predicted PBH abundances for PBH formation during an early MD epoch with PBH constraints from the literature, assuming an extended mass function that we derive. The results are presented in sections 3.4 and 3.5, and presented graphically in figures 3.4.1, 3.4.2, 3.5.1 and 3.5.2. These figures show that for a near-scale-invariant power spectrum compatible with the Planck 2018 results [3], current and potential PBH bounds from the 21 cm observations may constrain early MD if MD lasts for a duration of at least $\mathcal{A} = a_{\rm reh}/a_{\rm md} \gtrsim 10^5$, i.e. ~ 12 e-folds, and ends at a reheating temperature $T_{\rm min} < T_{\rm reh} \lesssim 10^{5.5}$ GeV, where $T_{\rm min}$ depends on the duration of MD, the spectral index $n_{\rm s}$, and $\alpha_{\rm s}$. For optimistic assumptions, our derived limits on the spectral index $n_{\rm s}$ extend into the Planck 2018 [3] 67% upper confidence region, to almost tangent their median $n_{\rm s}$, if we neglect the running $\alpha_{\rm s}$. Our bounds on the running $\alpha_{\rm s}$ shows that early MD is incompatible with $\alpha_{\rm s} \gtrsim 0$.

4.2 Discussion

Before stringent bounds on PBH abundances were derived from 21 cm observations, the enhanced production of PBHs associated with MD was not enough to produce abundances in conflict with observation. We made it our task to explore whether

the current and potential 21 cm bounds on PBHs, as presented in [28] and [58], are strong enough to change this conclusion, taking the route away from a monochromatic treatment and accounted for an extended mass function. Our analysis showed that, indeed, the new stronger bounds put us at right at the boundary where we can place new bounds on early MD. This is the main result of our work. However, because the red regions in figure 3.4.1 only slightly protrude over the value 0, we are not in a position to say with certainty that early MD is excluded. Thus, even small changes in our parameters can make the bounds disappear. For example, if the running $\alpha_{\rm s} = 0$, the bounds disappear when we go from $n_{\rm s}^{+} = 0.9649 + 0.014$ to $n_{\rm s} = 0.9649$, in which case we are just below the threshold. This means that we are extremely sensitive to the running $\alpha_{\rm s}$, since even small positive values, $\alpha_{\rm s} \gtrsim 0$, have significant effects on the power spectrum amplitude far away from the Planck pivot scale $k_* = 0.05\text{Mpc}^{-1}$. In section 3.2.4, e.g., we followed [26] to estimate the largest PBH mass $M_{\rm max}$ that forms. We thus imposed that an overdensity must have grown nonlinear by the time of reheating in order to continue collapsing against the radiation pressure, a condition we phrased as $\sigma_{\rm reh} = 1$. This meant that the modes must enter the horizon well before the end of MD to form PBHs. We briefly mentioned that this condition seemed rather arbitrary and could be replaced by some other number guided by simulations or other arguments. Had we instead chosen $\sigma_{\rm reh} = 1/3$, $M_{\rm max}$, as given by equation 3.33, we would pick up a factor $3^{3/2} \sim 5$. Thus, in order to achieve the same mass spectrum as before, the reheating temperature $T_{\rm reh}$ would need to be higher, which would lead to a longer period of RD afterwards. In section 2.4, we saw that the longer this period, the larger the relative enhancement of PBHs during RD and the larger the amplitude of the mass function. Thus, we would obtain stronger constraints if we relax the condition, i.e. let $1/3 \lesssim \sigma_{\rm reh} \lesssim 1$. In this regard, we believe our adoption of $\sigma_{\rm reh} = 1$ to be conservative, but note that a smaller value would moderately strengthen the constraints. We take the position that our results should be viewed as a positive sign that with current and near-future 21 cm observations [54] such as SKA [17], it is feasible that early MD may be constrained using (the non-observation of) PBHs, opening up a new window to the physics before BBN. This is very exciting and demands from the scientific community that great care is taken when deriving new constraints to eliminate sources of uncertainty [45]. It furthermore incentivizes new creative ways of using existing and future experiments to obtain even stronger bounds on PBHs.

For generality, we chose the form 2.138 and the parameters 2.139 for the scalar power

spectrum. While this equipped us with a simple scenario, it is not clear that this expansion accurately describes the power spectrum far away from the Planck pivot scale $k_* = 0.05\text{Mpc}^{-1}$. Since we are evaluating 2.138 at scales $\log_{10}(k/k_\star) \sim 16$, we are extrapolating many orders of magnitude. As a consequence, we must acknowledge that our bounds on early MD are very sensitive to this choice of the power spectrum. This suggests that a future study could complement our analysis by making use of predicted power spectra from inflationary models, thus eliminating the need for extrapolation. Indeed, we initialized such a study, but decided early on that this should be left for future work. If such a work is undertaken, one should study those inflationary models that give rise to power that is at least as UV-blue as the form 2.138 of the power spectrum if we set the running to zero. Similar analyses have already been performed in case of PBH formation during RD [7, 27]. Given that no conclusive evidence exists yet as to what model of inflation is correct [5], we believe our usage of the model-independent form 2.138 to be justified.

Another source of uncertainty comes from the analysis of the EDGES data [15, 45, 64]. The observed 21 cm signal in absorption is twice as large as, and flatter than, expected [15, 45]. This prompted many to invoke new physics as an explanation (e.g. [37]). Therefore, the importance of a true detection is massive. However, extraordinary results require extraordinary care and scrutiny, and comments were quickly made on their assumptions and foreground modeling choices [45, 64]. It was suggested that other justified modeling choices lead to different results that may not need new physics. [45] further points out that the modeling choices made in the original article [15] lead to unphysical parameters for the foregrounds, and concludes by remarking that while the observed 21 cm absorption feature may still be present in the data, more evidence is needed. Future 21 cm experiments are likely to shed more light on these issues and the results by [15]. This uncertainty propagates to our analysis via the derivation of bounds on PBHs in [68]. We mentioned earlier that while these limits are strong, they are not directly derived from EDGES data but assume that the global differential brightness temperature of the 21 cm signal be $T_{21} \lesssim -100$ mK for a 21 cm absorption feature in the same redshift range as that of the EDGES signal, which is much shallower than $T_{21} \sim -500$ mK according to the result presented in [15]. The approach in [68] to derive constraints on PBHs is thus somewhat justified, as it is yet to be shown that EDGES data indeed hints on the need for new physics. By the same argument, our adoption of their constraints is viable. Indeed, if the future 21 cm observations reveal that no

new physics is needed and that the absorption feature is consistent with predictions from stellar reionization, one could use the actual data to infer the global differential brightness temperature T_{21}, which for a measurement $T_{21} < -100$ mK would lead to even stronger constraints on PBHs than those we have applied.

We briefly mentioned the effect of angular momentum to suppress PBH formation during MD in section 3.2.3, but proceeded without considering this effect, with the remark that any potential constraints on MD would correspond to the optimistic scenario where the suppression due to angular momentum is negligible. An adequate analysis of angular momentum suppression of PBHs formation during MD is beyond the scope of this work but forms an important subject for a future study, in which the work in [40] is carefully revisited and implemented in a similar treatment to the present, in order to say with confidence that non-detection of PBHs may indeed probe early MD, inflationary scenarios, and pre-BBN physics.

4.3 Conclusions

We have explored the possibility of using primordial black holes (PBHs) to probe a period of early matter domination (MD). Our results are presented in section 4.1 and discussed in section 4.2. Under optimistic assumptions, we conclude that predictions of PBH formation during MD may be in conflict with observational bounds on PBHs if bounds from 21 cm observations are included. Without the addition of these bounds, we cannot exclude MD. We thus conclude that, while future work is required to shed more light onto our results as discussed in 4.2, (non-observation of) PBHs may potentially be used probe the pre-BBN universe, if the effect of angular momentum to suppress formation is small and the recent 21 cm bounds are strengthened or confirmed by further studies. PBHs may thus be employed to learn about the very early universe.

Bibliography

[1] Abbott, Benjamin P, Abbott, R, Abbott, TD, Abernathy, MR, Acernese, F, Ackley, K, Adams, C, Adams, T, Addesso, P, Adhikari, RX, et al. “GW150914: The Advanced LIGO detectors in the era of first discoveries”. In: *Physical review letters* 116.13 (2016), p. 131103.

[2] Aghanim, N, Armitage-Caplan, C, Arnaud, M, Ashdown, M, Atrio-Barandela, F, Aumont, J, Baccigalupi, C, Banday, AJ, Barreiro, RB, Bartlett, JG, et al. “Planck 2013 results. XXVII. Doppler boosting of the CMB: Eppur si muove”. In: *Astronomy & Astrophysics* 571 (2014), A27.

[3] Aghanim, Nabila, Akrami, Yashar, Ashdown, M, Aumont, J, Baccigalupi, C, Ballardini, M, Banday, AJ, Barreiro, RB, Bartolo, N, Basak, S, et al. “Planck 2018 results-VI. Cosmological parameters”. In: *Astronomy & Astrophysics* 641 (2020), A6.

[4] Akrami, Y, Arroja, F, Ashdown, M, Aumont, J, Baccigalupi, C, Ballardini, M, Banday, AJ, Barreiro, RB, Bartolo, N, Basak, S, et al. “Planck 2018 results. I. Overview and the cosmological legacy of Planck”. In: *arXiv preprint arXiv:1807.06205* (2018).

[5] Akrami, Y., Arroja, F., Ashdown, M., Aumont, J., Baccigalupi, C., Ballardini, M., Banday, A. J., Barreiro, R. B., Bartolo, N., and al., et. “Planck2018 results”. In: *Astronomy Astrophysics* 641 (Sept. 2020), A10. ISSN: 1432-0746. DOI: 10.1051/0004-6361/201833887. URL: http://dx.doi.org/10.1051/0004-6361/201833887.

[6] Allahverdi, Rouzbeh, Amin, Mustafa A, Berlin, Asher, Bernal, Nicolás, Byrnes, Christian T, Delos, M Sten, Erickcek, Adrienne L, Escudero, Miguel, Figueroa, Daniel G, Freese, Katherine, et al. “The first three seconds: a review of possible

expansion histories of the early universe". In: *arXiv preprint arXiv:2006.16182* (2020).

[7] Ballesteros, Guillermo, Rey, Julián, Taoso, Marco, and Urbano, Alfredo. "Primordial black holes as dark matter and gravitational waves from single-field polynomial inflation". In: *Journal of Cosmology and Astroparticle Physics* 2020.07 (2020), p. 025.

[8] Baumann, Daniel. "Cosmology: Part III mathematical tripos". In: *University lecture notes* 56 (2014).

[9] Baumann, Daniel. "TASI lectures on inflation". In: *arXiv preprint arXiv:0907.5424* (2009).

[10] Baumann, Daniel. *TASI Lectures on Primordial Cosmology*. 2018. arXiv: 1807.03098 [hep-th].

[11] Berlin, Asher, Hooper, Dan, and Krnjaic, Gordan. "PeV-scale dark matter as a thermal relic of a decoupled sector". In: *Physics Letters B* 760 (Sept. 2016), pp. 106–111. ISSN: 0370-2693. DOI: 10.1016/j.physletb.2016.06.037. URL: http://dx.doi.org/10.1016/j.physletb.2016.06.037.

[12] Bertone, Gianfranco and Hooper, Dan. "History of dark matter". In: *Reviews of Modern Physics* 90.4 (Oct. 2018). ISSN: 1539-0756. DOI: 10.1103/revmodphys.90.045002. URL: http://dx.doi.org/10.1103/RevModPhys.90.045002.

[13] Bertone, Gianfranco, Hooper, Dan, and Silk, Joseph. "Particle dark matter: evidence, candidates and constraints". In: *Physics Reports* 405.5-6 (Jan. 2005), pp. 279–390. ISSN: 0370-1573. DOI: 10.1016/j.physrep.2004.08.031. URL: http://dx.doi.org/10.1016/j.physrep.2004.08.031.

[14] Bird, Simeon, Cholis, Ilias, Muñoz, Julian B., Ali-Haïmoud, Yacine, Kamionkowski, Marc, Kovetz, Ely D., Raccanelli, Alvise, and Riess, Adam G. "Did LIGO Detect Dark Matter?" In: *Physical Review Letters* 116.20 (May 2016). ISSN: 1079-7114. DOI: 10.1103/physrevlett.116.201301. URL: http://dx.doi.org/10.1103/PhysRevLett.116.201301.

[15] Bowman, Judd D, Rogers, Alan EE, Monsalve, Raul A, Mozdzen, Thomas J, and Mahesh, Nivedita. "An absorption profile centred at 78 megahertz in the sky-averaged spectrum". In: *Nature* 555.7694 (2018), pp. 67–70.

[16] Byrnes, Christian T, Hindmarsh, Mark, Young, Sam, and Hawkins, Michael RS. "Primordial black holes with an accurate QCD equation of state". In: *Journal of Cosmology and Astroparticle Physics* 2018.08 (2018), p. 041.

[17] Carilli, C.L. and Rawlings, S. "Motivation, key science projects, standards and assumptions". In: *New Astronomy Reviews* 48.11-12 (Dec. 2004), pp. 979–984. ISSN: 1387-6473. DOI: 10.1016/j.newar.2004.09.001. URL: http://dx.doi.org/10.1016/j.newar.2004.09.001.

[18] Carr, B. J. "The primordial black hole mass spectrum." In: 201 (Oct. 1975), pp. 1–19. DOI: 10.1086/153853.

[19] Carr, B. J. "The primordial black hole mass spectrum." In: 201 (Oct. 1975), pp. 1–19. DOI: 10.1086/153853.

[20] Carr, B. J., Gilbert, J. H., and Lidsey, James E. "Black hole relics and inflation: Limits on blue perturbation spectra". In: *Physical Review D* 50.8 (Oct. 1994), pp. 4853–4867. ISSN: 0556-2821. DOI: 10.1103/physrevd.50.4853. URL: http://dx.doi.org/10.1103/PhysRevD.50.4853.

[21] Carr, Bernard, Clesse, Sebastien, Garcia-Bellido, Juan, and Kühnel, Florian. "Cosmic conundra explained by thermal history and primordial black holes". In: *Physics of the Dark Universe* 31 (2021), p. 100755.

[22] Carr, Bernard, Kohri, Kazunori, Sendouda, Yuuiti, and Yokoyama, Jun'ichi. "Constraints on primordial black holes". In: *arXiv preprint arXiv:2002.12778* (2020).

[23] Carr, Bernard and Kühnel, Florian. "Primordial black holes as dark matter: recent developments". In: *Annual Review of Nuclear and Particle Science* 70 (2020), pp. 355–394.

[24] Carr, Bernard, Kühnel, Florian, and Sandstad, Marit. "Primordial black holes as dark matter". In: *Physical Review D* 94.8 (2016), p. 083504.

[25] Carr, Bernard, Raidal, Martti, Tenkanen, Tommi, Vaskonen, Ville, and Veermäe, Hardi. "Primordial black hole constraints for extended mass functions". In: *Physical Review D* 96.2 (2017), p. 023514.

[26] Carr, Bernard, Tenkanen, Tommi, and Vaskonen, Ville. "Primordial black holes from inflaton and spectator field perturbations in a matter-dominated era". In: *Physical Review D* 96.6 (2017), p. 063507.

[27] Carrion, Karim, Hidalgo, Juan Carlos, Montiel, Ariadna, and Padilla, Luis E. “Complex Scalar Field Reheating and Primordial Black Hole production”. In: *arXiv preprint arXiv:2101.02156* (2021).

[28] Clark, Steven J, Dutta, Bhaskar, Gao, Yu, Ma, Yin-Zhe, and Strigari, Louis E. “21 cm limits on decaying dark matter and primordial black holes”. In: *Physical Review D* 98.4 (2018), p. 043006.

[29] Clesse, Sébastien and García-Bellido, Juan. “Massive primordial black holes from hybrid inflation as dark matter and the seeds of galaxies”. In: *Physical Review D* 92.2 (2015), p. 023524.

[30] Crawford, Matt and Schramm, David N. “Spontaneous generation of density perturbations in the early universe”. In: *Nature* 298.5874 (1982), pp. 538–540.

[31] Cui, Yanou, Lewicki, Marek, Morrissey, David E., and Wells, James D. “Probing the pre-BBN universe with gravitational waves from cosmic strings”. In: *Journal of High Energy Physics* 2019.1 (Jan. 2019). ISSN: 1029-8479. DOI: 10.1007/jhep01(2019)081. URL: http://dx.doi.org/10.1007/JHEP01(2019)081.

[32] Cyburt, Richard H., Fields, Brian D., Olive, Keith A., and Yeh, Tsung-Han. “Big bang nucleosynthesis: Present status”. In: *Reviews of Modern Physics* 88.1 (Feb. 2016). ISSN: 1539-0756. DOI: 10.1103/revmodphys.88.015004. URL: http://dx.doi.org/10.1103/RevModPhys.88.015004.

[33] D’Amico, Guido, Panci, Paolo, and Strumia, Alessandro. “Bounds on dark-matter annihilations from 21-cm data”. In: *Physical review letters* 121.1 (2018), p. 011103.

[34] Dalianis, Ioannis. “Constraints on the curvature power spectrum from primordial black hole evaporation”. In: *Journal of Cosmology and Astroparticle Physics* 2019.08 (Aug. 2019), pp. 032–032. ISSN: 1475-7516. DOI: 10.1088/1475-7516/2019/08/032. URL: http://dx.doi.org/10.1088/1475-7516/2019/08/032.

[35] Dodelson, Scott. *Modern cosmology*. Elsevier, 2003.

[36] Doroshkevich, AG. “Spatial structure of perturbations and origin of galactic rotation in fluctuation theory”. In: *Astrophysics* 6.4 (1970), pp. 320–330.

[37] Fraser, Sean, Hektor, Andi, Hütsi, Gert, Kannike, Kristjan, Marzo, Carlo, Marzola, Luca, Racioppi, Antonio, Raidal, Martti, Spethmann, Christian, Vaskonen, Ville, et al. “The EDGES 21 cm anomaly and properties of dark matter”. In: *Physics Letters B* 785 (2018), pp. 159–164.

[38] Green, Anne M. and Kavanagh, Bradley J. *Primordial Black Holes as a dark matter candidate*. 2020. arXiv: 2007.10722 [astro-ph.CO].

[39] Harada, Tomohiro, Yoo, Chul-Moon, and Kohri, Kazunori. “Threshold of primordial black hole formation”. In: *Physical Review D* 88.8 (Oct. 2013). ISSN: 1550-2368. DOI: 10.1103/physrevd.88.084051. URL: http://dx.doi.org/10.1103/PhysRevD.88.084051.

[40] Harada, Tomohiro, Yoo, Chul-Moon, Kohri, Kazunori, and Nakao, Ken-Ichi. “Spins of primordial black holes formed in the matter-dominated phase of the Universe”. In: *Physical Review D* 96.8 (2017), p. 083517.

[41] Harada, Tomohiro, Yoo, Chul-Moon, Kohri, Kazunori, Nakao, Ken-ichi, and Jhingan, Sanjay. “Primordial black hole formation in the matter-dominated phase of the Universe”. In: *The Astrophysical Journal* 833.1 (2016), p. 61.

[42] Hawking, S.W. “Black holes from cosmic strings”. In: *Physics Letters B* 231.3 (1989), pp. 237–239. ISSN: 0370-2693. DOI: https://doi.org/10.1016/0370-2693(89)90206-2. URL: https://www.sciencedirect.com/science/article/pii/0370269389902062.

[43] Hawking, Stephen. “Gravitationally collapsed objects of very low mass”. In: *Monthly Notices of the Royal Astronomical Society* 152.1 (1971), pp. 75–78.

[44] Hawking, Stephen W. “Black hole explosions?” In: *Nature* 248.5443 (1974), pp. 30–31.

[45] Hills, Richard, Kulkarni, Girish, Meerburg, P. Daniel, and Puchwein, Ewald. “Concerns about modelling of the EDGES data”. In: *Nature* 564.7736 (Dec. 2018), E32–E34. ISSN: 1476-4687. DOI: 10.1038/s41586-018-0796-5. URL: http://dx.doi.org/10.1038/s41586-018-0796-5.

[46] Inomata, Keisuke, Kawasaki, Masahiro, Mukaida, Kyohei, Tada, Yuichiro, and Yanagida, Tsutomu T. “Inflationary primordial black holes as all dark matter”. In: *Physical Review D* 96.4 (2017), p. 043504.

[47] Jedamzik, Karsten. “Primordial black hole formation during the QCD epoch”. In: *Physical Review D* 55.10 (1997), R5871.

[48] Kawamura, Seiji, Ando, Masaki, Seto, Naoki, Sato, Shuichi, Musha, Mitsuru, Kawano, Isao, Yokoyama, Jun’ichi, Tanaka, Takahiro, Ioka, Kunihito, Akutsu, Tomotada, et al. “Current status of space gravitational wave antenna DECIGO and B-DECIGO”. In: *arXiv preprint arXiv:2006.13545* (2020).

[49] Khlopov, M Yu, Malomed, BA, and Zeldovich, Ya B. “Gravitational instability of scalar fields and formation of primordial black holes”. In: *Monthly Notices of the Royal Astronomical Society* 215.4 (1985), pp. 575–589.

[50] Khlopov, M Yu and Polnarev, AG. “Primordial black holes as a cosmological test of grand unification”. In: *Physics Letters B* 97.3-4 (1980), pp. 383–387.

[51] Khlopov, M Yu and Polnarev, AG. “Primordial black holes as a cosmological test of grand unification”. In: *Physics Letters B* 97.3-4 (1980), pp. 383–387.

[52] Khlopov, MY and Polnarev, AG. “The stage of the superheavy particle dominance in the universe and primordial black holes”. In: *NASA STI/Recon Technical Report N* 81 (1980), p. 25890.

[53] Kolb, Edward W and Turner, Michael S. “The early universe”. In: *Nature* 294.5841 (1981), pp. 521–526.

[54] Koopmans, Leon, Barkana, Rennan, Bentum, Mark, Bernardi, Gianni, Boonstra, Albert-Jan, Bowman, Judd, Burns, Jack, Chen, Xuelei, Datta, Abhirup, Falcke, Heino, Fialkov, Anastasia, Gehlot, Bharat, Gurvits, Leonid, Jelić, Vibor, Klein-Wolt, Marc, Koopmans, Léon, Lazio, Joseph, Meerburg, Daan, Mellema, Garrelt, Mertens, Florent, Mesinger, Andrei, Offringa, André, Pritchard, Jonathan, Semelin, Benoit, Subrahmanyan, Ravi, Silk, Joseph, Trott, Cathryn, Vedantham, Harish, Verde, Licia, Zaroubi, Saleem, and Zarka, Philippe. *Peering into the Dark (Ages) with Low-Frequency Space Interferometers*. 2019. arXiv: 1908.04296 [astro-ph.IM].

[55] Kovetz, Ely D, Cholis, Ilias, and Kaplan, David E. “Bounds on ultralight hidden-photon dark matter from observation of the 21 cm signal at cosmic dawn”. In: *Physical Review D* 99.12 (2019), p. 123511.

[56] La, Daile and Steinhardt, Paul J. “Bubble percolation in extended inflationary models”. In: *Physics Letters B* 220.3 (1989), pp. 375–378.

[57] Lyth, David H and Liddle, Andrew R. *The primordial density perturbation: Cosmology, inflation and the origin of structure*. Cambridge University Press, 2009.

[58] Mack, Katherine J and Wesley, Daniel H. “Primordial black holes in the Dark Ages: Observational prospects for future 21cm surveys”. In: *arXiv preprint arXiv:0805.1531* (2008).

[59] Musco, Ilia and Miller, John C. “Primordial black hole formation in the early universe: critical behaviour and self-similarity”. In: *Classical and Quantum Gravity* 30.14 (2013), p. 145009.

[60] Phinney, S, Bender, P, Buchman, R, Byer, R, Cornish, N, Fritschel, P, Folkner, W, Merkowitz, S, Danzmann, K, DiFiore, L, et al. “The Big Bang Observer: Direct detection of gravitational waves from the birth of the Universe to the Present”. In: *NASA Mission Concept Study* (2004).

[61] Polnarev, AG and Khlopov, M Yu. “Cosmology, primordial black holes, and supermassive particles”. In: *Soviet Physics Uspekhi* 28.3 (1985), p. 213.

[62] Punturo, M, Abernathy, M, Acernese, F, Allen, B, Andersson, Nils, Arun, K, Barone, F, Barr, B, Barsuglia, M, Beker, M, et al. “The Einstein Telescope: a third-generation gravitational wave observatory”. In: *Classical and Quantum Gravity* 27.19 (2010), p. 194002.

[63] Ruderman, Josh. “New Physics at the Soft Photon Frontier”. In: Presented at Quantum Universe Lectures, DESY, Hamburg, 2021. URL: `https://indico.desy.de/event/28581/`.

[64] Tauscher, Keith, Rapetti, David, and Burns, Jack O. “Formulating and Critically Examining the Assumptions of Global 21 cm Signal Analyses: How to Avoid the False Troughs That Can Appear in Single-spectrum Fits”. In: *The Astrophysical Journal* 897.2 (2020), p. 132.

[65] Thorne, Kip S, Misner, Charles W, and Wheeler, John Archibald. *Gravitation*. Freeman, 2000.

[66] Weinberg, Steven. *Cosmology*. Oxford university press, 2008.

[67] Wouthuysen, SA. “On the excitation mechanism of the 21-cm (radio-frequency) interstellar hydrogen emission line.” In: *The Astronomical Journal* 57 (1952), pp. 31–32.

[68] Yang, Yupeng. “Constraints on primordial black holes and curvature perturbations from the global 21-cm signal”. In: *Phys. Rev. D* 102 (8 Oct. 2020), p. 083538. DOI: 10.1103/PhysRevD.102.083538. URL: https://link.aps.org/doi/10.1103/PhysRevD.102.083538.

[69] Zaldarriaga, Matias, Furlanetto, Steven R, and Hernquist, Lars. “21 Centimeter fluctuations from cosmic gas at high redshifts”. In: *The Astrophysical Journal* 608.2 (2004), p. 622.

[70] Zel’Dovich, Ya B. “Gravitational instability: An approximate theory for large density perturbations.” In: *Astronomy and astrophysics* 5 (1970), pp. 84–89.

[71] Zel’dovich, Ya. B. and Novikov, I. D. “The Hypothesis of Cores Retarded during Expansion and the Hot Cosmological Model”. In: 10 (Feb. 1967), p. 602.

TRITA TRITA-SCI-GRU 2021:058